Doctoral Dissertation

Development of Organically Bridged Silica Membranes and Application to Water Purification

(橋架けアルコキシドを用いた有機シリカ膜の開発と水処理への応用)

Rong Xu

Department of Chemical Engineering

Graduate School of Engineering, Hiroshima University

(広島大学大学院工学研究科 化学工学専攻)

September, 2013

Contents

Chapter 1

General Introduction

1.1 Water scarcity and desalination technology

The provision of clean, fresh water is a long-term challenge facing the world in the coming decades due to the well-known water scarcity [1-8]. Presently, more than 1.1 billion people in different countries, particularly in the Middle East and Africa, do not have access to safe drinking water [3]. A World Resources Institute analysis estimated that by 2025, around 3.9 billion people (nearly two-thirds of the Earth's population) would live in water-scare areas [4]. The growing population, the rapid economic development and the effect of climate change are likely to accelerate the water shortages. The global population growth is about 80 million a year, with increasing demands for fresh water [5]. Meanwhile, rapid economic development in the developing countries such as China and India, is typically accompanied by enormous energy consumption, which would further increase the stress on limited freshwater supplies [6]. Moreover, the rising temperature due to the climate change result in drier solid and less reliable rainfall, accelerating the loss of the already dwindling freshwater resources [7,8]. This growing demands for freshwater is therefore motivating the search for technological solutions that could alleviate the water crisis.

Desalination, a technology that converts saline water into clean freshwater, provides a seemingly permanent solution to this international water-shortage problem, since approximately 97% of total water resource on our planet is sea water. Desalination of brackish groundwater is also a choice for water supply in inland regions, where groundwater constitutes the most important available resources [9,10]. Today various technologies have been developed for desalination, including thermal-driven processes (e.g. multi-stage flash (MSF), multi-effect distillation (MED), and vapor compression distillation (VCD)) and membrane-based processes (electrically driven electrodialysis (ED), pressure-driven reverse osmosis (RO) and nanofiltration (NF)) [11-13].

Distillation consumes a large amount thermal energy to evaporate water, leaving the non-evaporated salts in the source water. Therefore, most distillation technologies are used in energy producing areas such as Middle East, where the cost of energy is inexpensive. Middle East has approximately 50% of the whole desalination capacity in the world and MSF technology accounts for more than half [14]. Although thermal-driven distillation is still the primary technology in the Middle East, membrane-based desalination technology has rapidly developed and now overtaken the conventional thermal technology. Today, reverse osmosis (RO) is the leading desalination technology and its popularity is expected to increase in the near future. Up to now, over 15,000 desalination plants have been installed in the world, and approximately 50% of plants using RO technology [15].

Figure 1-1 shows a schematic diagram of RO process. RO is a process of desalting water using a membrane that is permeable to the solvent but essentially impermeable to the solute. In order to force water to pass through the semi-permeable membrane, external high pressure must be applied to overcome the osmotic pressure (approximately 2.4 MPa for seawater) [16]. This semi-permeable membrane is called a RO membrane, which is effective in rejecting low molecular weight solutes such as inorganic salts or small organic molecules such as glucose. Solvent and solute transport RO membranes mainly according to a solution-diffusion mechanism, in which the permeating molecules dissolve into a membrane, diffuse through it, and desorb from the other side [17,18]. This transport mechanism will be described in detail in Chapter 3.

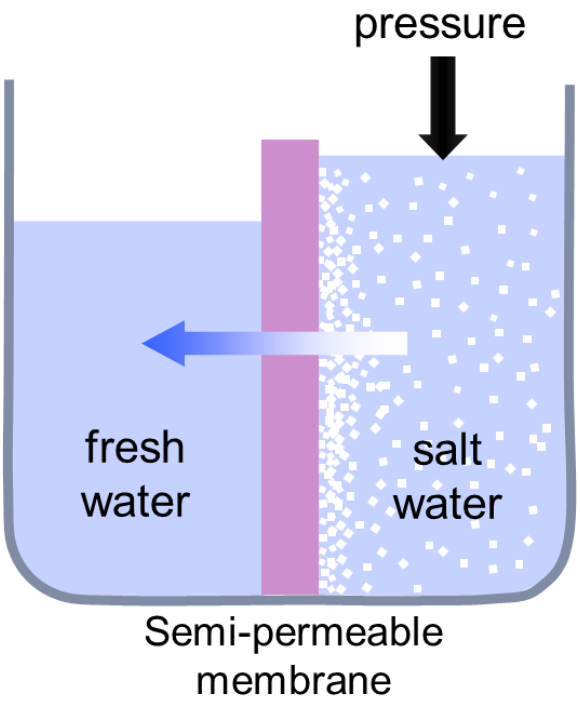

Figure 1-1. Schematic diagram of the RO process.

1.2 Conventional reverse osmosis (RO) membranes — materials and limits

A lot of membrane materials have been developed to prepare RO membranes. Polymeric RO membranes currently dominate the commercial market since they were first commercialized in RO application. One of the earliest reviews focused on polymeric RO membrane materials was reported by Cadotte in 1985 [19]. In 1993, a comprehensive review on composite RO membranes was presented by Petersen, focusing on the chemistry and composition of composite RO and NF membranes, especially for the membranes that have found commercial use [20]. In this section, a brief description of the most commercially important two types of polymers, cellulose acetate and aromatic polyamides, was given.

Cellulose acetate (CA) membranes

Asymmetric cellulose acetate (CA, the general chemical structure was shown in Figure 1-2) was the first commercially high-performance RO membrane material developed in

the early 1960s [21]. By 1970s, blending the initial cellulose diacetate with small amounts of cellulose triacetate (CTA) exhibited higher water permeability and salt rejection [22]. These blend membranes are major form of currently used CA membranes. Today, typical commercial CA membranes generally achieve NaCl rejection of 98-99% and have good flux for seawater feed. Even now, CA membranes still maintain a small fraction of the market, since they are easy to make, mechanically stable, and resistant to chlorine and other oxidants attack. For example, CA membranes can tolerate to chlorine up to 1 ppm, so the feed water can be chlorinated for biofouling control. However, the acetate group is prone to hydrolysis in both acidic and alkaline conditions, as well as sensitive to microbial fouling, limited the applications of CA membranes in a wider range [11,23].

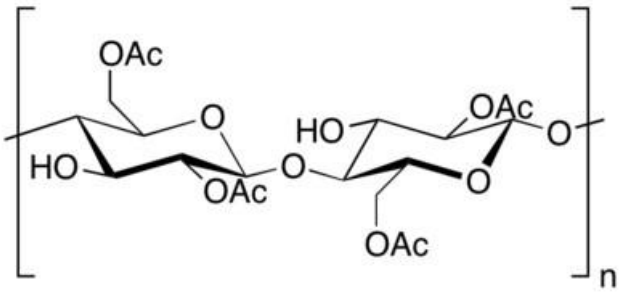

Figure 1-2. General chemical structure of cellulose acetate.

Aromatic polyamide (PA) membranes

A more commercially successful RO membrane for desalination is the thin film composite (TFC) aromatic polyamide membrane. The TFC polyamide membranes dominate the current water desalination market, mainly due to their very high salt rejection and high water permeability. For example, the classic FT-30 membrane, based on interfacial polymerization of 1,3-benzenediamine and trimesoyl chloride, exhibited a NaCl rejection of 99.2 % and a flux of nearly 1 $m^3/m^2 \cdot day$ operating at 5.5 MPa in seawater desalination test [24]. The main features of these commercialized polymeric RO membranes were presented in Table 1-1.

Table 1-1. Characteristics of some notable RO membranes.

Membrane (Material)	***Test Conditions***	***J_v*** [a] ***[$m^3/(m^2 \cdot d)$]***	***R_{obs}*** [b]	***Advantages/Disadvantages***	***Ref.***
Loeb-Sourirajan CA (Cellulose acetate)	>100 bar, 4% NaCl	**0.35**	**99%**	First RO membrane in practice; Cl[c] = 1 ppm / pH = 4-6; T < 35°C, less stable in organic solvents.	[25]
NS 100 (polyethylenimine - based)	>100 bar, 3.5% NaCl	**0.7**	**99%**	First TFC membrane achieved SWRO characteristics / Cl = 0 ppm.	[26]
PA 300/RC 100 (polyepiamine - based)	>69 bar, 3.5% NaCl	**1.0**	**99.4%**	First application in large SWRO plant / no tolerance to chlorine	[27]
FT-30 (Crosslinked fully aromatic polyamide)	68 bar, 3.5% NaCl	**1.2**	**99.3%**	Very high rejection and flux; wide pH range (2-11) / T < 45°C; Cl < 0.1 ppm.	[28]
SW30XLE (Crosslinked fully aromatic polyamide)	55 bar, 3.2% NaCl	**0.92**	**99.7%**	State-of-the-art SWRO membrane; pH = 2-11 / T < 45°C; Cl < 0.1 ppm.	[29]
ES10-D (Crosslinked fully aromatic polyamide)	7.5 bar, 0.15% NaCl	**1.7**	**99.5%**	Ultra-low pressure RO (energy saving); pH = 2-10 / T < 40°C; Cl = 0 ppm.	[30]

[a] J_v: volume flux of water; [b] R_{obs}: observed salt rejection; [c] Cl: chlorine tolerance.

Although aromatic PA membranes show better flux and rejection of salts and low-molecular-weight organic solutes than their predecessors such as CA membranes, they still have drawbacks. A significant problem is they are prone to biofouling, which severely diminishes filtration performance and shortens membrane lifetime. One simple way to reduced or even stopped biofouling is to add chlorine or hypochlorite disinfectants to the feed. Unfortunately, PA membranes are quite sensitive to chlorine, because the amide linkage in the membranes is susceptible to chlorine attack [31,32]. The degradation mechanism of PA membranes by hypochlorite was illustrated in Figure 1-3. To date, although the chlorine tolerance of the TFC polyamide membranes have been improved by various modifications, these membranes still cannot expose to feed water containing more than a few ppb levels of chlorine. Therofore, feed water, which is chlorinated for biofouling control, requires an additional pre-treatment step, dechlorination, before exposing to PA RO membranes. After passing through the membranes, the purified water is then rechlorinated before sent to other unit operations [33]. These costly dechlorination and rechlorination steps might be eliminated through use of new RO membranes which can tolerate high levels of chlorine in feed water.

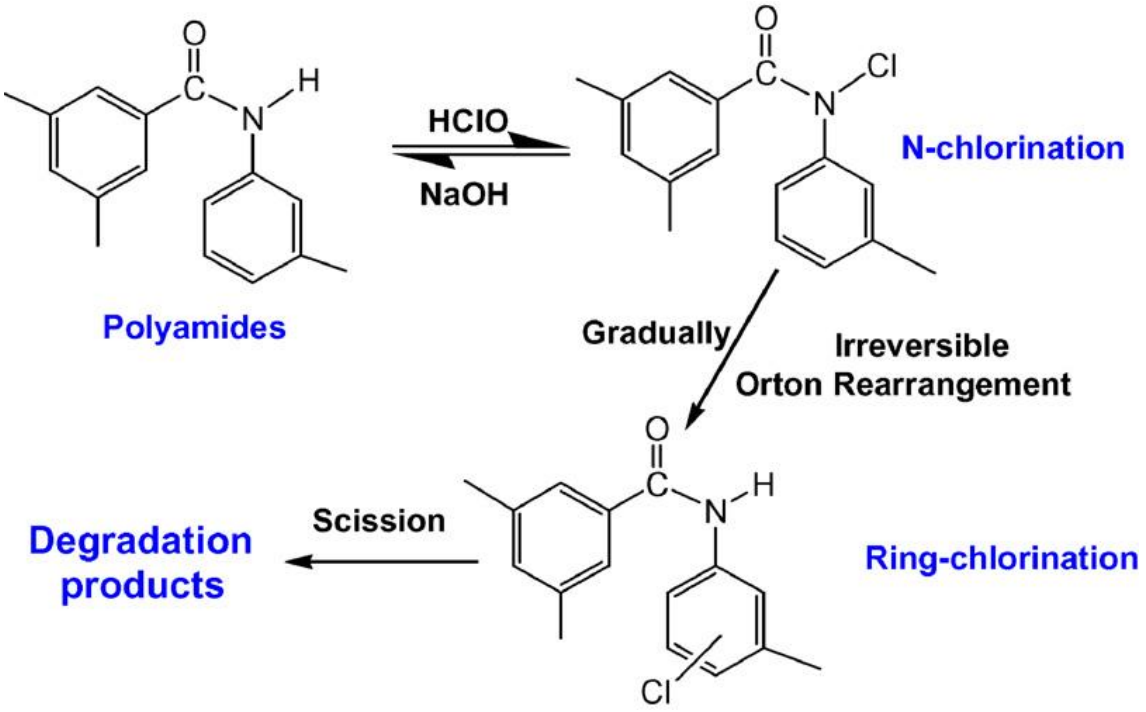

Figure 1-3. Proposed mechanism of hypochlorite degradation of polyamide membrane [34].

Another drawback of polyamide membranes is their low hydrothermal stability. Operation of RO at high temperatures is desired in many industrial applications, such as the food and textile industries [35]. Unfortunately, the maximum operating temperature for most polyamide membranes is normally below 55 °C [36]. Moreover, they are hardly used in non-aqueous solutions, since the substrate material, polysulfone, can be easily attacked by many organic solvents [35,37]. Therefore, the development of robust RO membranes, which possess highly chlorine tolerance and higher hydrothermal stability, remains a challenge for water purification.

1.3 New materials for RO membranes

A desired membrane should have high level in regard to water permeability, salt rejection, and stability under operating conditions. Given the limitations of TFC polyamide membranes mentioned above, extensive efforts have, therefore, been devoted to developing more attractive materials. Inorganic membranes have superior thermal and chemical stability with great potential for application to water desalination. The following

sections describe two of the most promising inorganic materials, zeolites and carbon nanotubes (CNTs).

Zeolite membranes

Zeolites are crystalline aluminosilicate materials with well-defined pores and narrow pore size distribution. Zeolite membranes have been extensively studied for gas separation and liquid pervaporation (PV) [38-41]. Due to their specific pore structure, zeolite membranes show great potential for RO desalination. Moreover, zeolites are in a wider range of solvents and can withstand at high temperature and high pressure. Recently, molecular dynamic simulation has shown that a perfect (single crystal) of ZK-4 zeolite membrane could reject 100% Na^+ ions through the RO process [42]. The first RO experimental research using a MFI-type silicalite-1 zeolite membrane (pore size: 0.56 nm, typical structure of MFI-type zeolite was shown in Figure 1-4) showed 76.7% rejection of Na^+ ions with a water flux of about 0.112 kg m^{-2} h^{-1} under applied pressure of 2.07 MPa [43]. Subsequently, a lot of work has been conducted to improve the water flux and salt rejection by modifying the zeolite structure and optimizing preparation technique [44-48]. The Si/Al ratio, which dominates the membrane wettability and surface charge, has been optimized to increase the flux and salt rejection. Adjustment of Al content in the zeolite membrane would tailor the surface hydrophilicity, therefore altering membrane affinity to water [49]. Recently, the comparison of zeolite membranes with varying Si/Al ratios was reported by Duke and his co-workers [47]. They developed silicalite (pure silica MFI zeolite) and ZSM-5 (Al-containing MFI zeolite) membranes for desalination. Silicalite membranes achieved highest rejections in RO due to their monopolar surface charge. Moreover, addition of alumina offered a tailorable property in ion-selective water filtration. However, these zeolite membranes typically require tedious synthesis procedures to form thin, defect-free film on porous substrates [50].

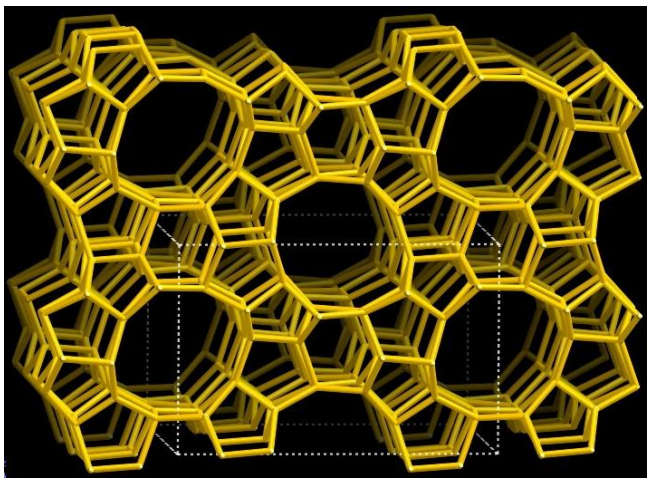

Figure 1-4. Three dimensional network of a MFI zeolite.

Carbon nanotubes (CNTs)

Recently, carbon nanotubes (CNTs) have attracted considerable attention due to their unusually high water flux, showing great promise in water purification [51-54]. The preliminary measurement with a CNTs membrane comprised of aligned double-wall CNTs with inner diameter less than 2 nm was reported by Holt et al [54]. The water flux through these microfabricated membranes was more than three orders of magnitude higher than the theoretically calculation. Further experiment with these CNTs membrane showed that ion exclusion that could be as high as 98% under certain conditions, and the ion exclusion mechanism in CNTs was dominated by electrostatic interactions (Donnan effect) rather than steric and hydrodynamic effects [55]. The mechanism of very fast transport of water through CNTs is still not completely clear, in spite of many academic discussions on this point [56-59]. Some research suggested that the formation of tight hydrogen-bonding network between the water molecules and hydrophobic inner walls of CNTs caused spontaneous filling of CNTs with an ordered chain of water molecules, which led to the rapid motion of water along the tube axis in a slug flow manner [51,58]. On the other hand, it also has been suggested that the frictionless water transport is due to the formation of liquid layer of water molecules inside the walls of CNTs, which shields the bulk flow from the hydrophobic carbon surface [59]. Despite the unusually high flux of each individual CNTs, producing of aligned CNTs membranes is complex costly

compared commercially viable membranes. In addition, CNTs membranes might be prone to fouling in water desalination given their high hydrophobic nature [60].

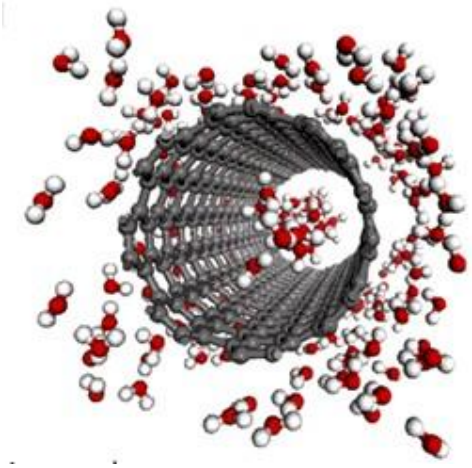

Figure 1-5. Schematic image of water molecules through carbon nanotubes (reproduced from Ref. [61])

1.4 Organosilica hybrid materials

Another promising candidate for RO desalination is amorphous microporous silica membranes owing to their excellent molecular sieving ability. These sol-gel derived silica membranes with pore sizes that range from 2-5 Å have been successfully used for gas separation and PV processes [62,63]. However, a low hydrothermal stability severely limits their application to water purification. Extensive efforts have, therefore, been devoted to improving the hydrothermal stability of silica membranes.

A significant breakthrough in hydrothermal stability came with the development of organic-inorganic hybrid silica materials with bridging organic groups. The synthesis of this hybrid material through hydrolysis and condensation of bridged organosilanes, $(R'O)_3Si\text{-}R\text{-}Si(OR')_3$, has been studied for a long time in the sol-gel chemistry field [64,65]. This new class of hybrid silica materials, known as periodic mesoporous organosilicas (PMOs), are highly promising for applications in various fields since they were first synthesized by three different research groups in 1999 [66-68]. In PMOs, the functional organic groups are homogeneously incorporated in the three-dimensional silica

networks as bridges. The versatility of organic bridges offers the ability to tune the bulk properties such as thermal stability, surface area, porosity, flexibility, chemical resistance and hydrophobicity [65]. Early PMOs was explored only with simple organic functions such as methyl, ethyl, ethylene, and benzene groups [66-68]. Now, a variety of complex functional groups have been introduced into PMOs, as described in specialized reviews [69-71].

However, for molecular separation application, PMOs with mesopores of larger than 2 nm has no molecular sieving properties. In 2008, Castricum *et al.* reported in a pioneering paper the development of microporous organosilica membranes by co-condensation of 1,2-bis(triethoxysilyl)ethane (BTESE) and methyltriethoxysilane (MTES). The resulting organosilica membranes showed a quite stable performance of 2 years for the pervaporative dehydration of butanol at 150 °C [72,73]. In their subsequent work, the BTESE membrane also showed a high degree of acid stability in long-term measurements at a pH value of ~2, and the membrane performance was reproducible for acidities that ranged from pH 2-8 [74]. Furthermore, the influences of size, flexibility, and shape of various alkyl and aryl bridges on the membrane pore size, nanostructure, and affinity was described to determine the relationship between the bridging group and the membrane properties [75]. Qi *et al.* employed the Nb-doped BTESE membranes for enhanced CO_2 separation, and found that the membranes possessed high hydrothermal stability under exposure to steam at 200 °C [76,77]. Moreover, bis(triethoxysilyl)methane (BTESM) derived organosilica membranes have already been developed for pervaporative dehydration and gas separation by different research groups [74,78,79]. It is particularly worth noting that polyamide-imide supported BTESE membranes were successfully prepared by plasma enhanced chemical vapor deposition and the pervaporation performance of resulting membranes is comparable with those of conventional ceramic supported membranes, which would further reduce time to market [80].

Our research group proposed a “spacer” technique to control silica networks, where the linking groups were introduced to design a loose structure for development of a highly permeable hydrogen separation membrane [81,82]. This organosilica membrane was also applied to pervaporative dehydration of acetic acid aqueous solutions and exhibited high

permselectivity with excellent stability [83]. Recently, we examined the possibility of using organosilica membranes for RO desalination under aggressive environments. Figure 1-6 shows the schematic diagram of bridged organosilica nanosieve networks for water desalination. The BTESE-derived organosilica membranes exhibited excellent resistance to chlorine and exceptional hydrothermal stability, as well as superior salt rejection of >97%, showing great promise as robust RO membranes. Moreover, the transport mechanism for these innovative membranes was also studied in our work [84,85].

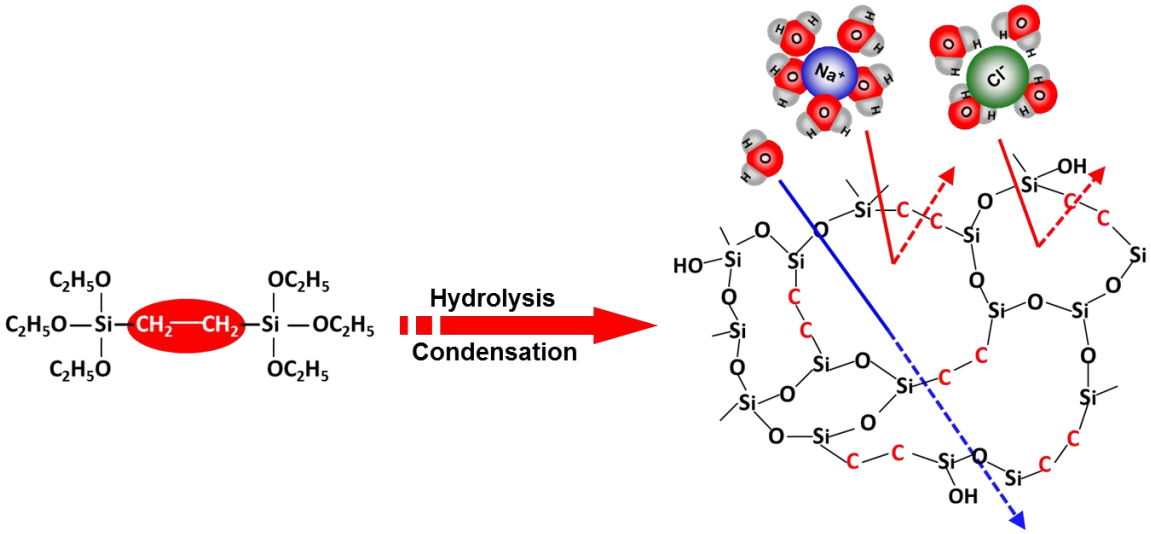

Figure 1-6. Schematic image of bridged organosilica networks for water desalination.

1.5 Objectives and organization of this research

The overall objective of this dissertation research is to develop robust organosilica membranes for water purification by reverse osmosis (RO). Given the limitations of conventional polyamide-based RO membranes, this research has been focusing on the development of advanced RO membranes using a new class of materials, bridged organosilicas, which are expected to possess high separation capability and high stability in harsh environments including chlorine-containing and high-temperature system. In addition, the transport mechanism for these innovative membranes has also been studied in this research. The following is the main work of this research.

(1) Development of BTESE-derived organosilica membranes for RO desalination in harsh environments.

(2) Investigation of transport mechanism in RO and comparison with the pervaporation and gas permeation properties using these organosilica membranes.

(3) Optimizing the separation performances by tailoring the structure of the organic links and making a comparative study of organosilica membranes with different functional groups.

This thesis consists of 6 chapters, as follows:

Chapter 1 is "***General introduction***", which introduces the research background and purpose of this study.

Chapter 2 is "***Development of chlorine-resistant and hydrothermal stable organosilica membranes for reverse osmosis***". A new type of microporous organosilica membrane derived from bis(triethoxysilyl)ethane (BTESE) has been developed for reverse osmosis (RO). Sol-gel derived BTESE RO membranes show a molecular weight cut-off below 100 Da and exhibit superior molecular sieving ability. Due to the introduction of an inherently stable hybrid network structure, the membrane withstands higher temperatures in comparison with commercial polyamide RO membranes, and is resistant to water to at least 90 °C with no obvious changes in filtration performance. Furthermore, the accelerated chlorine-resistance test confirmed excellent chlorine stability in this material, which demonstrates promise for a new generation of chlorine-resistant RO membrane materials.

Chapter 3 is "***Reverse osmosis performance of organosilica membranes and comparison with the pervaporation and gas permeation properties***". BTESE-derived organosilica membranes calcined at 300 °C almost completely rejected salts and neutral solutes with low molecular weight in RO. Increasing the operating pressure led to an increase in water flux and salt rejection, while the flux and rejection decreased as salt

concentration increased, which could be successfully explained by the solution-diffusion (SD) model. The water permeation mechanism differed from the viscous flow mechanism. Observed activation energies for permeation were larger for membranes with a smaller pore size, and were considerably larger than the activation energies for water viscosity. The applicability of the generalized SD model to RO and pervaporation (PV) desalination processes was examined, and the quantitative differences in water permeance were accurately predicted by the application of generalized transport equations.

Chapter 4 is "***Optimizing water permeability by introducing polarizable ethenylene bridges and aqueous ozone modification***". Bis(triethoxysilyl)ethylene (BTESEthy) was used as a novel precursor to develop a microporous organosilica membrane via the sol-gel technique. Water sorption measurements confirmed that ethenylene-bridged BTESEthy networks had a higher affinity for water than that of ethane-bridged organosilica materials. The introduction of polarizable and rigid ethenylene bridges in the network structure led to improved water permeability and high NaCl rejection (>98.5%) in RO. Moreover, the aqueous ozone modification promoted significant improvement in water permeability of the membrane. Despite a moderate rejection decrease from 98.8 to 92.3% after 60 min of ozone exposure, the water permeability reached 1.1×10^{-12} $m^3/(m^2 \cdot s \cdot Pa)$, which was close to that of the commercial seawater RO membrane, SW30HR.

Chapter 5 is "***Comparative study on structure-property of organosilica membranes with ethane, ethylene and acetylene bridging groups***". Acetylene-bridged organosilica membranes were prepared and compared with the previous organosilica membranes with ethane and ethylene bridges. BTESA sols showed a relatively narrow size distribution with small sol size. Like BTESE and BTESEthy membranes, BTESA membranes were thermally stable up to 300 °C in air. Compared with BTESE and BTESEthy membranes, BTESA membranes exhibited higher permeance and lower selectivity in gas permeation, probably due to its more loose structure. MWCO measurements suggested that BTESA membranes had the largest effective pore size among the three membranes, resulting in a relatively low level of NaCl rejection. However, BTESA membranes exhibited highest

water permeability of up to approximately 8.5×10^{-13} $m^3/(m^2 \cdot s \cdot Pa)$ in RO, owing to the introduction of the more polarizable and rigid acetylene bridges in the silica network.

Chapter 6 is "***Conclusions***". Main conclusions presented in this thesis were summarized and recommendations for future work were provided.

References

[1] M.A. Shannon, P.W. Bohn, M. Elimelech, J.G. Georgiadis, B.J. Marinas, A.M. Mayes, Science and technology for water purification in the coming decades, *Nature* 452 (2008) 301-310.

[2] M. Elimelech, W.A. Phillip, The future of seawater desalination: Energy, technology, and the environment, *Science* 333 (2011) 712-717.

[3] M.A. Montgomery, M. Elimelech, Water and sanitation in developing countries: including health in the equation, *Environ. Sci. Technol.* 41 (2007) 17-24.

[4] S.J. Kim, S.H. Ko, K.H. Kang, J. Han, Direct seawater desalination by ion concentration polarization, *Nature Nanotechnology* 5 (2010) 297-301.

[5] R.F. Service, *Science* 313 (2006) 1088-1090.

[6] C.J. Vörösmarty, P. Green, J. Salisbury, R.B. Lammers, Global water resources: Vulnerability from climate change and population growth, *Science* 289 (2000) 284-288.

[7] S.L. Piao, P. Ciais, Y. Huang, Z.H. Shen, S.S. Peng, J.S. Li, L.P. Zhou, H.Y. Liu, Y.C. Ma, Y.H. Ding, P. Friedlingstein, C.Z. Liu, K. Tan, Y.Q. Yu, T.Y. Zhang, J.Y. Fang, The impacts of climate change on water resources and agriculture in China, *Nature* 467 (2010) 43-51.

[8] L.M. Fry, J.R. Mihelcic, D.W. Watkins, Water and nonwater-related challenges of achieving global sanitation coverage, *Environ. Sci. Technol.* 42 (2008) 4298-4304.

[9] M.S. Mohsen, O.R. Al-Jayyousi, Brackish water desalination: an alternative for water supply enhancement in Jordan, *Desalination* 124 (1999) 163-174.

[10] A.R. Allam, M.A. Dawoud, Desalination of brackish groundwater in Egypt, *Desalination* 152 (2003) 19-26.

[11] R.W. Baker, Membrane Technology and Applications, Second Ed., John Wiley & Sons, Ltd.: West Sussex, England, (2004) 191-235.

[12] B. Van der Bruggen, C. Vandecasteele, Distillation vs. membrane filtration: overview of process evolutions in seawater desalination, *Desalination* 143 (2002)207-218.

[13] D. Li, H.T. Wang, Recent developments in reverse osmosis desalination membranes, *J. Mater. Chem.* 20 (2010) 4551-4566.

[14] R. Borsani, S. Rebagliati, Fundamentals and costing of MSF desalination plants and comparison with other technologies, *Desalination* 182 (2005) 29-37.

[15] L.F. Greenlee, D.F. Lawler, B.D. Freeman, B. Marrot, P. Moulin, Reverse osmosis desalination: Water sources, technology, and today's challenges, *Water Res.* 43 (2009) 2317-2348.

[16] C. Fritzmann, J. Löwenberg, T. Wintgens, T. Melin, State-of-the-art of reverse osmosis desalination, *Desalination* 216 (2007) 1-76.

[17] J.G. Wijmans, R.W. Baker, The solution-diffusion model: a review, *J. Membr. Sci.* 107 (1995) 1-21.

[18] T. Kataoka, T. Tsuru, S. Nakao, S. Kimura, Permeation equations developed for prediction of membrane performance in pervaporation, vapour permeation and reverse osmosis based on the solution-diffusion model, *J. Chem. Eng. Jpn.* 24 (1991) 326-333.

[19] J.E. Cadotte, Evolution of Composite Reverse Osmosis Membranes, in: Material Science of Synthetic Membranes, *ACS Symposium Series* 269 (1985) 273-294.

[20] R.J. Petersen, Composite reverse osmosis and nanofiltration membranes, *J. Membr. Sci.* 83 (1993) 81-150.

[21] S. Loeb, S. Sourirajan, Sea Water Demineralization by Means of an Osmotic Membrane, in: Saline Water Conversion - II, *Advances in Chemistry* 46 (1963) 117-132.

[22] W.M. King, D.L. Hoernschemeyer, C.W. Saltonstall, Cellulose acetate blend membranes, In: *Reverse Osmosis Membrane Research*, H.K. Lonsdale, H.E. Podall (Eds.), Plenum Press, New York (1972) 131-162.

[23] K.P. Lee, T.C. Arnot, D. Mattia, A review of reverse osmosis membrane materials for desalination-development to date and future potential, *J. Membr. Sci.* 370 (2011) 1-22.

[24] R.E. Larson, J.E. Cadotte, R.J. Petersen, The FT-30 seawater reverse osmosis membrane-element test results, *Desalination* 38 (1981) 473-483.

[25] S. Loeb, The Loeb-Sourirajan Membrane: How It Came About, in: Synthetic Membranes, American Chemical Society, Washington, D.C., (1981) 1-9.

[26] J.E. Cadotte, Reverse Osmosis Membrane, US Patent 4039440 (1977).

[27] R.L. Riley, R.L. Fox, C.R. Lyons, C.E. Milstead, M.W. Seroy, M. Tagami, Spiral-wound poly (ether/amide) thin-film composite membrane systems, Desalination 19

(1976) 113-126.

[28] J.E. Cadotte, Interfacially Synthesized Reverse Osmosis Membrane, US Patent 4277344 (1981).

[29] http://www.home-water-purifiers-and-filters.com/filmtec-seawater-RO-membranes.

[30] http://www.nitto.com/product/datasheet/menbren/003/

[31] J. Glater, S.K. Hong, M. Elimelech, The search for a chorine-resistant reverse osmosis membrane, *Desalination* 95 (1994) 325-345.

[32] V.T. Do, C.Y. Tang, M. Reinhard, J.O. Leckie, Degradation of polyamide nanofiltration and reverse osmosis membranes by hypochlorite, *Environ. Sci. Technol.* 46 (2012) 852-859.

[33] G.A. Tularam, M. Ilahee, Environmental concerns of desalinating seawater using reverse osmosis, *J. Environ. Monit.* 9 (2007) 805-813.

[34] G.D. Kang, C.J. Gao, W.D. Chen, X.M. Jie, Y.M. Cao, Q. Yuan, Study on hypochlorite degradation of aromatic polyamide reverse osmosis membrane, *J. Membr. Sci.* 300 (2007) 165-171.

[35] M.J.H. Snow, D. de Winter, R. Buckingham, J. Campbell, J. Wagner, New techniques for extreme conditions: high temperature reverse osmosis and nanofiltration, *Desalination* 105 (1996) 57-61.

[36] H. Saidani, N.B. Amar, J. Palmeri, A. Deratani, Interplay between the transport of solutes across nanofiltration membranes and the thermal properties of the thin active layer, *Langmuir* 26 (2010) 2574-2583.

[37] M. Mänttäri, A. Pihlajamäki, E. Kaipainen, M. Nyström, Effect of temperature and membrane pre-treatment by pressure on the filtration properties of nanofiltration membranes, *Desalination* 145 (2002) 81-86.

[38] J. Caro, M. Noack, Zeolite membranes-recent developments and progress, *Micropor. Mesopor. Mater.* 115 (2008) 215-233

[39] M. P. Bernal, G. Xomeritakis, M. Tsapatsis, Tubular MFI zeolite membranes made by secondary (seeded) growth, *Catal. Today* 67 (2001) 101-107.

[40] S. Gopalakrishnan, T. Yamaguchi, S.I. Nakao, Permeation properties of templated and template-free ZSM-5 membranes, *J. Membr. Sci.* 274 (2006) 102-107.

[41] B. Soydas, O. Dedea, A. Culfaza, H. Kalıpçılar, Separation of gas and organic/water mixtures by MFI type zeolite membranes synthesized in a flow system, *Micropor. Mesopor. Mater.* 127 (2010) 96-103.

[42] J. Lin, S. Murad, A computer simulation study of the separation of aqueous solution using thin zeolite membranes, *Mol. Phys.* 99 (2001) 1175-1181.

[43] L.X. Li, J.H. Dong, T.M. Nenoff, R. Lee, Desalination by reverse osmosis using MFI zeolite membranes, *J. Membr. Sci.* 243 (2004) 401-404.

[44] L.X. Li, N. Liu, B. McPherson, R. Lee, Enhanced water permeation of reverse osmosis through MFI-type zeolite membranes with high aluminum contents, *Ind. Eng. Chem. Res.* 46 (2007) 1584-1589.

[45] L.X. Li, J.H. Dong, T.M. Nenoff, Transport of water and alkali metal ions through MFI zeolite membranes during reverse osmosis, *Sep. Purif. Technol.* 53 (2007) 42-48.

[46] N. Liu, L.X. Li, B. McPherson, R. Lee, Removal of organics from produced water by reverse osmosis using MFI-type zeolite membranes, *J. Membr. Sci.* 325 (2008) 357-361.

[47] M.C. Duke, J. O'Brien-Abraham, N. Milne, B. Zhu, J.Y.S. Lin, J. Diniz da Costa, Seawater desalination performance of MFI type membranes made by secondary growth, *Sep. Purif. Technol.* 68 (2009) 343-350.

[48] J. Lu, N. Liu, L. Li, R. Lee, Organic fouling and regeneration of zeolite membrane in wastewater treatment, *Sep. Purif. Technol.* 72 (2010) 203-207.

[49] F. Jareman, J. Hedlund, J. Sterte, Effects of aluminum content on the separation properties of MFI membranes, *Sep. Purif. Technol.* 32 (2003) 159-163.

[50] M.C. Duke, S. Mee, J.C.D. da Costa, Performance of porous inorganic membranes in non-osmotic desalination, *Water Res.* 41 (2007) 3998-4004.

[51] G. Hummer, J.C. Rasaiah, J.P. Nowotyta, Water conduction through the hydrophobic channel of a carbon nanotube, *Nature* 414 (2001) 188-190.

[52] B.J. Hinds, N. Chopra, T. Rantell, R. Andrews, V. Gavalas, L.G. Bachas, Aligned multiwalled carbon nanotube membranes, *Science* 303 (2004) 62-65.

[53] M. Majumder, N. Chopra, R. Andrews, B.J. Hinds, Nanoscale hydrodynamics: Enhanced flow in carbon nanotubes, *Nature* 438 (2005) 44.

[54] J.K. Holt, H.G. Park, Y. Wang, M. Stadermann, A.B. Artyukhin, C.P. Grigoropoulos,

A. Noy, O. Bakajin, Fast mass transport through sub-2-nanometer carbon nanotubes, *Science* 312 (2006) 1034-1037.

[55] F. Fornasiero, H.G. Park, J.K. Holt, M. Stadermann, C.P. Grigoropoulos, A. Noy, O. Bakajin, Ion exclusion by sub-2-nm carbon nanotube pores, *Proc. Natl. Acad. Sci.* 105 (2008) 17250-17255.

[56] A. Striolo, The mechanism of water diffusion in narrow carbon nanotubes, *Nano Lett.* 6 (2006) 633-639.

[57] S. Joseph, N.R. Aluru, Why are carbon nanotubes fast transporters of water, *Nano Lett.* 8 (2008) 452-458.

[58] A. Kalra, S. Garde, G. Hummer, Osmotic water transport through carbon nanotubes membranes, *Proc. Natl. Acad. Sci.* 100 (2003) 10175-10180.

[59] E.M. Kotsalis, J.H. Walther, P. Koumoutsakos, Multiphase water flow inside carbon nanotubes, *Int. J. Multiphase Flow* 30 (2004) 995-1010.

[60] B. Corry, Designing carbon nanotube membranes for efficient water desalination, *J. Phys. Chem. B* 112 (2008) 1427-1434.

[61] https://www.llnl.gov/news/newsreleases/2008/NR-08-06-09.html.

[62] R.M. de Vos, H. Verweij, High-Selectivity, High-Flux Silica Membranes for Gas Sep7aration, *Science* 279 (1998) 1710-1711.

[63] J.E. ten Elshof, C.R. Abadal, J. Sekulić, S.R. Chowdhury, D.H.A. Blank, Transport mechanisms of water and organic solvents through microporous silica in the pervaporation of binary liquids, *Micropor. Mesopor. Mater.* 65 (2003) 197-208.

[64] D.A. Loy, K.J. Shea, Bridged polysilsesquioxanes. Highly porous hybrid organic-inorganic materials, *Chem. Rev.* 95 (1995) 1431-1442.

[65] K.J. Shea, D.A. Loy, Bridged Polysilsesquioxanes. Molecular-Engineered Hybrid Organic-Inorganic Materials, *Chem. Mater.* 13 (2001) 3306-3319.

[66] S. Inagaki, S. Guan, Y. Fukushima, T. Ohsuna, O. Terasaki, Novel Mesoporous Materials with a Uniform Distribution of Organic Groups and Inorganic Oxide in Their Frameworks, *J. Am. Chem. Soc.* 121 (1999) 9611-9614.

[67] T. Asefa, M.J. MacLachlan, N. Coombs, G.A. Ozin, Periodic mesoporous organosilicas with organic groups inside the channel walls, *Nature* 402 (1999) 867-871.

[68] B.J. Melde, B.T. Holland, C.F. Blanford, A. Stein, Mesoporous Sieves with Unified Hybrid Inorganic/Organic Frameworks, *Chem. Mater.* 11 (1999) 3302-3308.

[69] P. Van Der Voort, D. Esquivel, E. De Canck, F. Goethals, I. Van Driessche, F.J. Romero-Salguero, Periodic Mesoporous Organosilicas: from simple to complex bridges; a comprehensive overview of functions, morphologies and applications, *Chem. Soc. Rev.* 42 (2013) 3913-3955.

[70] F. Hoffmann, M. Cornelius, J. Morell, M. Froeba, Silica-based mesoporous organic-inorganic hybrid materials, *Angew. Chem., Int. Ed.* 45 (2006) 3216-3251.

[71] B. Hatton, K. Landskron, W. Whitnall, D. Perovic, G.A. Ozin, Past, Present, and Future of Periodic Mesoporous Organosilicas－The PMOs, *Acc. Chem. Res.* 38 (2005) 305-312.

[72] H.L. Castricum, A. Sah, R. Kreiter, D.H.A. Blank, J.F. Vente, J.E. ten Elshof, Hybrid ceramic nanosieves: stabilizing nanopores with organic links, *Chem. Commun.* 2008, 1103-1105.

[73] H.L. Castricum, A. Sah, R. Kreiter, D.H.A. Blank, J.F. Vente, J.E. ten Elshof, Hydrothermally stable molecular separation membranes from organically linked silica, *J. Mater. Chem.* 18 (2008) 2150-2158.

[74] H.M. van Veen, M.D.A. Rietkerk, D.P. Shanahan, M.M.A. van Tuel, R. Kreiter, H.L. Castricum, J.E. ten Elshof, J.F. Vente, Pushing membrane stability boundaries with HybSi® pervaporation membranes, *J. Membr. Sci.* 380 (2011) 124-131.

[75] H.L. Castricum, G.G. Paradis, M.C. Mittelmeijer-Hazeleger, R. Kreiter, J.F. Vente, J.E. ten Elshof, Tailoring the Separation Behavior of Hybrid Organosilica Membranes by Adjusting the Structure of the Organic Bridging Group, *Adv. Func. Mater.* 21 (2011) 2319-2329.

[76] H. Qi, J. Han, N.P. Xu, H.J.M. Bouwmeester, Hybrid organic-inorganic microporous membranes with high hydrothermal stability for the separation of carbon dioxide, *ChemSusChem* 3 (2010) 1375-1378.

[77] H. Qi, J. Han, N.P. Xu, Effect of calcination temperature on carbon dioxide separation properties of a novel microporous hybrid silica membrane, *J. Membr. Sci.* 382 (2011) 231-237.

[78] R. Kreiter, M.D.A. Rietkerk, H.L. Castricum, H.M. vanVeen, J.E. tenElshof, J.F. Vente, Stable hybrid silica nanosieve membranes for the dehydration of lower alcohols, *ChemSusChem* 2 (2009) 158-160.

[79] M. Kanezashi, M. Kawano, T. Yoshioka, T. Tsuru, Organic-inorganic hybrid silica membranes with controlled silica network size for propylene/propane separation, *Ind. Eng. Chem. Res.* 51 (2012) 944-953.

[80] P.H.T. Ngamou, J.P. Overbeek, R. Kreiter, H.M. van Veen, J.F. Vente, I.M. Wienk, P.F. Cuperus, M. Creatore, Plasma-deposited hybrid silica membranes with a controlled retention of organic bridges, *J. Mater. Chem. A* 1 (2013) 5567-5576.

[81] M. Kanezashi, K. Yada, T. Yoshioka, T. Tsuru, Design of Silica Networks for Development of Highly Permeable Hydrogen Separation Membranes with Hydrothermal Stability, *J. Am. Chem. Soc.* 131 (2009) 414-415.

[82] M. Kanezashi, K. Yada, T. Yoshioka, T. Tsuru, Organic-inorganic hybrid silica membranes with controlled silica network size: preparation and gas permeation characteristics, *J. Membr. Sci.* 348 (2010) 310-318.

[83] T. Tsuru , T. Shibata, J.H. Wang, H.R. Lee, M. Kanezashi, T. Yoshioka, Pervaporation of acetic acid aqueous solutions by organosilica membranes, *J. Membr. Sci.* 421-422 (2012) 25-31.

[84] R. Xu, J.H. Wang, M. Kanezashi, T. Yoshioka, T. Tsuru, Development of Robust Organosilica Membranes for Reverse Osmosis, *Langmuir* 27 (2011) 13996-13999.

[85] R. Xu, J.H. Wang, M. Kanezashi, T. Yoshioka, T. Tsuru, Reverse osmosis performance of organosilica membranes and comparison with the pervaporation and gas permeation properties, *AIChE J.* 59 (2013) 1298-1307.

Chapter 2

Development of chlorine-resistant and hydrothermal stable organosilica membranes for reverse osmosis

2.1 Introduction

Today, reverse osmosis (RO) is the most commonly used technology for water purification in a variety of applications [1]. Polyamide thin-film composite (TFC) RO membranes currently dominate the commercial market. However, polyamide membranes are prone to biofouling, which severely diminishes filtration performance and shortens membrane lifetime. The membrane biofouling could be reduced or even stopped if the oxidizing agents such as chlorine could be added to the feed. Unfortunately, polyamide membranes are quite sensitive to chlorine, because the amide linkage in the membranes is susceptible to chlorine attack [2]. Numerous attempts have therefore been made to develop chlorine-resistant RO membranes, including elimination of chlorine-sensitive sites (amide nitrogen functions), modifications of the polymer structure and protection of chlorine-sensitive sites [3]. Although these approaches are successful in improving chlorine resistance, some of them require a complex fabrication process or show limited desalination performance. For example, RO membranes fabricated using sulfonated aromatic polyethersulfones as the active layer exhibit high chlorine resistance. However, salt rejection of the membrane (around 90%) merits further improvement [4]. Moreover, operation of RO at high temperatures is desired in many industrial applications, such as the food and textile industries [5,6]. Unfortunately, the maximum operating temperature for most polyamide membranes is normally below 55 °C [6,7]. Therefore, the development of robust RO membranes, which possess highly chlorine tolerance and hydrothermal stability, remains a challenge.

Inorganic membranes have superior thermal and chemical stability with great potential for application to water desalination. Zeolite membranes such as MFI-type (silicalite and ZSM-5) zeolite, have been tried for RO desalination because of their well-defined

sub-nanometer pore structures [8-10]. These zeolite membranes, however, typically require tedious synthesis procedures to form thin, defect-free film on porous substrates. Another promising candidate for RO desalination is amorphous microporous silica membranes with molecular sieving permeation characteristics. These sol-gel derived silica membranes with pore sizes that range from 2-5 Å have been successfully used for gas separation and pervaporation (PV) processes [11-13]. The main obstacle to the use of silica membranes for water purification is structural instability in the presence of water, due to hydrolysis of the siloxane bonds and rearrangement of the silanol groups, which eventually results in a loss of separation performance [14]. Some alternative approaches have been proposed to improve the hydrothermal stability of silica membranes, such as modification of silica matrix with metal oxides [15,16] or methyl ($-CH_3$) groups [17,18].

Recently, the durability of the membrane has been greatly improved by incorporating hydrolytically stable organic groups as integral bridging components into the nanoporous silica network [19-22]. Castricum et al. [19,20] developed the microporous membranes derived from co-condensation of bis(triethoxysilyl) ethane (BTESE) and methyltriethoxysilane for the dehydration of n-butanol by pervaporation, where the feed and the permeate were liquid and gas phases, respectively. These hybrid organosilica membranes could withstand long-term operation of up to 2 years at 150 °C. In a previous study, we proposed a design of the silica networks using BTESE as a silica precursor for development of a highly permeable hydrogen separation membrane with hydrothermal stability [21]. The resultant membranes showed approximately 1 order of magnitude higher H_2 permeance compared with previously reported silica membranes using tetraethoxysilane. Qi et al. [22] employed the Nb-doped BTESE membranes for enhanced CO_2 separation, and found that the membranes possessed high hydrothermal stability under exposure to steam at 200 °C. However, no work has reported the use of these organosilica materials for the preparation of RO membranes, which need immersing in chlorine-containing, more severe aqueous environments. In this study, we present the first report of the development of organosilica RO membranes using BTESE material as a single precursor. These membranes demonstrated excellent chlorine tolerance and exceptional hydrothermal stability, as well as superior molecular sieving properties.

2.2 Experimental

2.2.1 Synthesis of organosilica polymer sol

Organosilica membranes were prepared using the sol-gel technique via a polymeric route with $(EtO)_3Si\text{-}CH_2CH_2\text{-}Si(OEt)_3$ (BTESE) as a precursor. BTESE (Gelest, Inc.) sol was synthesized by hydrolysis and polymerization reaction of the precusor with water and HCl, in ethanol. A required amount of BTESE was mixed with ethanol. Subsequently, premixed water and HCl were added dropwise to the precursor mixture under continuous stirring. The molar composition of the reactants was BTESE/H_2O/HCl = 1: 60: 0.1, and the weight percent of BTESE was kept at 5.0 wt%. After stirring for 2 h at room temperature, the BTESE polymer sols were used to prepare the separation layer of the organosilica membranes.

2.2.2 Membrane preparation

The organosilica composite membranes were prepared as follows. First, α-alumina particles were coated onto the outer surface of α-alumina tubular supports (porosity: 50%, average pore size: 1μm, outside diameter: 10 mm, length: 100 mm), and were fired at 550 °C for 30 min. This procedure was repeated several times to remove large pores that might result in pinholes in the membrane. Then, SiO_2-ZrO_2 (molar ratio of Si/Zr=1/1) colloidal sols were coated onto the outer surface of the substrate and fired at 550 °C to form an intermediate layer. Finally, the BTESE sol was deposited onto the intermediate layer, followed by calcination at 100 or 300 °C in nitrogen for 30 min.

2.2.3 Instruments

The sizes of freshly prepared BTESE sol were measured by dynamic light scattering at 25 °C in a Malvern Zetasizer Nano (Malvern, ZEN3600). Membrane morphology and thickness were examined using scanning electron microscopy (JEOL, JCM-5700) with an acceleration voltage of 20 kV. Fourier transform infrared (FTIR) spectroscopy (Shimadzu, FTIR-8300) was performed to confirm the functional groups and chemical structures of the membrane. The samples for measurement were prepared by coating the polymer sols onto quartz plates, followed by firing at 300 °C for 30 min.

2.2.4 Reverse osmosis

The RO experiment was conducted in cross-flow filtration systems at a pressure of 1.15 MPa and a temperature of 25 °C unless otherwise specified. The feed solution, pressurized with a plunger pump, was introduced at an approximate flow of 30 mL/min to a RO cell, and the retentate was recycled back to the feed container. The concentrations of feed solutions were 2000 ppm of NaCl, and 500 ppm of $MgSO_4$, methanol, ethanol, isopropanol and glucose. RO Performance of the membrane was evaluated by water permeability and observed rejection. Water permeability, L_p, was calculated from the volume flux J_v divided by the effective transmembrane pressure, $\Delta P - \Delta\pi$ [Eq. (1)].

$$J_v = L_p(\Delta P - \Delta\pi) \quad (1)$$

Where L_p is the water permeability and, ΔP ($=P_1 - P_2$) and $\Delta\pi$ ($=\pi_1 - \pi_2$) are the differences in applied pressure and osmotic pressure, respectively.

For sufficiently dilute solutions, osmotic pressure difference, $\Delta\pi$, for NaCl was determined from the van′t Hoff equation [23]:

$$\Delta\pi \cong 2RT(C_f - C_p) \quad (2)$$

where R is the gas constant, T is the absolute temperature, C_p is the permeate concentration, and C_f is the feed concentration. The effect of concentration polarization was rationally ignored in this work due to low permeate flux.

An observed rejection, R_{obs}, was expressed as follows:

$$R_{obs} = (1 - C_p/C_f) \times 100\% \quad (3)$$

The concentrations of feed and permeate were measured with a conductivity meter (HORIBA, ES-51) for NaCl and a total organic carbon analyzer (Shimadzu, TOC-V_E) for neutral solutes.

2.2.5 Chlorine resistance test

The accelerated chlorine resistance test was performed using a commercial sodium hypochlorite solution (NaClO, active chlorine: 10%) at room temperature. The concentration of the fresh chlorine solution was 500 ppm and pH was adjusted to 7 using a 0.2 M KH_2PO_4 buffer solution. The membrane was periodically immersed in, and removed from a chlorine solution, which was placed in a sealed, stirred, dark glass bottle.

The RO performances were then tested after a thorough rinse with deionized water. The total exposure of the membrane to chlorine was expressed as the product of chlorine concentration (ppm) and exposure time (h).

2.3 Results and Discussion

2.3.1 Molecular sieving ability

The size distribution of BTESEthy sols with a silica concentration of 0.3 mol L^{-1} was determined by dynamic light scattering at 25 °C, as presented in Figure 2-1. The freshly synthesized BTESE sol showed a small mean radius of 2.9 nm and a narrow size distribution, which was desirable for preparing a thin, microporous separation layer [24].

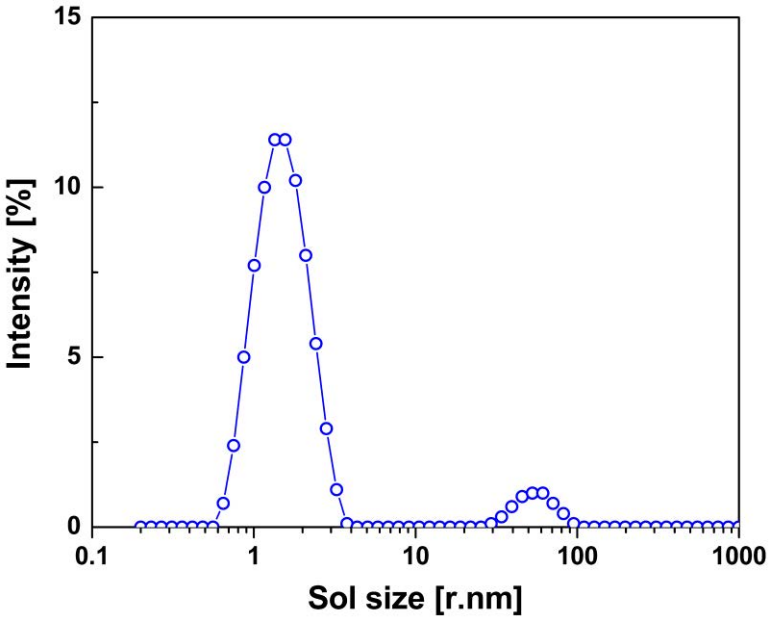

Figure 2-1. Size distribution of the BTESE sol determined by dynamic light scattering.

A hybrid silica layer was prepared by coating BTESE polymer sol onto the silica-zirconia intermediate layer, followed by drying and calcination at 100 °C or 300 °C. The scanning electron microscopy (SEM) image (Figure 2-2.) clearly showed that a crack-free, continuous separation layer was formed on top of the SiO_2-ZrO_2 intermediate layer, and the thin separation layer had a thickness of less than 300 nm.

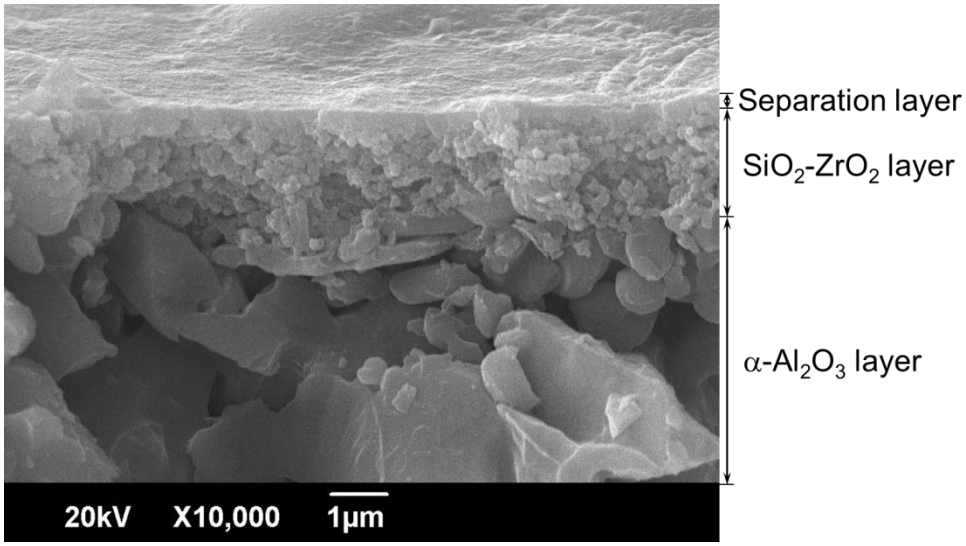

Figure 2-2. Cross-sectional SEM image of the BTESE-derived organosilica membrane.

The effective pore sizes of the BTESE membranes were evaluated by measuring rejections for a series of neutral solutes: methanol (MW 32), ethanol (46), isopropanol (60) and glucose (180). As shown in Figure 2-3, both BTESE-100 and BTESE-300 membranes, which were prepared by calcination at 100 and 300 °C, respectively, showed quite high rejection for neutral solutes of low molecular weight (isopropanol: 76.0% (BTESE100) and 95.6% (BTESE300); glucose: >98.5%). Compared with the commercial polyamide SW30HR membrane [25], the BTESE-300 membrane showed a higher rejection curve, indicating its small pore size and strong molecular sieving ability. Moreover, the pore size of the membranes could be tuned by calcination temperatures due to a sintering of the silica networks. A smaller pore size was obtained by calcination at a higher temperature, which resulted in a higher rejection and lower water permeability. It should be noted that the pore sizes of BTESE membranes, controlled by the size of the gel network, are smaller than the inorganic nanofiltration membranes, which are typically prepared by colloidal sol route [26].

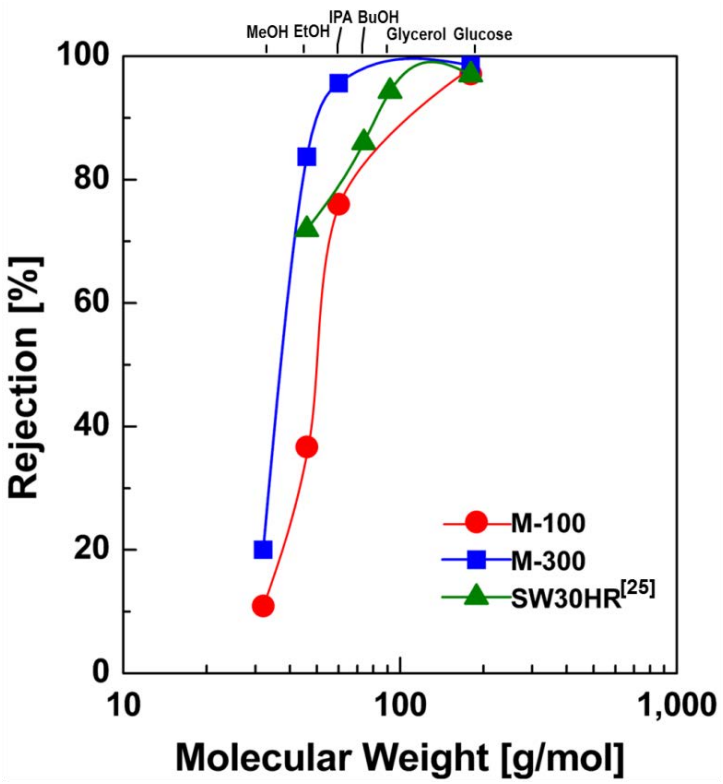

Figure 2-3. Comparison of the rejection of neutral solutes for BTESE membranes and the commercial polyamide RO membrane, SW30HR (Dow FilmTec).

2.3.2 Hydrothermal stability

Figure 2-4(a) shows the temperature dependence of water permeability and NaCl rejection. With an increase in feed temperature from 25 to 90 °C step-by-step, water permeability of the membrane was increased approximately 8-fold. Interestingly, a trade-off relationship between permeability and selectivity was not observed in this process. On the contrary, rejection increased slightly as temperature increased and reached 98.2% at 90 °C from an initial value of 97.3% at 25 °C. Subsequently, the temperature was kept at 90 °C for 180 min, and water permeability and rejection remained almost constant during this continuous RO process (Figure 2-4(b)). This suggested that the pores of the membranes were still sufficiently small to enable molecular sieving separation under such a high temperature. As the temperature returned to the starting level, water permeability reduced gradually to approximately the initial value and the membrane still maintained a high salt rejection (Figure 2-4(a)). These superior desalination properties were also evaluated in the pervaporation process, where the salt rejection remained stable

at the level of 99.9% during increase in temperature from 30 to 90 °C (Figure 2-5). Only a few polymeric nanofiltration membranes could withstand a temperature of 65 °C with no significant change in filtration performance [5,7], thereby indicating an outstanding hydrothermal stability and high reproducibility in temperature cycle of the BTESE membranes.

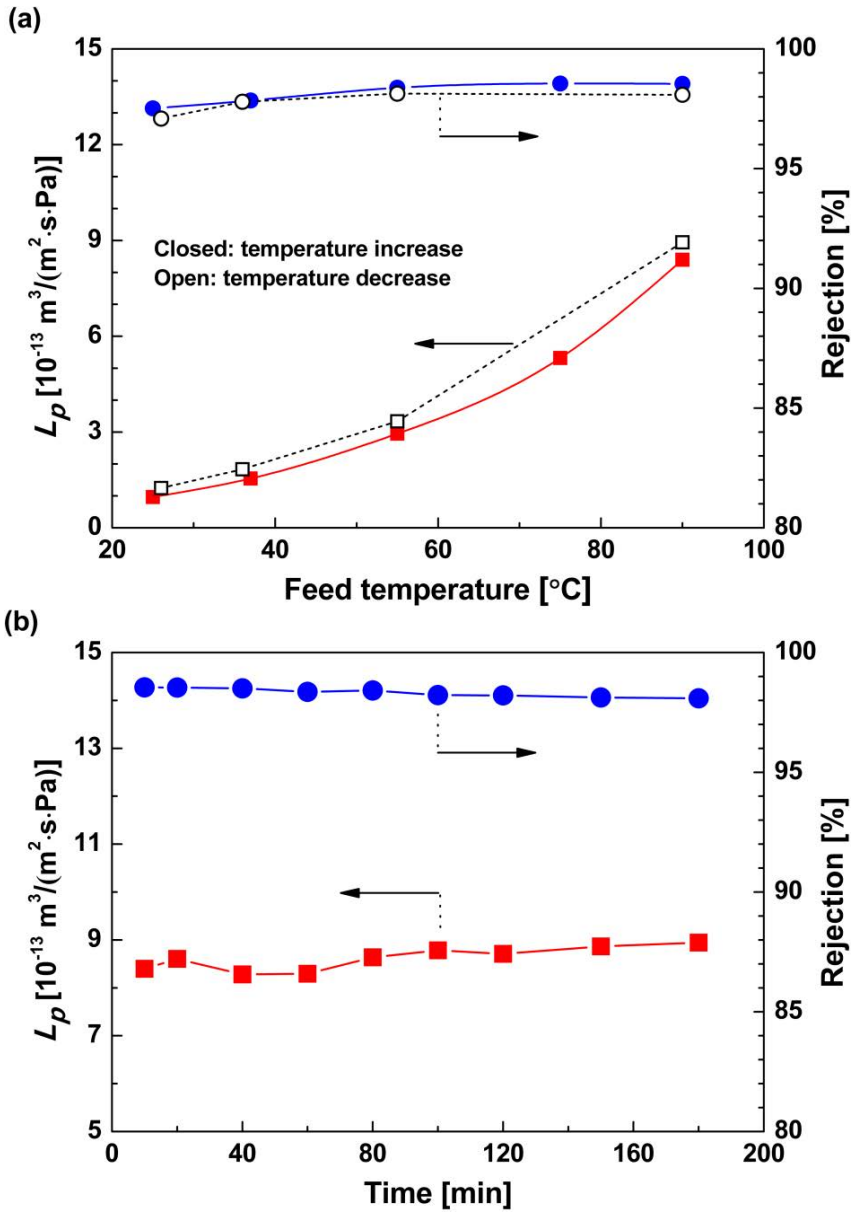

Figure 2-4. (a) Water permeability and NaCl rejection as a function of temperature cycles for the BTESE-300; (b) Water permeability and salt rejection as a function of operating time at a high temperature of 90 °C.

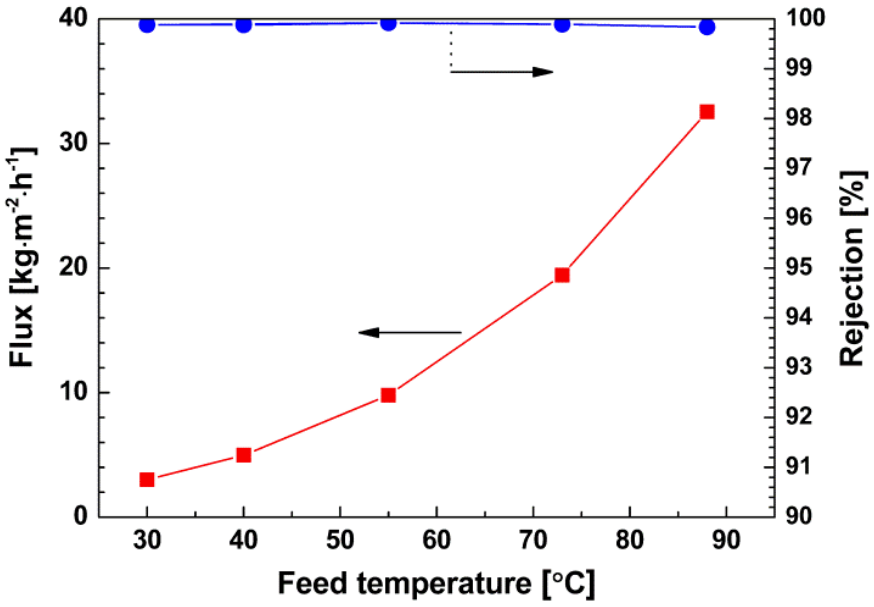

Figure 2-5. Temperature dependence of flux and rejection for the BTESE-300 membrane in a pervaporation process (2000ppm-NaCl; permeate pressure < 2 Torr).

2.3.3 Chlorine tolerance

An accelerated chlorine-resistance test was performed by soaking tests under various chlorine concentrations [27]. The BTESE membrane was periodically immersed in, and removed from, an aqueous solution of chlorine; the membrane performance was then tested after a thorough rinse with deionized water. The total exposure of the membrane to chlorine was expressed as the product of chlorine concentration (ppm) and exposure time (h). As presented in Figure 2-6(a), the BTESE membrane exhibited high chlorine resistance under a wide range of chlorine concentrations. Even after a total chlorine exposure of as high as 35,000 ppm·h (equivalent to 4 years of exposure to a chlorine level of 1 ppm), there was no significant change in either water permeability or NaCl rejection. The excellent chlorine stability can be attributed to the inherently stable hybrid network structure of BTESE membranes. The main body of this structure consists of chemically strong bonds such as Si-C and Si-O, so it inherently lacks the amide linkages that are sensitive to attack by aqueous chlorine. The chlorine-stable structure was further confirmed by FTIR analysis of the membrane before and after exposure to chlorine (Figure 2-6(b)). The formation of Si-O-Si was verified by the characteristic bands located

at 1033 and 1093 cm^{-1}, while the broad band in the region of 2875-2950 cm^{-1} was regarded as evidence of the presence of the bridging ethane groups [20,28]. After chlorine exposure from 5,000-35,000 ppm·h, these characteristic peaks did not change in the FTIR spectrum compared with that of the virgin membrane.

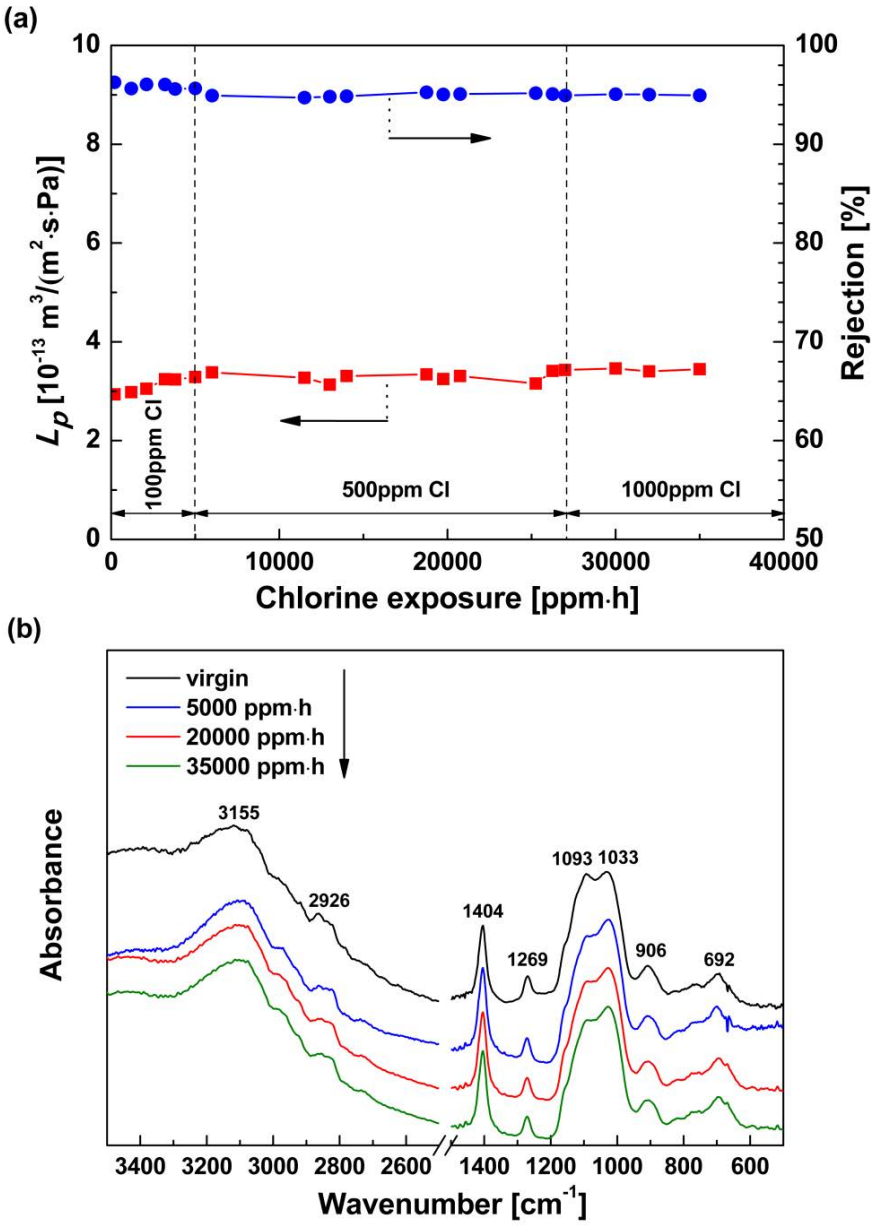

Figure 2-6. (a) Effect of chlorine exposure on rejection and water permeabilitiy of BTESE-300 under various chlorine concentrations. (feed concentration: 2000 ppm NaCl, pH: 7.0); (b) FTIR spectra of virgin and chlorine-exposed BTESE-300 membranes.

The molecular sieving ability of these membranes was further confirmed by a RO desalination process, and the separation performances were compared with those of inorganic, and polymeric RO membranes. As shown in Table 2-1, BTESE membranes showed higher water permeabilities than inorganic zeolite membranes such as ZSM-5 and silicalite. Even at a low pressure of 1.15 MPa, the BTESE-300 membrane almost completely (>95-99%) rejected the salts of NaCl (hydrated size of $Na^{+}_{(aq)}$: 0.72 nm and $Cl^{-}_{(aq)}$: 0.66 nm) [29] and $MgSO_4$ (hydrated size of $Mg^{2+}_{(aq)}$: 0.86 nm and $SO_4^{2-}{}_{(aq)}$: 0.76 nm) [30]. Although higher water permeabilities were reported for the aromatic polyamide membranes, SW30HR (seawater RO membrane) [25] and ES10 (low pressure RO membrane) [31], these commercial RO membranes suffered from poor resistance to aqueous chlorine, the concentration of which was normally recommended to be lower than 0.1 ppm [32]. BTESE membranes, however, had already exhibited high chlorine tolerance over a wide range of chlorine concentration (from 100 to 1000 ppm active chlorine), showing great promise as a new type of chlorine-resistant RO membrane materials.

Table 2-1. Comparison of performances of BTESE membranes and some typical RO membranes.

Membrane	Testing conditions	Flux [L/(m^{2}h)]	Water permeability [m^3/(m^2·s·Pa)]	Rejection [%]	Ref.
ZSM-5, Si/Al=50	25 °C, 2.76 MPa, 0.1M-NaCl	1.129	1.4×10^{-13}	92.9	[9]
Silicalite	25 °C, 2.76 MPa, 0.1M-NaCl	0.112	1.4×10^{-14}	90.6	[9]
Silicalite	25 °C, 2.76 MPa, 0.1M-NaCl	0.35	4.3×10^{-14}	99.4	[10]
BTESE-100	25 °C, 1.15 MPa, 2000 ppm-NaCl	/	$(2.8\text{-}3.2)\times10^{-13}$	93.8-94.4	This work
BTESE-300	25 °C, 1.15 MPa, 2000 ppm-NaCl	/	$(0.9\text{-}2.8)\times10^{-13}$	96.3-99.0	This work
	25 °C, 1.15 MPa, 500 ppm-$MgSO_4$	/	$(0.9\text{-}1.9)\times10^{-13}$	97.9-99.4	
SW30HR (FilmTec) [a]	21±1 °C, 2.76 MPa, 2000 ppm-NaCl	21±5	$(2.2\pm0.5)\times10^{-12}$	98.5±0.7	[25]
ES 10 (Nitto Denko) [b]	24 °C, 1.0 MPa, 104 ppm-NaCl	/	$(1.2\pm0.16)\times10^{-11}$	99.2	[31]

[a] Membrane type: aromatic polyamide; Free chlorine tolerance: <0.1 ppm. [b] Membrane type: aromatic polyamide; Residual chlorine: zero [33]

2.4 Conclusions

A robust microporous organosilica membrane has been developed for water purification by reverse osmosis (RO). The organosilica membranes derived from BTESE exhibit superior molecular sieving ability for neutral solutes of low molecular weight. Exceptional hydrothermal stability has been obtained due to the introduction of an inherently stable, organically bridged silica network structure, significantly broadening the applications of this silica-based membrane in water treatment. Furthermore, these organosilica RO membranes already show excellent chlorine stability under a wide range of chlorine concentrations; e.g., after a total chlorine exposure of up to 35,000 ppm·h, there was no obvious change in separation performance.

References

[1] L.F. Greenlee, D.F. Lawler, B.D. Freeman, B. Marrot, P. Moulin, Reverse osmosis desalination: Water sources, technology, and today's challenges, *Water Res.* 43 (2009) 2317-2348.

[2] G.D. Kang, C.J. Gao, W.D. Chen, X.M. Jie, Y.M. Cao, Q. Yuan, Study on hypochlorite degradation of aromatic polyamide reverse osmosis membrane, *J. Membr. Sci.* 300 (2007) 165-171.

[3] J. Glater, S.K. Hong, M. Elimelech, The search for a chorine-resistant reverse osmosis membrane, *Desalination* 95 (1994) 325-345.

[4] G.M. Geise, H.S. Lee, D.J. Miller, B.D. Freeman, J.E. McGrath, D.R. Paul, Water purification by membranes: The role of polymer science, *J. Polym. Sci., Part B: Polym. Phys.* 48 (2010) 1685-1718.

[5] M.J.H. Snow, D. de Winter, R. Buckingham, J. Campbell, J. Wagner, New techniques for extreme conditions: high temperature reverse osmosis and nanofiltration, *Desalination* 105 (1996) 57-61.

[6] M. Mänttäri, A. Pihlajamäki, E. Kaipainen, M. Nyström, Effect of temperature and membrane pre-treatment by pressure on the filtration properties of nanofiltration membranes, *Desalination* 145 (2002) 81-86.

[7] H. Saidani, N.B. Amar, J. Palmeri, A. Deratani, Interplay between the transport of solutes across nanofiltration membranes and the thermal properties of the thin active layer, *Langmuir* 26 (2010) 2574-2583.

[8] L.X. Li, J.H. Dong, T.M. Nenoff, R. Lee, Desalination by reverse osmosis using MFI zeolite membranes, *J. Membr. Sci.* 243 (2004) 401-404.

[9] L.X. Li, N. Liu, B. McPherson, R. Lee, Enhanced water permeation of reverse osmosis through MFI-type zeolite membranes with high aluminum contents, *Ind. Eng. Chem. Res.* 46 (2007) 1584-1589.

[10] N. Liu, L.X. Li, B. McPherson, R. Lee, Removal of organics from produced water by reverse osmosis using MFI-type zeolite membranes, *J. Membr. Sci.* 325 (2008) 357-361.

[11] R.M. de Vos, H. Verweij, High-selectivity, high-flux silica membranes for gas

separation, *Science* 279 (1998) 1710-1711.

[12] T. Yoshioka, E. Nakanishi, T. Tsuru, M. Asaeda, Experimental study of gas permeation through microporous silica membranes, *AIChE J.* 47 (2001) 2052-2063.

[13] J.E. ten Elshof, C.R. Abadal, J. Sekulić, S.R. Chowdhury, D.H.A. Blank, Transport mechanisms of water and organic solvents through microporous silica in the pervaporation of binary liquids, *Micropor. Mesopor. Mater.* 65 (2003) 197-208.

[14] M.C. Duke, J.C.D. da Costa, D.D. Do, P.G. Gray, G.Q. Lu, Hydrothermally robust molecular sieve silica for wet gas separation, *Adv. Funct. Mater.* 16 (2006) 1215-1220.

[15] R. Igi, T. Yoshioka, Y.H. Ikuhara, Y. Iwamoto, T. Tsuru, Characterization of Co-doped silica for improved hydrothermal stability and application to hydrogen separation membranes at high temperatures, *J. Am. Ceram. Soc.* 91 (2008) 2975-2981.

[16] V. Boffa, D.H.A. Blank, J.E. ten Elshof, Hydrothermal stability of microporous silica and niobia-silica membranes, *J. Membr. Sci.* 319 (2008) 256-263.

[17] R.M. de Vos, W.F. Maier, H. Verweij, Hydrophobic silica membranes for gas separation, *J. Membr. Sci.* 158 (1999) 277-288.

[18] J. Campaniello, C.W.R. Engelen, W.G. Haije, P.P.A.C. Pex, J.F. Vente, Long-term pervaporation performance of microporous methylated silica membranes, *Chem. Commun.* (2004) 834-835.

[19] H.L. Castricum, A. Sah, R. Kreiter, D.H.A. Blank, J.F. Vente, J.E. ten Elshof, Hybrid ceramic nanosieves: stabilizing nanopores with organic links, *Chem. Commun.* (2008) 1103-1105.

[20] H.L. Castricum, A. Sah, R. Kreiter, D.H.A. Blank, J.F. Vente, J.E. ten Elshof, Hydrothermally stable molecular separation membranes from organically linked silica, *J. Mater. Chem.* 18 (2008) 2150-2158.

[21] H. Qi, J. Han, N.P. Xu, H.J.M. Bouwmeester, Hybrid organic-inorganic microporous membranes with high hydrothermal stability for the separation of carbon dioxide, *ChemSusChem* 3 (2010) 1375-1378.

[22] M. Kanezashi, K. Yada, T. Yoshioka, T. Tsuru, Design of Silica Networks for Development of Highly Permeable Hydrogen Separation Membranes with Hydrothermal Stability, *J. Am. Chem. Soc.* 131 (2009) 414-415.

[23] M.L. Lind, D.E. Suk, T.V. Nguyen, E.M.V. Hoek, Tailoring the structure of thin film nanocomposite membranes to achieve seawater RO membrane performance, *Environ. Sci. Technol.* 44 (2010) 8230-8235.

[24] H.L. Castricum, G.G. Paradis, M.C. Mittelmeijer-Hazeleger, R. Kreiter, J.F. Vente, J.E. ten Elshof, Tailoring the Separation Behavior of Hybrid Organosilica Membranes by Adjusting the Structure of the Organic Bridging Group, Adv. Func. Mater. 21 (2011) 2319-2329.

[25] E.S. Hatakeyama, C.J. Gabriel, B.R. Wiesenauer, J.L. Lohr, M.J. Zhou, R.D. Noble, D.L. Gin, Water filtration performance of a lyotropic liquid crystal polymer membrane with uniform, sub-1-nm pores, *J. Membr. Sci.* 366 (2011) 62-72.

[26] T. Tsuru, Nano/subnano-tuning of porous ceramic membranes for molecular separation, *J. Sol-Gel Sci. Technol.* 46 (2008) 349-361.

[27] Y.N. Kwon, J.O. Leckie, Hypochlorite degradation of crosslinked polyamide membranes: II. Changes in hydrogen bonding behavior and performance, *J. Membr. Sci.* 282 (2006) 456-464.

[28] X.M. Guo, H.D. Guo, L.S. Fu, R.P. Deng, W. Chen, J. Feng, S. Dang, H.J. Zhang, Synthesis, spectroscopic properties and stabilities of ternary europium complex in SBA-15 and periodic mesoporous organosilica: A comparative study, *J. Phys. Chem. C* 113 (2009) 2603-2610.

[29] M.J. Zhou, P.R. Nemade, X.Y. Lu, X.H. Zeng, E.S. Hatakeyama, R.D. Noble, D.L. Gin, New type of membrane material for water desalination based on a cross-linked bicontinuous cubic lyotropic liquid crystal assembly, *J. Am. Chem. Soc.* 129 (2007) 9574-9575.

[30] L. Firdaous, F. Quéméneur, J.P. Schlumpf, J.P. Maléríat, Modification of the ionic composition of salt solutions by electrodialysis, *Desalination* 167 (2004) 397-402.

[31] Y. Kiso, K. Muroshige, T. Oguchi, M. Hirose, T. Ohara, T. Shintani, Pore radius estimation based on organic solute molecular shape and effects of pressure on pore radius for a reverse osmosis membrane, *J. Membr. Sci.* 369 (2011) 290-298.

[32] N. Soice, A. Maladono, D. Takigawa, A. Norman, W. Krantz, A. Greenberg, Oxidative degradation of polyamide reverse osmosis membranes: studies of molecular

model compounds and selected membranes, *J. Appl. Polym. Sci.* 90 (2003) 1173-1184.

[33] S.P. Nunes, K.V. Peinemann, Membrane materials and membrane preparation, In: *Membrane technology in the chemical industry*, S.P. Nunes, K.V. Peinemann (Eds.), Weinheim: Wiley-VCH (2001) 1-68.

Chapter 3

Reverse osmosis performance of organosilica membranes and comparison with the pervaporation and gas permeation properties

3.1 Introduction

The provision of clean, fresh water for continuously growing populations is a long-term challenge facing the world today. Reverse osmosis (RO) is now the leading technology for the production of drinking water from seawater and brackish water, and its popularity is expected to increase in the near future [1,2]. A typical RO membrane is composed of a crosslinked aromatic polyamide thin film on the surface of a microporous polysulfone support via interfacial polymerization. However, polyamide TFC membranes are quite susceptible to chlorine, which is widely used as a disinfectant in water treatment for preventing biological growth. Even a few parts per million of chlorine in feed water could lead to a significant membrane degradation [3]. Extensive efforts have, therefore, been devoted to developing new chlorine-resistant RO membranes, such as the recently exploited membranes based on cross-linked lyotropic liquid crystals and sulfonated block copolymers [4,5]. Although the resulting membranes exhibit excellent chlorine tolerance, some of them require complex fabrication process or show limited desalination performance. Amorphous microporous silica membranes are promising candidate for desalination owing to their excellent molecular sieving ability and good chemical resistance [6,7]. However, the low hydrothermal stability severely limited their application in water purification.

Some research groups have recently reported the utilization of organically bridged *bis*-silyl precursors for the fabrication of microporous organosilica membranes. The stability of the membranes has been greatly enhanced by incorporating organic linking groups between two silicon atoms [8-12]. Castricum et al. [8,9] developed microporous

membranes derived from co-condensation of 1,2-bis(triethoxysilyl)ethane (BTESE) and methyltriethoxysilane (MTES) for the dehydration of 95 wt.% n-butanol by PV. The results demonstrated that these organosilica membranes could withstand long-term operation of up to 2 years at 150 °C. BTESE and bis(triethoxysilyl)methane (BTESM) membranes showed a high degree of acid stability in long-term measurements at a pH value of ~2, and the membrane performance was reproducible for acidities that ranged from pH 2-8 [10]. Our research group proposed a "spacer" technique to control silica networks, using an organically linked alkoxide for the development of a highly permeable hydrogen separation membrane with hydrothermal stability. Organosilica membranes derived from BTESE showed approximately one order of magnitude higher H_2 permeance, compared with previously reported tetraethoxysilane (TEOS)-derived silica membranes [11,12].

A number of transport equations have been proposed for the transport mechanism. Gas permeation through porous membranes is governed by the viscous, Knudsen, surface diffusion, and molecular sieving mechanisms, depending on the pore size and the molecular size. One major transport theory for nonporous membranes is the solution-diffusion (SD) model in which the permeating molecules dissolve into a membrane, diffuse through it, and desorb from the other side. In liquid-phase separation, viscous flow is the accepted mechanism for the permeation of solvents in the range of MF to NF, while SD is the most widely accepted mechanism for transport in RO. The SD model was also applied to PV. Although the SD model has been used successfully for RO, PV and gas separation (GS), different types of SD equations have been used and the relationship among them is not clear. Several research groups have proposed a generalized SD model [13-16]. The more general equations provide a good description of transport behavior in all of these processes, and can be compared with each other. The generalized SD mode is valuable in predicting the flux in gas separation, PV and RO. However, only a limited number of papers have discussed the generalized SD model and examined its applicability.

Our most recent study examined the possibility of using BTESE-derived organosilica membranes to desalinate water by RO. These organosilica membranes exhibited

exceptional chlorine tolerance and hydrothermal stability in our preliminary study, showing great promise as a new type of robust RO membrane materials [17]. For a better understanding of the permeation properties of this membrane, more detail is needed regarding the factors that affect membrane performance. In this paper, we present the results of a series of studies including the effects of solute species, calcination temperatures and operational variables on membrane performances. Moreover, 3 different membrane processes, including RO, PV and gas permeation, were performed using the same organosilica membrane to study the transport properties in each process, and a quantitative comparison of water permeances in PV and RO was made by using generalized SD equations.

3.2 Theory

3.2.1 Conventional solution-diffusion model

The solution-diffusion model is widely accepted for the explanation of transport behavior in RO, PV, and gas permeation [13,14]. The schema of permeation in a solution-diffusion film are schematically presented with symbols in Figure 3-1 together with symbols.

In the case of RO, the volume flux of water, J_v, is expressed as follows.

$$J_v = L_p(\Delta P - \Delta\pi), \quad (1)$$

where L_p is the water permeability and, ΔP ($=P_1 - P_2$) and $\Delta\pi$ ($=\pi_1 - \pi_2$) are the differences in applied pressure and osmotic pressure, respectively. The osmotic pressure, π, is given by

$$\pi = \phi C_s RT \quad (2)$$

where ϕ is the osmotic coefficient, C_s is the molar concentration of ions, R is the gas constant, and T is the absolute temperature. For dilute solutions, ϕ is reasonably assumed to be unity for the Van′t Hoff equation. Similarly, according to the SD model, a simplified expression for salt flux, J_s, is given by

$$J_s = B(C_f - C_p) \quad (3)$$

where B is the salt permeability and, C_f and C_p are the salt concentrations in the feed and

permeate, respectively.

Flux in PV can be expressed with permeance in PV, P_{PV}, and vapor pressure difference across a membrane, ($P_{sat} - P_2$), since the driving force of the permeating molecules is the vapor pressure, $P_{sat} = P_1$. When the vapor pressure in the permeate P_2 is assumed to be zero, permeate flux can be expressed as follows.

$$J = P_{PV}\left(P_{sat} - P_2\right) = P_{PV} \cdot P_{sat} \tag{4}$$

a similar equation is conventionally applied to gas permeation, using pressure difference between the feed and permeate sides, as follows.

$$J = P_{GS}\left(P_1 - P_2\right) \tag{5}$$

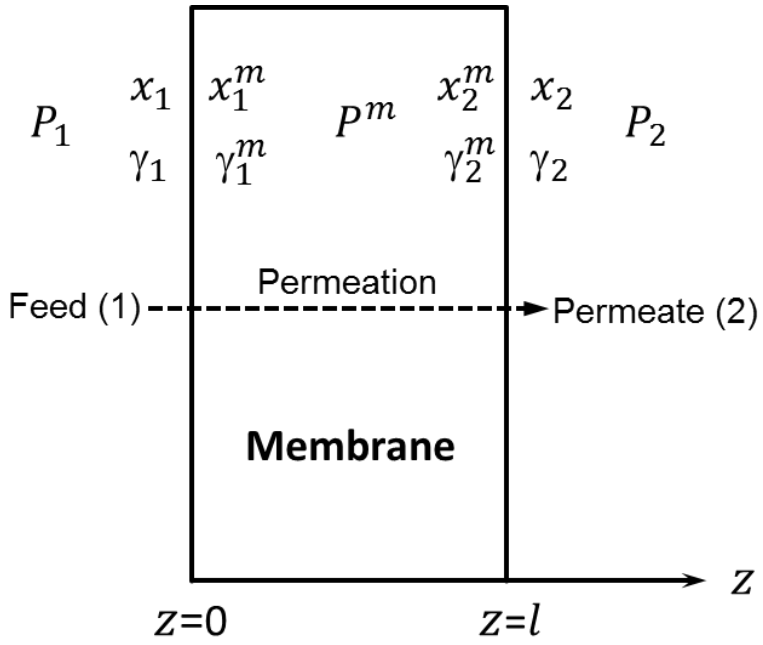

Figure 3-1. Schematic illustration of permeation through a solution-diffusion membrane.

3.2.2 Generalized solution-diffusion model

The generalized SD model assumes that the diffusion coefficient, D, activity coefficient, γ^m, and total molar concentration, C^m, are constant; the pressure within a membrane, P^m, is uniform and equal to upstream pressure, P_1; and, the molar volume of a permeant, $\bar{v}$, is constant, and is not dependent on the pressure. According to the SD model,

permeating molar flux is obtained as the product of diffusivity & concentration difference in the membrane and formulated for RO & PV as follows.

$$\text{RO:}\quad J = \frac{DC^m}{\ell}\left(\frac{\gamma_1 x_1}{\gamma^m} - \frac{\gamma_2 x_2}{\gamma^m}\exp\left(\frac{\bar{v}}{RT}\left(P_2 - P_1\right)\right)\right) \tag{6}$$

The osmotic pressure, π, is defined, using activity, a (= γx), as follows.

$$\pi = \frac{RT}{\bar{v}}\ln(a) = \frac{RT}{\bar{v}}\ln(\gamma x) \tag{7}$$

Thus, Eqs. (6) and (7) can be combined to yield

$$\begin{aligned} J &= \frac{DC^m}{\ell}\left(\frac{\gamma_1 x_1}{\gamma^m} - \frac{\gamma_1 x_1}{\gamma^m}\exp\left(\frac{\bar{v}}{RT}\left(\pi_1 - \pi_2\right)\right)\exp\left(\frac{\bar{v}}{RT}\left(P_2 - P_1\right)\right)\right) \\ &= \frac{DC^m}{\gamma^m \ell}\gamma_1 x_1\left(1 - \exp\left(\frac{\bar{v}}{RT}\left(\Delta P - \Delta\pi\right)\right)\right) \end{aligned} \tag{8}$$

Under the RO test conditions, ΔP (=$P_1 - P_2$) = 1.15×10^6 Pa, $\Delta\pi$ (=$\pi_1 - \pi_2$) ≈ 0.17×10^6 Pa, T = 298-363K, and $\bar{v}$ = 18×10^{-6} m^3/mol; the term $\bar{v}\left(\Delta P - \Delta\pi\right)/RT$ is from 5.8×10^{-3} to 7.1×10^{-3}. Since this term is very small, the simplification 1−exp (x) → x as x → 0 can be applied, and a very good approximation of Eq. (8) can be written as follows.

$$J = \frac{DC^m}{\gamma^m \ell}\gamma_1 x_1 \frac{\bar{v}}{RT}\left(\Delta P - \Delta\pi\right) \tag{9}$$

$$\text{PV:}\quad J = \frac{DC^m}{\ell}\left(\frac{\gamma_1 x_1}{\gamma^m} - \frac{P_2 x_2}{\gamma^m P_{sat}}\exp\left(\frac{\bar{v}}{RT}\left(P_{sat} - P_1\right)\right)\right) \tag{10}$$

Under the PV test conditions, $\bar{v}$ = 18×10^{-6} m^3/mol, P_1 = 10^5 Pa, T = 363K, P_{sat} ≈ 0.7×10^5 Pa; the term $\exp\left(\bar{v}\left(P_{sat} - P_1\right)/RT\right) \approx 1$. Eq. (10) can be written as

$$J = \frac{DC^m}{\ell}\left(\frac{\gamma_1 x_1}{\gamma^m} - \frac{P_2 x_2}{\gamma^m P_{sat}}\right) = \frac{DC^m}{\gamma^m \ell}\left(\gamma_1 x_1 - \frac{P_2 x_2}{P_{sat}}\right) \tag{11}$$

Therefore, the permeance in PV, combining Eqs. (4) and (11), can be expressed as follows.

$$P_{PV} = \frac{DC^m \gamma_1 x_1}{\gamma^m \ell}\frac{1}{P_{sat}} \tag{12}$$

While the permeance in RO, P_{RO}, is defined on a molar basis, a comparison of Eqs. (1)

and (9) is, as follows:

$$P_{RO} = \frac{L_p}{\bar{v}} = \frac{DC^m \gamma_1 x_1}{\gamma^m \ell} \frac{\bar{v}}{RT} \tag{13}$$

Eqs. (12) and (13) give the conversion relationship between conventional and generalized SD model, and a quantitative comparison of permeance in RO and PV.

3.3 Experimental

3.3.1 Synthesis of BTESE-derived organosilica sol

BTESE polymer sols were synthesized by the hydrolysis and polymerization reaction of BTESE (Gelest, Inc.) in ethanol. The detailed procedure has been described elsewhere [17]. Briefly, BTESE was mixed at the molar ratio of BTESE/H_2O/HCl = 1/60/0.1 with the equivalent weight of BTESE kept at 5.0 wt%. After stirring for 2 h at room temperature, the BTESE polymer sols were used to prepare the separation layer of the organosilica membranes.

3.3.2 Membrane fabrication and characterization

Tubular α-alumina microfiltration membranes (porosity, 50%; average pore size, 1μm; outside diameter, 10 mm; length, 100 mm) were used as the supports. The detailed procedure for synthesis of SiO_2-ZrO_2 colloidal sols has been described elsewhere [18]. First, two kinds of α-alumina particles (average particle size is 1.9 μm and 0.2 μm, respectively) were deposited onto the outer surface of the support using the SiO_2-ZrO_2 colloidal sol (2 wt.%) as a binder, and the substrate was fired at 550 °C for 30 min. This procedure was repeated 6 times to form the particle layer. Then, SiO_2-ZrO_2 (molar ratio of Si/Zr = 1/1, 0.5 wt.%) colloidal sols were coated on the particle layer by the hot-coating methods, where the substrate was first heated up to around 180 °C before coating, followed by quickly contacting the substrate with a wet cloth with the SiO_2-ZrO_2 sols. Subsequently, the substrate was fired at 550 °C for 15min in air. This hot-coating and calcination procedures were repeated approximately 6 times to form the intermediate layer. Finally, the BTESE polymer sol was deposited onto the intermediate layer by wipe

coating using a wet cloth with the BTESE sol (0.5 wt.%), followed by a flash calcination in air at 100 or 300 °C for 20 min. After preparation, the membrane morphology and thickness were examined using a scanning electron microscope (SEM) (JCM-5700, JEOL) with an acceleration voltage of 20 kV.

3.3.3 Reverse osmosis, gas permeation and pervaporation experiments

Figure 3-2 shows the schematic diagram of the RO experimental apparatus. The membrane was installed vertically inside a RO cell. The feed solution, pressurized with a plunger pump in the range of 0.5 to 1.5 MPa, was vigorously agitated using a magnetic stirrer at 600 rpm in the cell, and the retentate was recycled back to the feed container at an approximate flow of 30 mL/min. The permeate stream was maintained at atmospheric pressure, and collected using a micro tube pump. The temperature of the feed solution was controlled at 25-90 °C using a water bath. The concentrations of solute in the feed (C_f) and permeate (C_p) were measured with a conductivity meter (HORIBA, ES-51) for electrolytes and a total organic carbon analyzer (Shimadzu, TOC-V_E) for neutral solutes. The observed rejection, R_{obs}, is expressed as follows:

$$R_{obs} = (1 - C_p/C_f) \times 100\ \% \quad (14)$$

The effect of concentration polarization was rationally ignored in this study due to the low permeate flux. Each RO test lasted for at least 3 h to confirm a steady water flux and rejection, and then the permeate sample was collected at a predetermined time interval. Each experimental data point reported in this paper is the average value of 3 samples. The variation in water permeability and observed rejection during each measurement was found to be less than 3.6% and 0.7%, respectively.

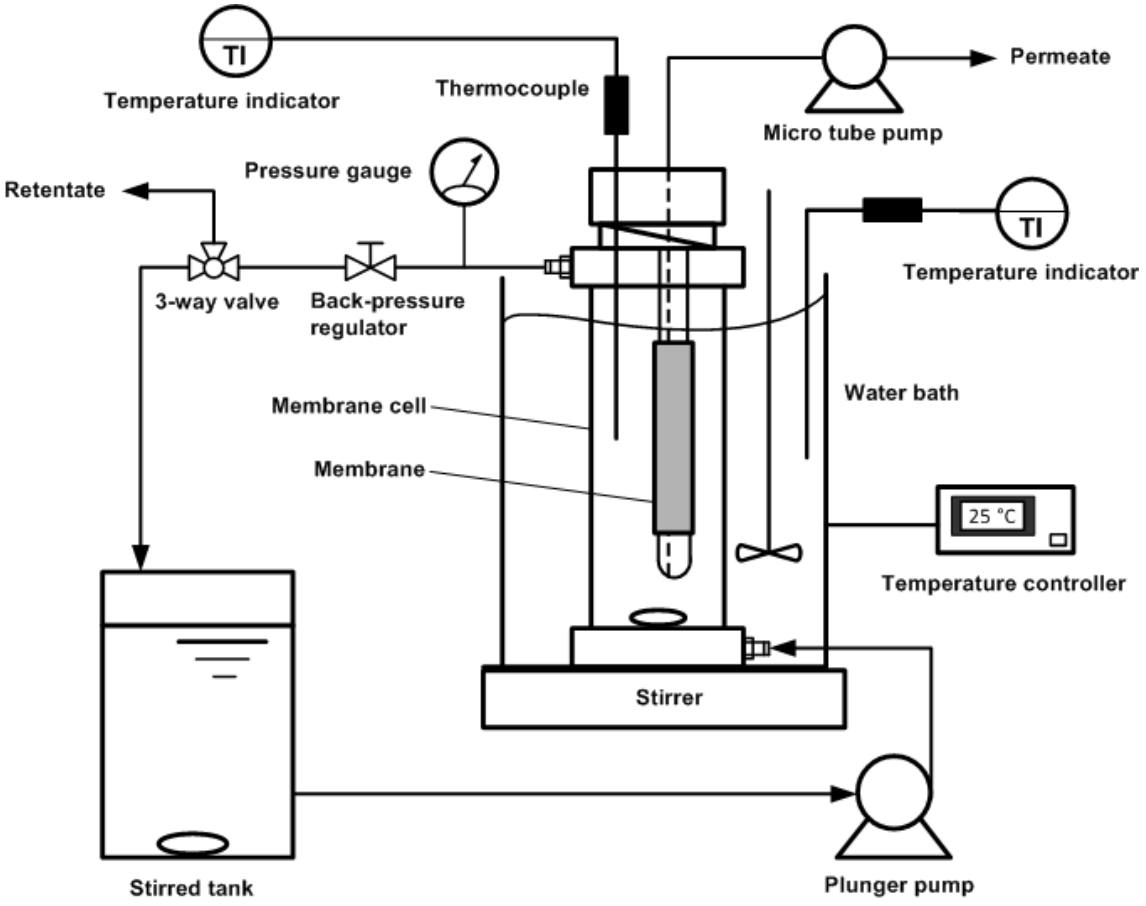

Figure 3-2. Schematic diagram of the reverse osmosis experiment.

Gas permeation measurements were performed at 200 °C using a testing apparatus as shown in Figure 3-3. A high-purity single component of He, H_2, CO_2, N_2, CH_4, C_3H_8 and SF_6 was used in the experiment. Prior to the measurement, the membrane was first pretreated for 8-10 h in a He flow of 50 mL/min at 200 °C to remove the adsorbed water from the membrane pores. The permeate side was kept at atmospheric pressure, and the pressure drop through the membrane was maintained at 1 bar. The permeation rate was measured using a soap-film flow meter.

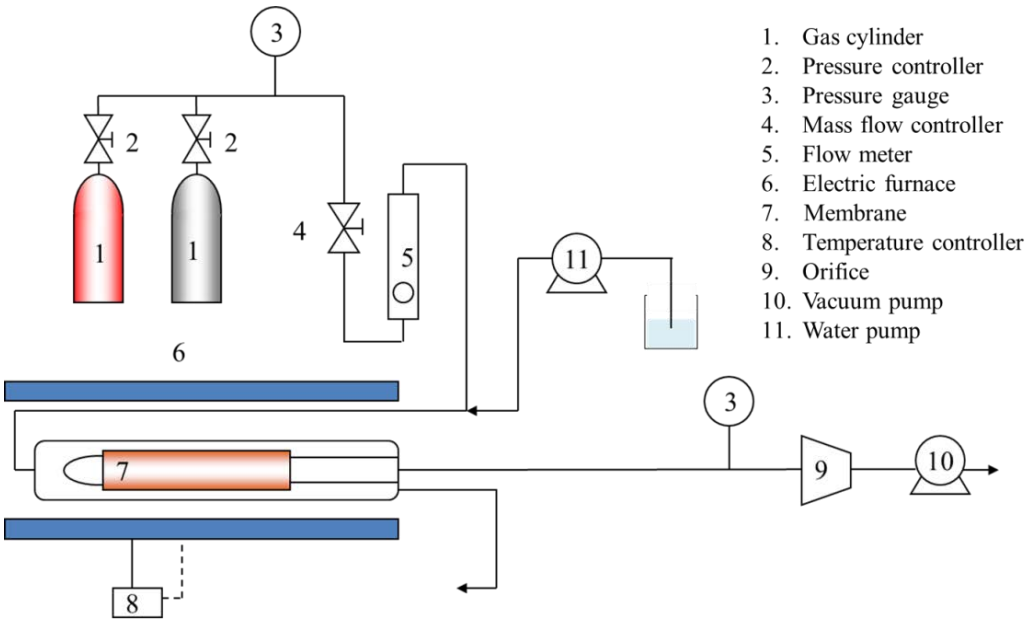

Figure 3-3. Schematic diagram of experimental apparatus for single gas permeation measurement.

The PV experiments were carried out using a typical PV testing apparatus as previously reported [18]. The membrane was dipped into a 2000 ppm NaCl solution, which was circulated vigorously to minimize the effect of concentration polarization on the membrane surface. The pressure on the feed side was maintained at atmospheric pressure, whereas the permeate side was evacuated to less than 300 Pa using a vacuum pump. The permeate was collected in liquid nitrogen cold traps during a predetermined time interval.

3.4 Results and discussion

3.4.1 Membrane morphology and reverse osmosis performance

A hybrid organosilica layer was prepared by coating BTESE polymer sol onto the silica-zirconia intermediate layer, followed by drying and calcination at either 100 or 300 °C. Figure 3-4 presents the SEM image of a cross-section of a BTESE-derived organosilica membrane. As shown in this micrograph, a crack-free, continuous separation layer formed on the top of the SiO_2-ZrO_2 intermediate layer, and the thin separation layer had a thickness of approximate 300 nm.

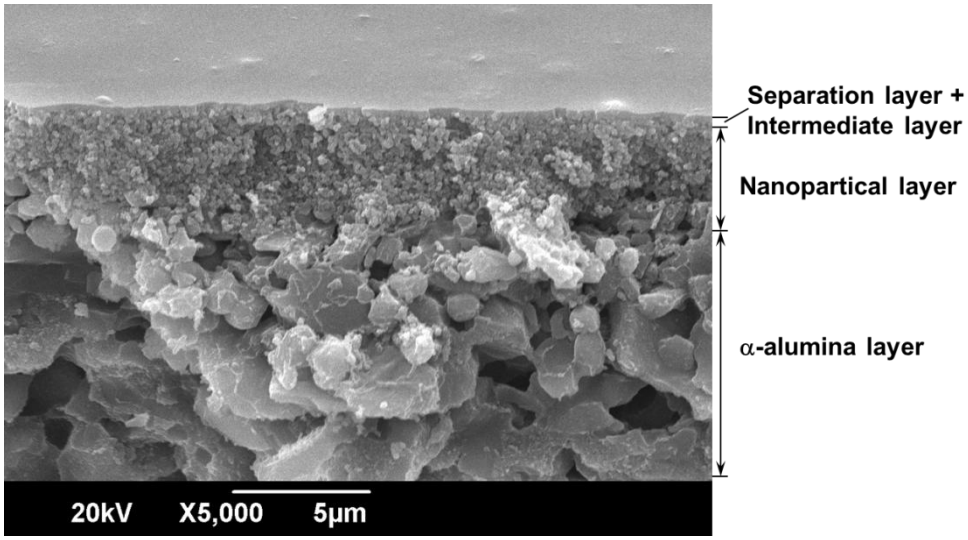

Figure 3-4. Cross-sectional SEM image of BTESE-derived organosilica membrane.

The observed rejection and water permeability of the membranes were measured at 25 °C and 1.15 MPa, using a series of electrolytes and neutral solutes of different sizes: NaCl (hydrated size of $Na^{+}_{(aq)}$: 0.72 nm, and $Cl^{-}_{(aq)}$: 0.66 nm); $MgSO_4$ ($Mg^{2+}_{(aq)}$: 0.86 nm, and $SO_4^{2-}{}_{(aq)}$: 0.76 nm) [19]; ethanol (Stokes diameter: 0.4 nm); isopropanol (IPA, 0.48 nm); and, glucose (0.73 nm) [20]. Figure 3-5 shows the RO performance of a BTESE-derived organosilica membrane for these probe molecules of different sizes. At a pressure of 1.15 MPa, the membrane calcined at 300 °C (BTESE-300) almost completely rejected electrolytes (>98%) and neutral solutes of low molecular weight (IPA, 96.9%; glucose, 98.3%), approximately the same level of rejections as seawater desalination membranes. The incomplete rejection of glucose might be due to the pore size distribution of amorphous silica networks. The preparation procedure will be further optimized to obtain a sharp pore size distribution. However, ethanol afforded only moderate rejection (～ 76.0%), because the Stokes diameter of ethanol is smaller than other neutral molecules (IPA, glucose). Its superior capacity for rejection of salts and small organic molecules demonstrated that the BTESE membrane showed great promise as a RO membrane. In addition, the neutral solutes with a larger Stokes diameter showed a higher rejection in the RO process. Since the Donnan effect was ineffective on these neutral solutes, this observation led us to the tentative conclusion that the transport mechanism for the BTESE membrane was primarily based on the molecular sieving effect. This assumption will be

further discussed in the following sections.

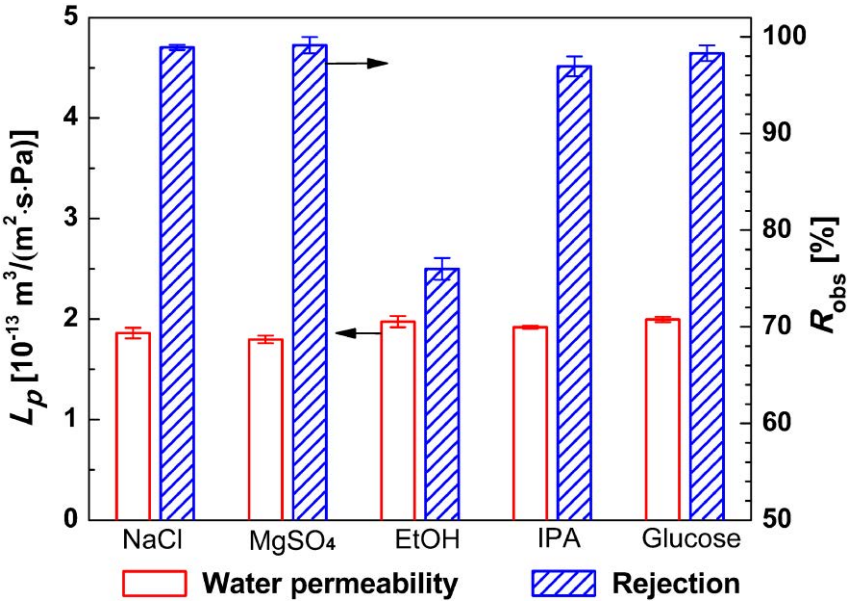

Figure 3-5. Rejection and water permeability of the BTESE-300 membrane for 5 types of probe molecules at a temperature of 25 °C and a pressure of 1.15 MPa.

3.4.2 Effects of operating pressure and feed concentration

Figure 3-6 shows the effect of feed pressure on permeation of water and salt, using two organosilica membranes with different calcination temperatures. Both the water flux (J_v) and the salt rejection (R_{obs}) of BTESE-100 and BTESE-300 membranes increased continuously as operating pressure increased from 0.7 to 1.5 MPa (Figure 3-6(a)). The water permeability (L_p) and salt permeability (B) of the two membranes, obtained by Eqs. (1) and (3), were almost constant (Figure 3-6(b)). This can be explained by the conventional SD model described by the simplified Eqs. (1) through (3). The transmembrane pressure difference ($\Delta P - \Delta\pi$) is the driving force for water transport across the membrane. Therefore, the water flux increased linearly with increasing the operating pressure, and the water permeability remained almost constant throughout the operating pressure range. However, the driving force for ion permeation through the membrane, according to Eq. (3), is the transmembrane concentration gradient. In other words, the salt flux (J_s) is independent of the operating pressure. Therefore, the salt permeability (B) was

nearly constant, as shown in Figure 3-6(b). Eventually, the salt rejection increased gradually with feed pressure due to the enhanced water permeation (Figure 3-6(a)). Using the relationships of water and salt permeability, the theoretical salt rejection of the SD model can be expressed as follows [21].

$$R = \frac{L_p(\Delta P - \Delta\pi)}{L_p(\Delta P - \Delta\pi) + B} \times 100\% \tag{15}$$

Eq. (15) relates salt rejection to intrinsic transport properties of the membrane (L_p and B), and the operating conditions (ΔP and $\Delta\pi$). The dotted curves in Figure 3-6(a) were calculated using averages for L_p and B, as shown in Figure 3-6(b), and showed excellent agreement with experimentally obtained flux, J_v, and rejection, R_{obs}.

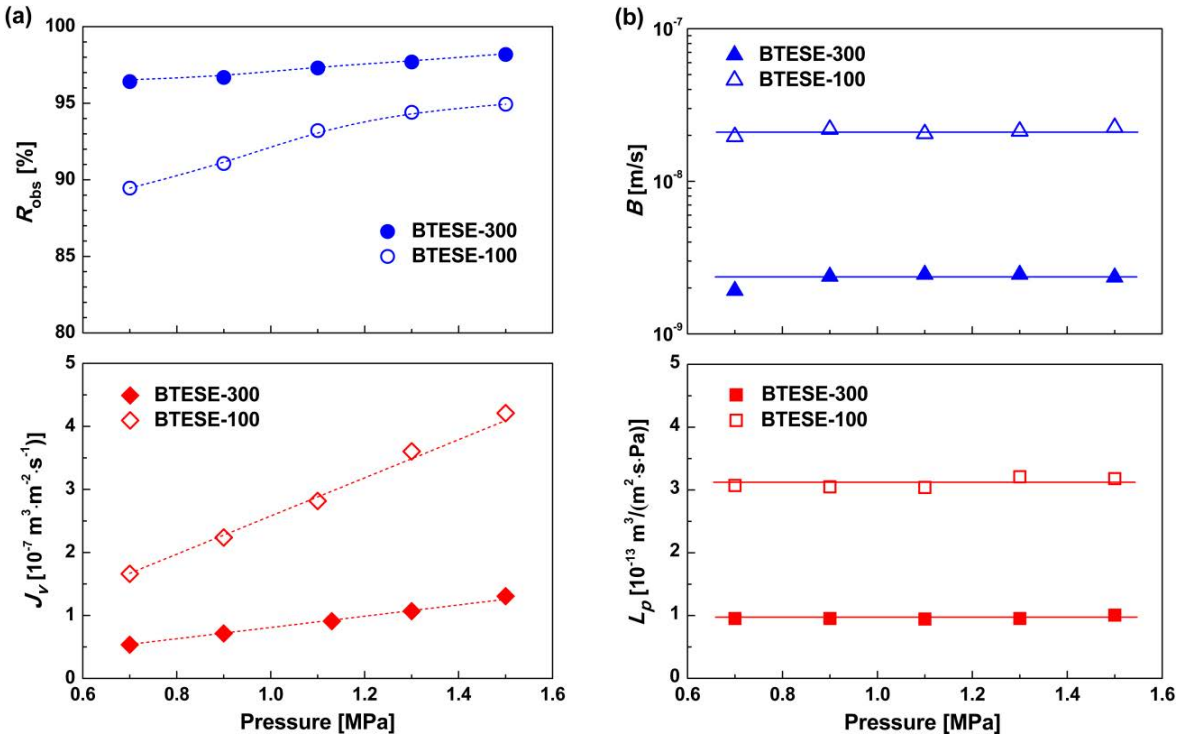

Figure 3-6. Effect of operating pressure on water flux and salt rejection (a), and on water permeability and salt permeability (b) at 25 °C and 2000-ppm NaCl feed (Dotted curves are calculated using Eqs. (1), (2), (3), and (15) with membrane parameters L_p and B).

It should be noted that the BTESE-300 membrane exhibited higher rejection and lower water flux than the BTESE-100 membrane. This difference in the separation performance can be attributed to effective pore size variation of the organosilica network that occurred

in the calcination process. Calcination at higher temperatures accelerated the condensation reaction of silanol groups (dehydroxylation) on the network and the formation of siloxane bonds, thus resulting in a denser silica network structure [22,23].

The desalination performance of the BTESE-300 membrane was evaluated using NaCl concentrations varied from 500 to 10000 ppm. The filtration performances of these NaCl solutions at a constant pressure of 1.5 MPa are illustrated in Figure 3-7. Increasing the feed concentration led to a decrease in transmembrane pressure difference ($\Delta P - \Delta\pi$) because of the increased osmotic pressure (π) at high ion concentrations (at 25 °C, π = 0.04 MPa and π = 0.85 MPa, respectively, for 500-ppm and 10000-ppm NaCl solution). Consequently, at a constant operating pressure, the water flux fell linearly from 1.9×10^{-7} to 1.0×10^{-7} $m^3/(m^2\cdot s)$ in the concentration range, while the water permeability was nearly constant at approximately 1.3×10^{-13} $m^3/(m^2\cdot s\cdot Pa)$. Since the concentration gradient across the membrane is the driving force for ion permeation, salt flux increased linearly with feed concentration, and salt permeability at any concentration, remained relatively constant. Ultimately, as shown in Figure 3-7, the salt rejection decreased slightly as the concentration increased, which is in agreement with Eq. (15). Meanwhile, the salt permeability clearly did not show obvious changes. As is well known, the rejection behavior of the solutes in NF and RO is governed by the charge (Donnan) effect and/or steric (sieving) effect. If the charge effect plays a major role, an increase in the ion concentrations should result in a significant drop in salt rejection, which is often observed for many nanofiltration membranes [24]. Therefore, the observation that the salt permeability remained approximately constant indicates that the influence of charge-charge interactions between the ions and micropores of silica networks has only a minor effect on the transport of ions through the membrane. This provides additional evidence that the transport mechanism for the BTESE RO membranes is governed by the molecular sieving effect.

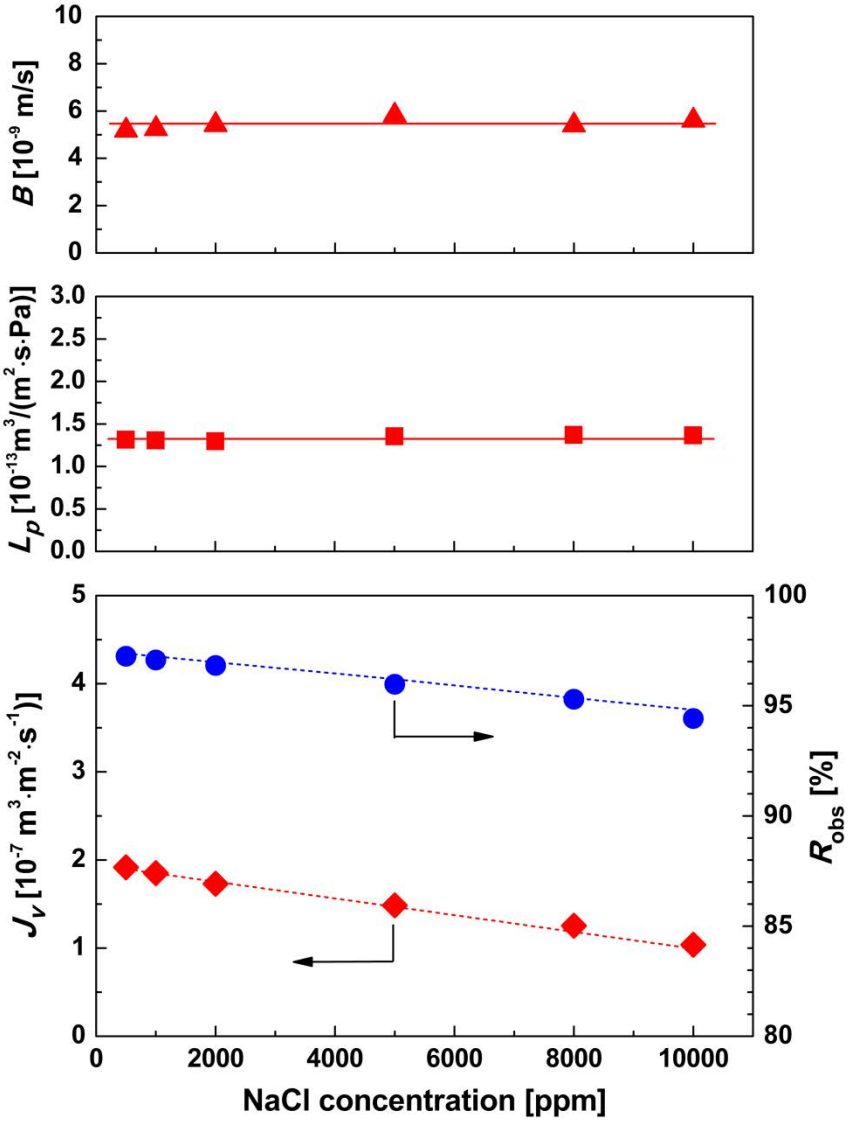

Figure 3-7. Influence of NaCl concentration on permeation performances for the BTESE-300 membrane at 25 °C and 1.5 MPa (Dotted curves are calculated using Eqs. (1), (2), (3), and (15) with membrane parameters L_p and B).

3.4.3 Temperature dependence of RO performance

The water permeation performance of the membrane as a function of temperature is shown in Figure 3-8. As temperature increased from 25 to 55 °C, the water permeability of two BTESE membranes with different calcination temperatures increased 2- to 3-fold. According to the viscous flow mechanism, the permeability through porous membranes (effective pore size, r_p; effective membrane thickness, Δx; and porosity, A_k) is formulated as the following Hagen-Poiseuille equation [25]:

$$L_p\mu = r_p^2 A_k / 8\Delta x \quad (16)$$

If the transport mechanism through these micropores is the viscous flow mechanism, the viscosity-corrected water permeability, $L_p\mu$, defined as L_p multiplied by the viscosity of bulk water, (μ), should be constant irrespective of the permeation temperature, since the structural parameters on the right side of Eq. (16) are considered to be constant. As shown in Figure 3-8, the $L_p\mu$ of the two kinds of BTESE membranes was not constant and clearly increased with temperature. Our group and others have observed a similar temperature dependency for inorganic NF membranes in water and many different organic solvents systems [25-27]. Figure 3-9 shows $L_p\mu$ normalized with that at 25 °C for the BTESE RO membranes in a comparison with the previous SiO_2-ZrO_2 and TiO_2 NF membranes. The normalized $L_p\mu$ should be unity if the water permeation obeys the viscous flow mechanism. However, it is obvious that the normalized $L_p\mu$ increased as temperature increased, and the slope increased on the order of BTESE-300>BTESE-100>SiO_2-ZrO_2>TiO_2, which is in accordance with the order of MWCO values (Table 3-1). The membrane with smaller pores showed a larger deviation from the viscous flow behavior. The dependency on permeation temperature can be evaluated by the Arrhenius equation with the activation energy of permeability. Table 3-1 summarizes the observed activation energies of L_p and $L_p\mu$ for BTESE, SiO_2-ZrO_2 and TiO_2 membranes. Clearly, the membrane with the smaller pore size showed larger activation energy. Meanwhile, the observed activation energies were larger than the corresponding viscosity activation energy, which again suggests that the water permeation through BTESE-derived organosilica membranes was different from viscous flow.

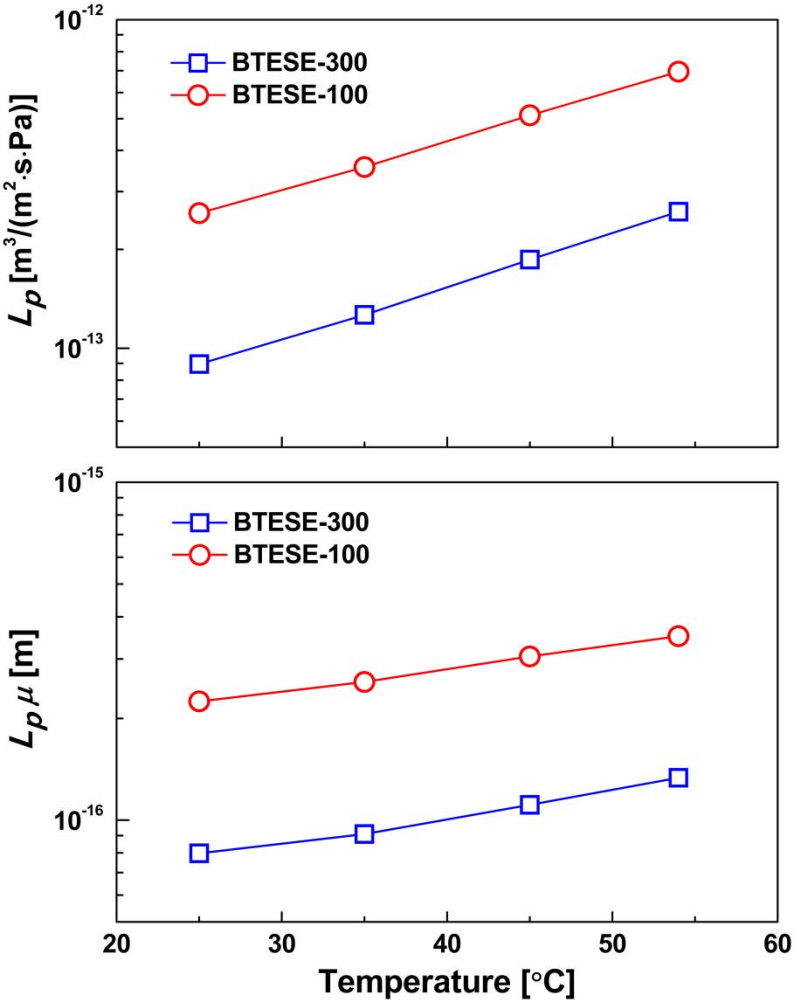

Figure 3-8. Temperature dependence of water permeability, L_p, and viscosity-corrected water permeability, $L_p\mu$, for BTESE-300 and BTESE-100 membranes.

Table 3-1. Activation Energy of L_p and $L_p\mu$ for BTESE RO membranes, compared with silica-zirconia and titania NF membranes.

Membrane	BTESE-300[17] (MWCO[c]: 50)	BTESE-100[17] (MWCO: 100)	SiO_2-ZrO_2[25] (MWCO: 200)	TiO_2[26] (MWCO: 600)	Viscous flow[b]
$\Delta E(L_p)$ (kJ/mol)[a]	30.8	27.1	24.6	22.7	15.4
$\Delta E(L_p\mu)$ (kJ/mol)[a]	15.3	12.1	/	8.2	0

[a]Activation energies $\Delta E(L_p)$ and $\Delta E(L_p\mu)$ were obtained using $L_p = (L_p)_0 \exp(-\Delta E(L_p)/RT)$, and $L_p\mu = (L_p\mu)_0 \exp(-\Delta E(L_p\mu)/RT)$. [b]Activation energy of viscous flow was calculated from the temperature dependence of the water viscosity, μ, in the bulk assuming a constant $L_p\mu$. [c]Molecular weight cut-off (MWCO, g/mol) is defined as the molecular weight at which 90% of a non-charged solute will be retained by the membrane.

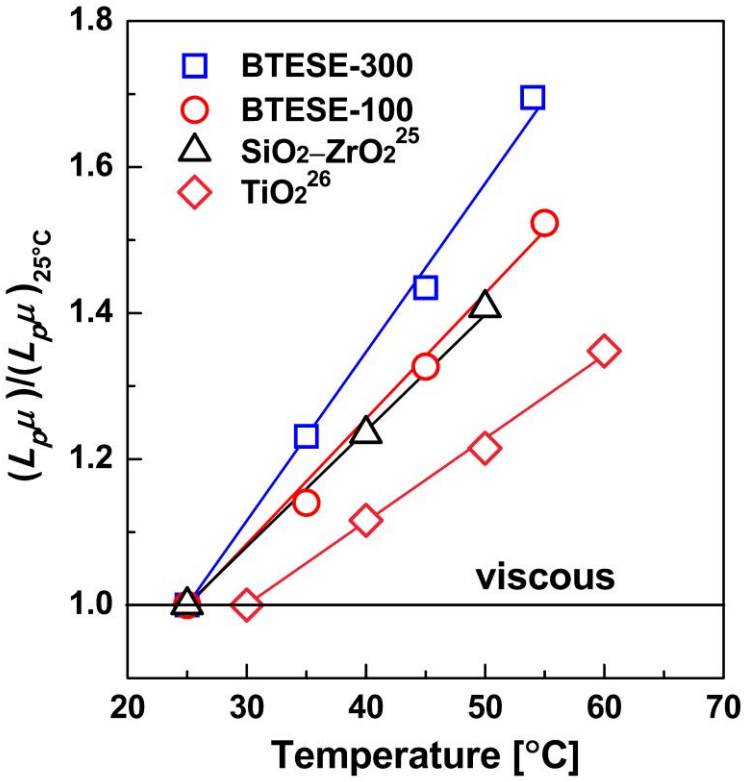

Figure 3-9. Normalized of $L_p\mu$ as a function of temperature.

There are several possible reasons for these phenomena. The first is that water permeation is an activated process in which water molecules permeate through the micropores via a repulsive force from the pore walls. Since the average pore size of the BTESE membrane is estimated to be approximately 0.5 nm [12], water molecules are expected to have strong friction with the pore walls. As the temperature increases, a portion of water molecules that have sufficient thermal energy to jump the energy barrier can pass through the micropores. Another explanation might be based on adsorption of water on the pore wall. Water can adsorb to hydrophilic parts of the organosilica pore wall that are covered with small amounts of silanol groups. The thickness of adsorbed water decreases with temperature, resulting in larger effective pores for water permeation. Third, the viscosity of water in micropores is different from that in a bulk solution [25]. Therefore, the temperature dependence of viscosity in these pores might be higher than that of the bulk solution.

To further investigate the influence of temperature on desalination performance, the

water permeability and NaCl rejection of the BTESE-300 membrane were measured in temperature cycle experiments. As presented in Figure 3-10, the feed temperature was increased and decreased step by step. After each step reached a steady state (approximately 3 hours), the membrane performance was then measured. With an increase in temperature from 25 to 90 °C, the water permeability increased approximately 8-fold. Surprisingly, a tradeoff between water permeability and water/salt selectivity was not observed during this process. On the contrary, NaCl rejection increased slightly as temperature increased and reached 98.3% at 90 °C, from an initial value of 97.3% at 25 °C. This contrasts with polymeric desalination membranes, for which increased water permeability generally comes at the expense of salt rejection due to thermal expansion of the polymer at high temperature [28]. For example, with the well-known commercial polyamide membrane, NF90, rejection of KCl decreased from 96.6 to 93.2% and water permeability increased from 3.5 to 11.5 kg/(m^2·h·bar) as the feed temperature increased from 20 to 60 °C (at 0.6 MPa, pH 6, and 20 mM KCl) [29]. However, thermal expansion effects were assumed to be less pronounced for these silica-based hybrid membranes, and therefore the pore size appeared to be unchanged in this temperature range. Increasing the temperature resulted in increased water permeability probably due to decreased viscosity and activated diffusion, whereas the large hydrated ions were still severely hindered due to the small pore sizes of BTESE silica networks. When the feed temperature was decreased gradually back to the starting level, water permeability returned to approximately the initial value, and high salt rejection was maintained. Only a few polymeric NF membranes withstood a temperature cycle of up to 65 °C without a significant change in filtration performance [30,31]. The high reproducibility of the RO performance in temperature cycles indicated superior hydrothermal stability of the BTESE membranes, which would benefit applications of high-temperature reverse osmosis.

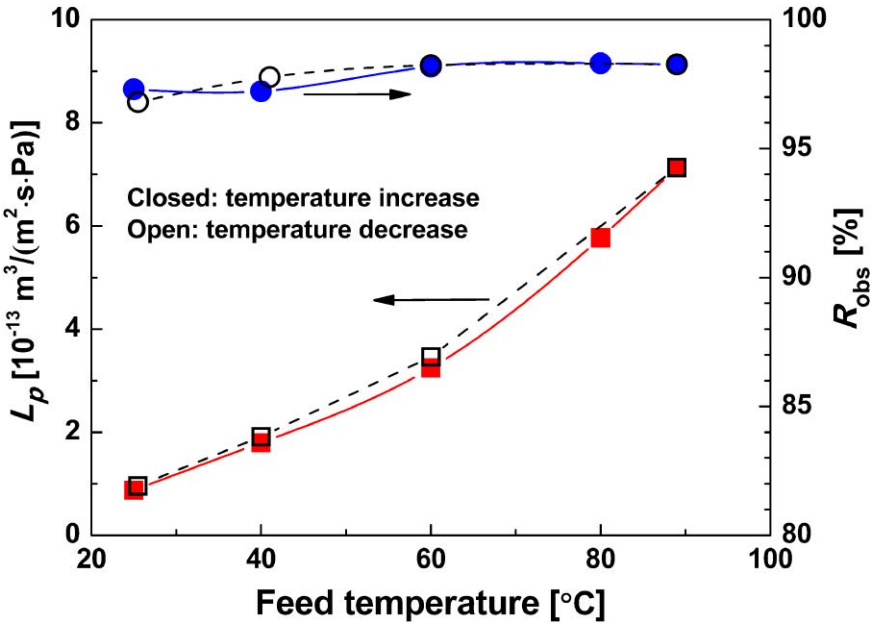

Figure 3-10. Water permeability and observed salt rejection for the BTESE-300 membrane as a function of temperature cycles at 1.15 MPa and 2000-ppm NaCl feed.

3.4.4 Comparison of transport properties and desalination performances

Figure 3-11 shows water permeances in PV and RO desalination processes with the BTESE-300 membrane, and compares them with gas permeances to develop deeper insight into the properties of water transport through the organosilica membrane. The single gas permeance results revealed that the membrane had hydrogen permeance as high as 1×10^{-6} mol m^{-2} s^{-1} Pa^{-1} with a high H_2/SF_6 permeance ratio of 5700. Water permeance in the PV was nearly one order of magnitude higher than the permeance of gases with similar kinetic diameters, such as He and H_2. This can probably be attributed to an increment in the adsorptive property of the water molecules. Water molecules that adsorbed to the hydrophilic parts of the organosilica networks could easily diffuse through the membrane by surface diffusion mechanism, avoiding strong interactions between water molecules and membrane pore walls. Similar observations have been reported in zeolite-4A membranes [32] and carbon membranes [33]. It is noteworthy that the transmembrane pressure difference was approximately 1 MPa in RO, resulting in a water flux of 2.4 kg/(m^2·h), whereas the vapor pressure difference was approximately 70 kPa in PV at 90 °C, giving a flux of 34.9 kg/(m^2·h). For comparison, L_p [$m^3/(m^2 \cdot s \cdot Pa)$] was

converted to P_{RO} ($P_{RO} = L_p / v_w$) in mol/(m^2·s·Pa), and very low water permeance was obtained in RO.

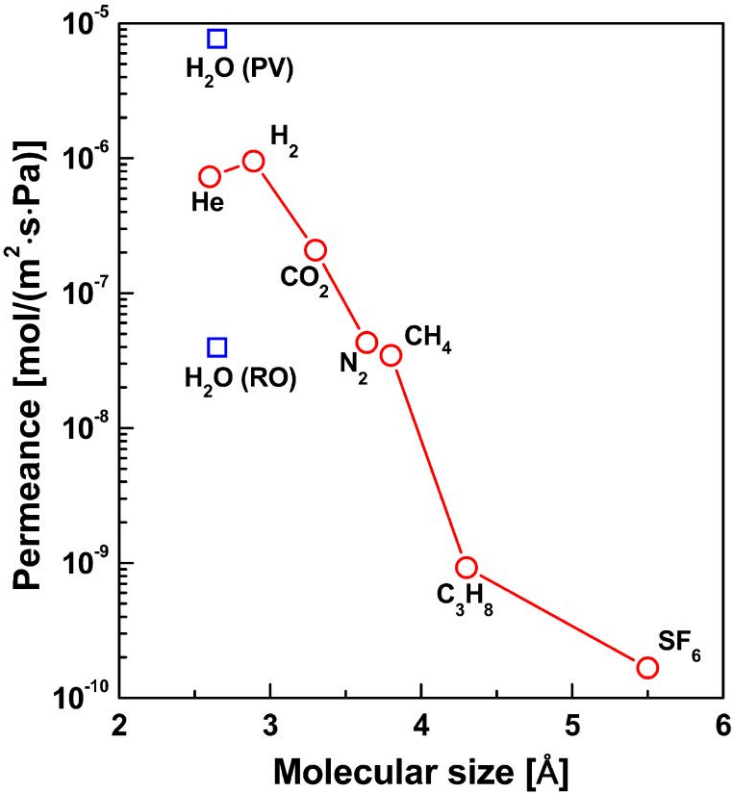

Figure 3-11. Gas permeance for the BTESE-300 membrane as a function of kinetic diameter at 200 °C and its comparison with water permeance in PV and RO processes at 90 °C.

The difference in water permeance, as shown in Figure 3-11, can be explained by application of the generalized SD equations for RO and PV processes. Within the context of the generalized SD model, by comparing Eqs. (12) and (13), the permeance difference in PV and RO is found in the terms $1/P_{sat}$ and $\bar{v}/RT$. The generalized transport equations suggest that the PV and RO are directly connected, and the permeation performance in one mode can be used to provide an initial estimate of performance in the other mode. For example, one can calculate theoretical PV desalination performance using the RO desalination performance data. In this study, the theoretical ratio of water permeance in RO to that in PV was calculated to be approximately 0.04% at 90 °C, and the experimentally obtained ratio was 0.5% at this temperature. The generalized SD

model successfully explained the drastic decrease in RO permeance, compared with that of PV. This is because a larger chemical potential difference could be provided for PV due to very low permeate pressure. Quantitatively, the water permeance in PV was predicted to be overstated, since the prediction of PV performance was made under ideal conditions. First, the PV process is theoretically considered as isothermal in the radial direction to the membrane. In reality, however, there is usually a noticeable temperature decrease from the bulk liquid to the upstream membrane surface [34]. This temperature drop in the liquid boundary layer could lead to a significant drop in water permeance due to the decrease in water vapor pressure, and therefore the driving force. Second, the nanoporous intermediate layer of this membrane is suspected to offer extra resistance to the transport of water molecules, particularly in PV with high flux, thus inhibiting the observation of expected high-water permeance in PV [35]. Third, in the PV desalination experiment, small amounts of hydrated Na and Cl ions may have diffused through to the permeate side and built up on the surface of the permeate side, since they cannot evaporate under a vacuum [36]. The accumulation of ions on the permeate surface would increase with experimental time, and decrease the water permeance.

3.5 Conclusions

Hybrid organosilica membranes were prepared by a sol-gel technique using bis(triethoxysilyl)ethane (BTESE), and were applied to desalination by reverse osmosis (RO). The influences of solute species, calcination temperatures, operating pressure, feed concentration and feed temperature were systematically studied to determine the permeation performance and transport mechanism of this new type of RO membrane. The generalized solution-diffusion (SD) equations were applied for a quantitative comparison of water permeance in PV and RO desalination processes using the same organosilica membrane.

(1) BTESE-derived organosilica membrane showed superior retention performance for mono- and bivalent ions and neutral solutes of low molecular weight, such as isopropanol and glucose. The membrane calcined at 300 °C exhibited higher salt rejection and lower

water flux compared with the membrane prepared at 100 °C, due to the formation of a denser silica network structure in the calcination process.

(2) As the operating pressure increased from 0.7 to 1.5 MPa, both the water flux and the salt rejection increased continuously, and the water permeability and salt permeability were almost constant. The pressure dependence of the permeation performance was explained well by the conventional SD model. The theoretical salt rejection and water flux showed excellent agreement with the experimental values.

(3) The water flux decreased linearly as the salt concentration increased from 500 to 10000 ppm, and the salt rejection decreased slightly with salt concentration. The nearly constant salt permeability in the concentration range excluded governance of the transport mechanism by the charge effect, thus supporting the molecular sieving mechanism for the organosilica RO membranes.

(4) The water permeation mechanism was found to differ from the viscous flow mechanism. Observed activation energies of permeation increased with a smaller pore size (lower MWCO values) for RO and NF membranes, and were considerably larger than the activation energies of the solvent viscosity. The organosilica membranes showed exceptional hydrothermal stability in temperature cycles in comparison with commercial polyamide RO membranes. The water permeability increased approximately 7-fold and salt rejection also increased slightly with an increase in temperature up to 90 °C.

(5) The applicability of the generalized SD model was examined in RO and PV desalination processes. The generalized transport equations were useful in providing a quick prediction for permeation performance based on performance observed in one mode. The water permeance differences in RO and PV processes agreed with the predictions made by using the generalized SD equations.

Notation

a = activity, dimensionless

A_k = surface porosity, dimensionless

B = salt permeability, $m \cdot s^{-1}$

C = concentration, $mol \cdot m^{-3}$

D = diffusivity, $m^2 \cdot s^{-1}$

J = permeation flux, $m^3 \cdot m^{-2} \cdot s^{-1}$

L_p = water permeability, $m^3 \cdot m^{-2} \cdot s^{-1} \cdot Pa^{-1}$

P = pressure, Pa

P_{sat} = saturation vapor pressure, Pa

P_{PV}, P_{RO}, and P_{GS} = permeance in pervaporation, reverse osmosis, and gas separation, $mol \cdot m^{-2} \cdot s^{-1} \cdot Pa^{-1}$

R = gas constant, $J \cdot mol^{-1} \cdot K^{-1}$

R_{obs} = observed rejection, dimensionless

R = theoretical salt rejection, dimensionless

r_p = pore radius, m

T = temperature, K

x = mole fraction, dimensionless

Δx, ℓ = membrane thickness, m

Greek letters

ϕ = osmotic coefficient, dimensionless

γ = activity coefficient, dimensionless

μ = viscosity, Pa·s

$\bar{v}$ = molar volume, $m^3 \cdot mol^{-1}$

π = osmotic pressure, Pa

Superscripts

m = inside the membrane

Subscripts

f, p = feed stream, permeate stream

s = salts

w = water

$1, 2$ = feed and permeate stream in diffusion

References

[1] M.A. Shannon, P.W. Bohn, M. Elimelech, J.G. Georgiadis, B.J. Marinas, A.M. Mayes, Science and technology for water purification in the coming decades, *Nature* 452 (2008) 301-310.

[2] L. Malaeb, G.M. Ayoub, Reverse osmosis technology for water treatment: State of the art review, *Desalination* 267 (2011) 1-8.

[3] K.P. Lee, T.C. Arnot, D. Mattia, A review of reverse osmosis membrane materials for desalination-development to date and future potential, *J. Membr. Sci.* 370 (2011) 1-22.

[4] M.J. Zhou, P.R. Nemade, X.Y. Lu, X.H. Zeng, E.S. Hatakeyama, R.D. Noble, D.L. Gin, New type of membrane material for water desalination based on a cross-linked bicontinuous cubic lyotropic liquid crystal assembly, *J. Am. Chem. Soc.* 129 (2007) 9574-9575.

[5] H.B. Park, B.D. Freeman, Z.B. Zhang, M. Sankir, J.E. McGrath, Highly chlorine-tolerant polymers for desalination, *Angew. Chem., Int. Ed.* 47 (2008) 6019-6024.

[6] R.M. de Vos, H. Verweij, High-selectivity, high-flux silica membranes for gas separation, *Science* 279 (1998) 1710-1711.

[7] B.N. Nair, K. Keizer, H. Suematsu, Y. Suma, N. Kaneko, S. Ono, T. Okubo, S.I. Nakao, Synthesis of Gas and Vapor Molecular Sieving Silica Membranes and Analysis of Pore Size and Connectivity, *Langmuir* 16 (2000) 4558-4562.

[8] H.L. Castricum, A. Sah, R. Kreiter, D.H.A. Blank, J.F. Vente, J.E. ten Elshof, Hybrid ceramic nanosieves: stabilizing nanopores with organic links, *Chem. Commun.* (2008) 1103-1105.

[9] H.L. Castricum, A. Sah, R. Kreiter, D.H.A. Blank, J.F. Vente, J.E. ten Elshof, Hydrothermally stable molecular separation membranes from organically linked silica, *J. Mater. Chem.* 18 (2008) 2150-2158.

[10] H.M. van M.D.A. Veen, Rietkerk, D.P. Shanahan, M.M.A. van Tuel, R. Kreiter, H.L. Castricum, J.E. ten Elshof, J.F. Vente, Pushing membrane stability boundaries with HybSi® pervaporation membranes. *J Membr Sci.* 380 (2011) 124-131.

[11] M. Kanezashi, K. Yada, T. Yoshioka, T. Tsuru, Design of Silica Networks for

Development of Highly Permeable Hydrogen Separation Membranes with Hydrothermal Stability, *J. Am. Chem. Soc.* 131 (2009) 414-415.

[12] M. Kanezashi, K. Yada, T. Yoshioka, T. Tsuru, Organic-inorganic hybrid silica membranes with controlled silica network size: preparation and gas permeation characteristics, *J. Membr. Sci.* 348 (2010) 310-318.

[13] J.G. Wijmans, R.W. Baker, The solution-diffusion model: a review, *J. Membr. Sci.* 107 (1995) 1-21.

[14] T. Kataoka, T. Tsuru, S. Nakao, S. Kimura, Permeation equations developed for prediction of membrane performance in pervaporation, vapour permeation and reverse osmosis based on the solution-diffusion model, *J. Chem. Eng. Jpn.* 24 (1991) 326-333.

[15] T. Kataoka, T. Tsuru, S. Nakao, S. Kimura, Membrane transport properties of pervaporation and vapor permeation in ethanol-water system using polyacrylonitrile and cellulose acetate membranes, *J. Chem. Eng. Jpn.* 24 (1991) 334-339.

[16] D.R. Paul, Reformulation of the solution-diffusion theory of reverse osmosis, *J. Membr. Sci.* 241 (2004) 371-386.

[17] R. Xu, J.H. Wang, M. Kanezashi, T. Yoshioka, T. Tsuru, Development of robust organosilica membranes for reverse osmosis, *Langmuir* 27 (2011) 13996-13999.

[18] T. Tsuru, A. Sasaki, M. Kanezashi, T. Yoshioka, Pervaporation of methanol/dimethyl carbonate using SiO_2 membranes with nano-tuned pore sizes and surface chemistry, *AIChE J.* 57 (2011) 2079-2089.

[19] L. Firdaous, F. Quéméneur, J.P. Schlumpf, J.P. Maléríat, Modification of the ionic composition of salt solutions by electrodialysis, *Desalination* 167 (2004) 397-402.

[20] X.L. Wang, T. Tsuru, S. Nakao, S. Kimura, The electrostatic and steric-hindrance model for the transport of charged solutes through nanofiltration membranes, *J. Membr. Sci.* 135 (1997) 19-32.

[21] G.M. Geise, H.B. Park, A.C. Sagle, B.D. Freeman, J.E. McGrath, Water permeability and water/salt selectivity tradeoff in polymers for desalination, *J. Membr. Sci.* 369 (2011) 130-138.

[22] R.M. de Vos, W.F. Maier, H. Verweij, Hydrophobic silica membranes for gas separation, *J. Membr. Sci.* 158 (1999) 277-288.

[23] L.T. Zhuravlev, The surface chemistry of amorphous silica. Zhuravlev model, *Colloids Surf., A: Physicochem. Eng. Asp.* 173 (2000) 1-38.

[24] J.M.M. Peeters, J.P. Boom, M.H.V. Mulder, H. Strathmann, Retention measurements of nanofiltration membranes with electrolyte solutions, *J. Membr. Sci.* 145 (1998) 199-209.

[25] T. Tsuru, S. Izumi, T. Yoshioka, M. Asaeda, Temperature effect on transport performance by inorganic nanofiltration membranes, *AIChE J.* 46 (2000) 565-574.

[26] T. Tsuru, K. Ogawa, M. Kanezashi, T. Yoshioka, Permeation characteristics of electrolytes and neutral solutes through titania nanofiltration membranes at high temperatures, *Langmuir* 26 (2010) 10897-10905.

[27] A. Dobrak, B. Verrecht, H. Van den Dungen, A. Buekenhoudt, I.F.J. Vankelecom, B. Van der Bruggen, Solvent flux behavior and rejection characteristics of hydrophilic and hydrophobic mesoporous and microporous TiO_2 and ZrO_2 membranes, *J. Membr. Sci.* 346 (2010) 344-352.

[28] C.K. Kim, J.H. Kim, I.J. Roh, J.J. Kim, The changes of membrane performance with polyamide molecular structure in the reverse osmosis process, *J. Membr. Sci.* 165 (2000) 189-199.

[29] M. Nilsson, G. Trägårdh, K. Östergren, Influence of temperature and cleaning on aromatic and semi-aromatic polyamide thin-film composite NF and RO membrane, *Sep. Purif. Technol.* 62 (2008) 717-726.

[30] M. Mänttäri, A. Pihlajamäki, E. Kaipainen, M. Nyström, Effect of temperature and membrane pre-treatment by pressure on the filtration properties of nanofiltration membranes, *Desalination* 145 (2002) 81-86.

[31] H. Saidani, N.B. Amar, J. Palmeri, A. Deratani, Interplay between the transport of solutes across nanofiltration membranes and the thermal properties of the thin active layer, *Langmuir* 26 (2010) 2574-2583.

[32] W. Zhu, L. Gora, A.W.C. van den Berg, F. Kapteijn, J.C. Jansen, J.A. Moulijn, Water vapour separation from permanent gases by a zeolite-4A membrane, *J. Membr. Sci.* 253 (2005) 57-66.

[33] M. Yoshimune, K. Haraya, Olefin gas dehydration using carbon hollow fiber

membranes derived from sulfonated poly(phenyl oxide), *J. Jpn. Petrol. Inst.* 54 (2011) 119-123.

[34] E. Favre, Temperature polarization in pervaporation, *Desalination.* 154 (2003) 129-138.

[35] R.Y.M. Huang, X. Feng, Resistance model approach to asymmetric polyetherimide membranes for pervaporation of isopropanol/water mixtures, *J. Membr. Sci.* 84 (1993) 15-27.

[36] C.H. Cho, K.Y. Oh, S.K. Kim, J.G. Yeo, P. Sharma, Pervaporative seawater desalination using NaA zeolite membrane: Mechanisms of high water flux and high salt rejection, *J. Membr. Sci.* 371 (2011) 226-238.

Chapter 4

Optimizing water permeability by introducing polarizable ethenylene bridges and aqueous ozone modification

4.1 Introduction

Due to global water scarcity and a growing demand for freshwater, the development of new and more efficient membranes for water purification is becoming an especially important task [1,2]. Polyamide-based thin film composite membranes dominate the current reverse osmosis (RO) and nanofiltration membrane markets, mainly because of their high salt rejection and high water permeability [3]. The main drawback of polyamide membranes is their susceptibility against chlorine, which is the most widely used disinfectant or as a membrane cleaning agent [4]. Therefore, numerous attempts have been made to explore robust RO membranes with high permeability and selectivity, as well as improved durability. Zeolite membranes (silicalite and ZSM-5) with good chemical resistance have successfully been explored for RO removal of salt ions and small organic molecules from water. In general, superior rejection has been achieved *via* charge- and/or size-based exclusion, but these zeolite membranes require tedious synthesis procedures to form defect-free ultrathin layers [5-7]. Microporous inorganic silica membranes are another promising candidate owing to their excellent molecular sieving ability. Highly permselective silica membranes are used in gas separation and pervaporation processes [8,9]. However, a low hydrothermal stability severely limits their application to water purification.

A significant breakthrough in hydrothermal stability came with the development of organosilica membranes, which were prepared *via* the hydrolysis and condensation of organically bridged bis-silyl precursors [10-15]. The introduction of covalently bridging groups into silica networks greatly improved membrane durability in water-containing system. Castricum *et al*. [10,11] reported a quite stable performance of 2 years for the pervaporative dehydration of butanol at 150 °C, using organosilica membranes derived

from the co-condensation of bis(triethoxysilyl)ethane (BTESE) and methyltriethoxysilane. More importantly, the versatility of organic bridges offers the ability to fine-tune the chemical-physical properties of a membrane at the molecular level. We proposed a "spacer" technique to control the silica networks, where the ethane groups were introduced to design a loose structure for development of a highly permeable hydrogen separation membrane [13]. Furthermore, the influences of size, flexibility, and shape of various alkyl and aryl bridges on the membrane pore size, nanostructure, and affinity was described to determine the relationship between the bridging group and the membrane properties [14].

Recently, we examined the possibility of applying organosilica membranes to water desalination under aggressive environments. The BTESE-derived organosilica membranes exhibited exceptional hydrothermal stability at 90 °C and excellent tolerance to chlorine, showing great promise as robust RO membranes [15]. The only weakness of the BTESE membrane was the relatively low water permeability, mainly due to the hydrophobic nature of the ethane bridges, which would not allow water to rapidly pass through the membrane. Consequently, the chemical structure of organosilica networks must be altered to improve membrane affinity to water, in order to improve the rate of water permeation. A modification strategy was only recently reported by incorporating of hydrophilic amino-functionalized precursors in a BTESE matrix, which led to highly water-permeable membranes for pervaporation [16].Yet, the co-condensation of organosilanes with terminal amine groups would result in a less durable structure and wider pore size distribution [17].

Here we present the first results on the development of ethenylene-bridged organosilica membranes with improved water permeability while maintaining a high selectivity and robustness in water purification. The organosilica membranes with ethenylene (–CH=CH–) bridges were prepared from bis(triethoxysilyl)ethylene (BTESEthy), a novel precursor for membrane materials. The π-bond electrons are more polarizable in the –CH=CH– bridges than electrons of σ-bond in the alkyl bridges, making the membrane more attractive to polar water molecules. The covalently bridged network architecture also suggests superior hydrothermal stability. Moreover, the unsaturated ethenylene bridges are reactive and

therefore provide plenty of opportunities for further chemical modification, such as bromination, sulfonation, and epoxidation [18-20]. In the present study, we tried a new and convenient method, namely ozone-assisted affinity modification, to further improve the water permeability of the membrane. The use of ozone treatment on periodic mesoporous organosilicas (PMOs) was recently reported by Polarz *et al.* for the creation of advanced, functionalized pore walls [21]. However, gas-phase ozone treatment resulted in a complete removal of the organic moieties in the ethenylene-bridged PMOs. In the present work, low levels of aqueous ozone were utilized to modify the innovative BTESEthy membranes.

4.2 Experimental

4.2.1 Sol synthesis

1,2-Bis(triethoxysilyl)ethylene (BTESEthy, 95%, ~80% trans isomer, Gelest, Inc.) sol was synthesized by hydrolysis and polymerization reaction of a precursor $(EtO)_3SiCH=CHSi(OEt)_3$ with water and HCl, in ethanol. A required amount of BTESEthy was mixed with ethanol. Subsequently, premixed water and HCl were added dropwise to the precursor mixture under continuous stirring. The molar composition of the reactants was BTESEthy/H_2O/HCl = 1: 60: 0.1, and the weight percent of BTESEthy was kept at 5.0 wt%. The solution was stirred for 2 h at 25 °C before coating. BTESEthy-derived gel powder was prepared by drying at 40 °C in air, and was ground using a mortar. 1,2-bis(triethoxysilyl)ethane (BTESE) sol and gel powder were prepared under the same conditions as the BTESEthy.

4.2.2 Membrane preparation

Tubular α-alumina microfiltration membranes (porosity, 50%; average pore size, 1μm; outside diameter, 10 mm; and, length, 100 mm) were used as the supports. First, two kinds of α-alumina particles (average particle size is 1.9 μm and 0.2 μm, respectively) were deposited onto the outer surface of the support using the SiO_2-ZrO_2 colloidal sol (2 wt.%) as a binder, and the substrate was fired at 550 °C for 30 min. This procedure was

repeated 6 times to form a particle layer. Then, SiO_2-ZrO_2 (molar ratio of Si/Zr = 1/1, 0.5 wt.%) colloidal sols were coated on the particle layer by the hot-coating methods, where the substrate was first heated up to around 180 °C before coating, followed by quickly contacting the substrate with a wet cloth with the SiO_2-ZrO_2 sols. Subsequently, the substrate was fired at 550 °C for 15min in air. This hot-coating and calcination procedures were repeated approximately 6 times to form an intermediate layer. Finally, the BTESEthy sol was deposited onto the intermediate layer by wipe coating using a wet cloth with the BTESEthy sol (0.5 wt.%), followed by a flash calcination at 300 °C in air for 20min.

4.2.3 Characterization

The size distribution of the sols was measured by dynamic light scattering (DLS) at 25 °C using a Malvern Zetasizer Nano-ZS (ZEN3600). Thermogravimetric/Differential Thermal Analysis (TG/DTA) was carried out in air using a DTG-60 instrument with a heating rate of 10 °C min^{-1}. The membrane structure and morphology were examined by Field Emission Scanning Electron Microscopy (FE-SEM, S-4800) with an acceleration voltage of 15 kV. X-ray Photoelectron Spectroscopy (XPS, ESCA3400) measurements were performed on the membrane sample that was used for SEM analysis. Depth profiles of the concentrations of C, Si and Zr in the membrane were calculated from the C 1s, Si 2p and Zr 3d energy bands via sputtering with 0.6 kV Ar^+ at 80 nm min^{-1}. Fourier Transform Infrared Spectrometer (FT/IR-4100) was applied to confirm the chemical structure of the BTESEthy films before and after ozone exposure. Films for FTIR and static contact angle (CA) measurements were obtained by coating the organosilica sols onto clean silicon wafers, followed by calcination at 300 °C for 20 min. The microstructures and surface properties of organosilica networks were studied by nitrogen (at 77 K) and water sorption (at 298 K), respectively, using a Belsorp-Max (Bel Japan, Inc.) instrument. Before analysis, the samples were outgassed at 200 °C overnight under vacuum. The Brunauer-Emmett-Teller (BET) method in the relative pressure range of P/P_0 = 0.01-0.25 was used to calculate the specific surface area. The pore size distribution was obtained through the analysis of the adsorption branch of nitrogen isotherms using

the MP method. The micropore volume was estimated using the *t*-plot method.

4.2.4 Performance evaluation

Single gas permeation measurements were performed at 200, 150, 100 and 50 °C in this sequence, using high-purity of He, H_2, CO_2, N_2, C_3H_6, C_3H_8, and SF_6. Prior to measurement, the membrane was dried for 8 h at 200 °C in a He flow of 20 mL min^{-1}. The permeate stream was kept at atmospheric pressure, and the pressure drop through the membrane was maintained at 1 bar. The permeation rate was measured using a soap-film flow meter.

Water desalination experiments were carried out using a 2,000 ppm NaCl solution, and molecular weight cut-off (MWCO) measurements were performed using 500 ppm neutral solutes: ethanol, isopropanol, glucose, and sucrose. RO experiments were conducted using a typical RO testing apparatus as previously described [22]. The feed solution, pressurized with a plunger pump, was vigorously agitated in the RO cell, and the retentate was recycled at an approximate flow of 30 mL min^{-1}. Water permeability, L_p, was calculated from the volume flux, J_v, divided by the effective transmembrane pressure, $\Delta P - \Delta\pi$.

$$J_v = L_p(\Delta P - \Delta\pi)$$

where L_p is the water permeability and, ΔP ($=P_1 - P_2$) and $\Delta\pi$ ($=\pi_1 - \pi_2$) are the differences in applied pressure and osmotic pressure, respectively. The observed rejection, R_{obs}, can be expressed as follows:

$$R_{obs} = (1 - C_p/C_f) \times 100\%$$

The concentrations of feed (C_f) and permeate (C_p) were measured with a conductivity meter for NaCl and a total organic carbon analyzer (Shimadzu, TOC-V_E) for neutral solutes.

4.2.5 Chlorine tolerance tests

The accelerated chlorine resistance test was performed using a commercial sodium hypochlorite solution (NaClO, active chlorine: 10%) at room temperature. The concentration of the fresh chlorine solution was 500 ppm and pH was adjusted to 7 using a 0.2 M KH_2PO_4 buffer solution. The membrane was periodically immersed in, and

removed from a chlorine solution, which was placed in a sealed, stirred, dark glass bottle. The RO performances were then tested after a thorough rinse with deionized water. The total exposure of the membrane to chlorine was expressed as the product of chlorine concentration (ppm) and exposure time (h).

4.2.6 Ozone modification

The ozone treatment experiments were performed using the setup shown in Figure 4-1. Ozone was produced from high-purity oxygen gas using an ozone generator (Fuji Electric, PO-10), which allowed control of the ozone concentration and the flow rate. Ozone must be injected continuously into the water due to its instability. A pre-injection of about 3 hours was required to establish a steady level of dissolved ozone. The concentration of ozone in water was maintained at 1 ppm, which was periodically analyzed using the indigo method [23]. BTESEthy membranes were periodically soaked in the aqueous ozone system for a predetermined time interval. The filtration performances were then evaluated after rinsing with deionized water.

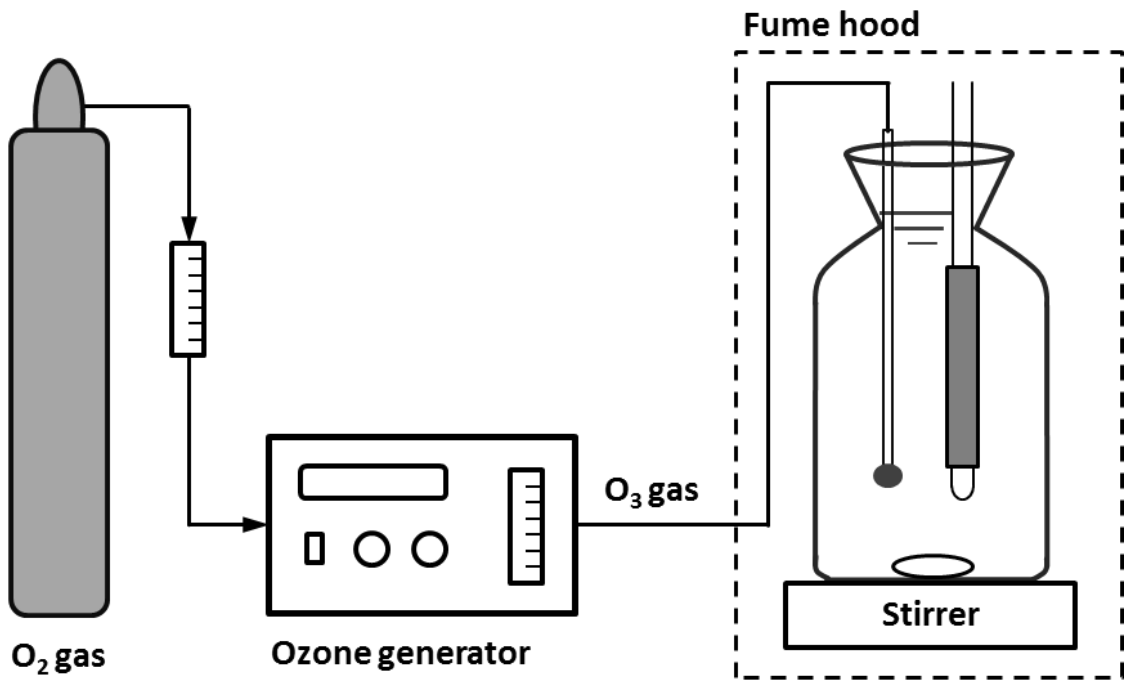

Figure 4-1. Experimental set-up for ozone modification of the BTESEthy membrane.

4.3 Results and Discussion

4.3.1 Physicochemical properties

Size distribution of the BTESEthy sol with a silica concentration of 0.3 mol L^{-1} was determined by dynamic light scattering at 25 °C, as presented in Figure 4-2. The freshly synthesized BTESEthy sol showed a small mean radius of 2.1 nm and a narrow monomodal size distribution, which was desirable for preparing a thin, microporous separation layer. After storage at 0 °C for two months, only a slight increase in mean particle size was observed, ranging from 2.1 to 3.7 nm, with no broadening of the size distribution. The slight increase in size was probably dominated by the polymerization reaction of the monomer species, rather than by the aggregation of nanoparticals, since even a very small fraction of aggregation would result in a dramatic size increase of the sol and a broadening of its size distribution [14,24].

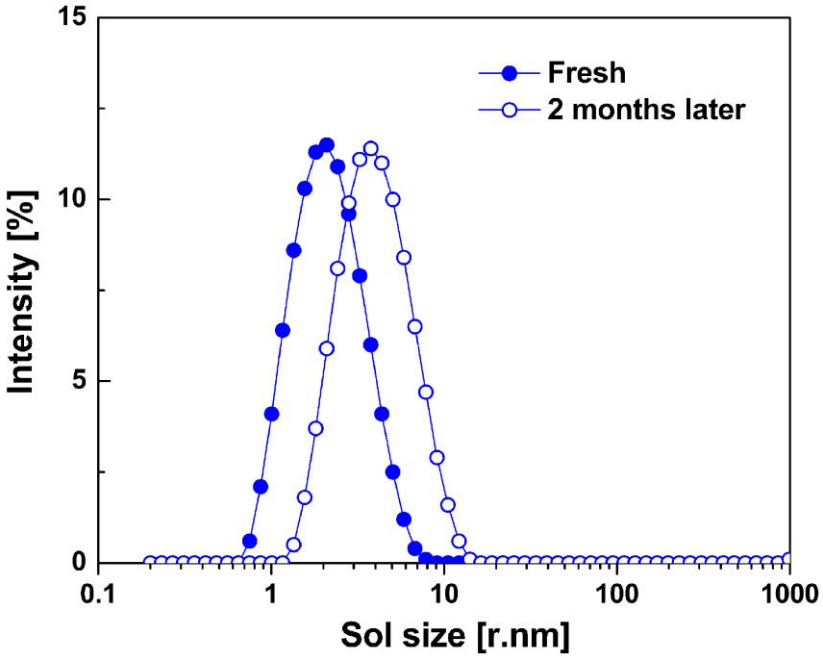

Figure 4-2. Size distribution of the BTESEthy sol determined by DLS.

TG/DTA was conducted to evaluate the thermal stability of the ethenylene-bridged network in air (Figure 4-3). The TG curve shows that a weight loss occurred in three steps. The first weight loss of about 14% below ~150 °C was assigned to the removal of physisorbed water. A minor weight loss of ~5% was observed for temperatures ranging from 150 to 350 °C, most likely due to ongoing condensation reaction of silanol groups

(dehydroxylation) [25] and the desorption of small amounts of chemisorbed water. Above approximately 350 °C, a continuous decrease in weight (~10%) was attributed to the decomposition of organic groups in the network (as revealed by the exothermic DTA peak). The BTESEthy material was confirmed to be thermally stable up to ~350 °C in air atmosphere.

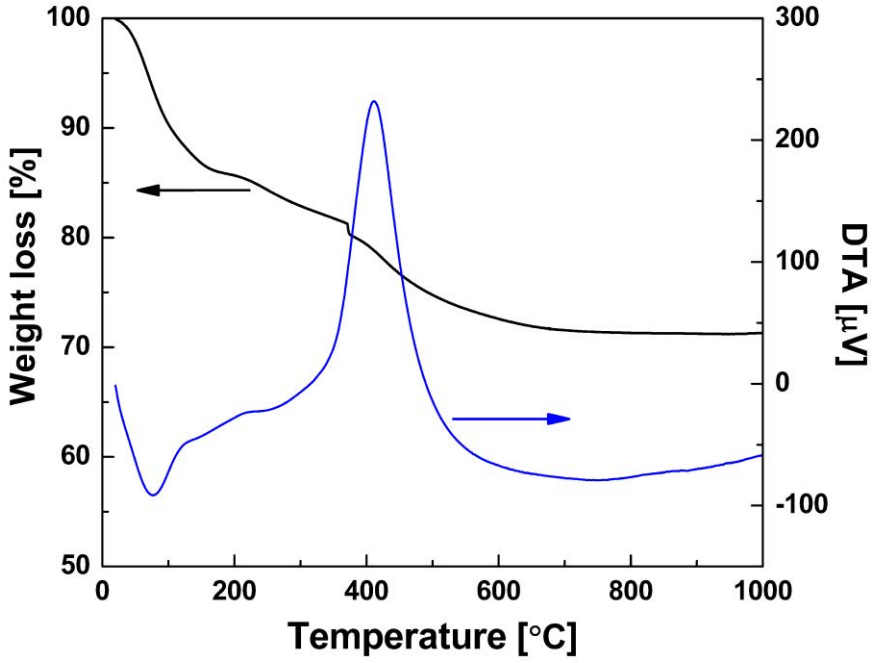

Figure 4-3. TG and DTA curves of BTESEthy gel powder measured in air with a heating rate of 10 °C/min.

To probe the pore structure, the N_2 adsorption-desorption isotherms of BTESEthy together with BTESE for a comparison, are presented in Figure 4-4(a). Both of the N_2 isotherms show type-I characteristics, with a significant uptake of N_2 at low relative pressure, which is typical of microporous materials. No hysteresis was observed in the isotherms, indicating the absence of mesopores [26]. Details of the physicochemical properties are given in Table 4-1. The BTESEthy sample exhibited a higher BET specific surface area together with a slightly larger volume of micropores, compared with the BTESE material. The incorporation of ethenylene bridges imparted higher rigidity within the networks, which would prevent the collapse of pores and the formation of dead-end pores during the calcination process, hence affording a more open and accessible pore

structure [27]. Both materials had a narrow pore size distribution with a maximum at the nominal pore diameter of 0.6 nm (Figure 4-4(b)), which is in good agreement with effective pore size of ~0.5 nm as estimated by gas permselectivities for the BTESE membrane [28].

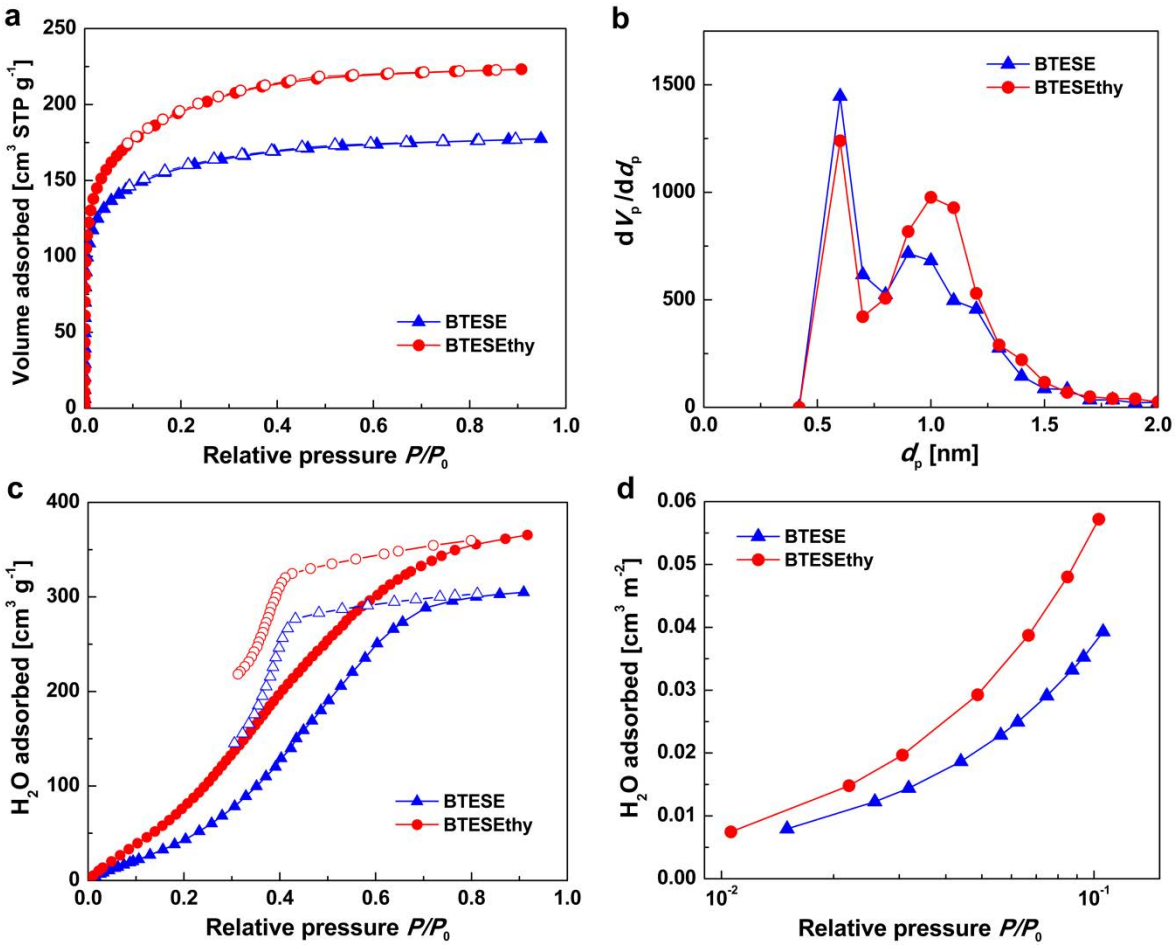

Figure 4-4. (a) Nitrogen adsorption-desorption isotherms of BTESE and BTESEthy samples (77 K) and (b) pore size distribution (calculated by MP method). (c) Water sorption isotherms of the samples (298 K) and (d) plots of samples at low pressure normalized to their specific surface area.

Figure 4-4(c) shows the water sorption isotherms of BTESE and BTESEthy materials measured at 298 K. Overall, a higher sorption capacity of water (366 cm^3 g^{-1}) was observed for BTESEthy, partly due to its larger surface area. In addition, the non-closed isotherms demonstrated that the adsorbed water could not completely desorb from the

pore surface of the network, suggesting a strong chemisorption of water molecules in the two materials. Since the chemisorption at low pressure is primarily driven by water vapor loading, whereas physisorption at high pressure depends mainly on the surface area, the differences in sorption behavior at low pressure are more significant to confirm the internal water affinity of the two kinds of networks. Thus, the water sorption capacities normalized by their specific surface area were further compared at low water vapor pressure up to 0.1 atm (Figure 4-4(d)). Apparently, a more rapid growth of water uptake was observed for the BTESEthy, demonstrating the stronger water affinity of the internal network. The results were consistent with the contact angles of the thin films (Table 4-1), which also showed a higher surface hydrophilicity of the BTESEthy material.

Table 4-1. Physicochemical properties of BTESE and BTESEthy materials.

Sample	BET surface area	Micropore volume	Micropore diameter	Contact angles
	A_{BET} (m^2/g)	V_p (cm^3/g)	d_p (nm)	CA (°)
BTESE	571	0.27	0.6	66.8 ± 1.4
BTESEthy	696	0.34	0.6	50.4 ± 2.1

Figure 4-5 shows a cross-sectional SEM image of a BTESEthy-derived organosilica membrane. Although it is difficult to distinguish the uppermost separation layer from the SiO_2-ZrO_2 intermediate layer, a thin and defect-free separation layer can be observed on top of the intermediate layer, with a total thickness of approximately 200 nm. The thickness of the BTESEthy-derived separation layer was further confirmed by the XPS depth profile analysis (Figure 4-6). The concentration of C atoms that is attributed to Si–CH=CH–Si bonds was detected on the membrane surface and showed a sharp decrease at a depth from 0 to 60 nm. This suggested that the effective separation layer had a thickness of about 60 nm. The concentration of Zr, which was obtained from the SiO_2-ZrO_2 intermediate layer, was also detected near the surface and increased with an increase in depth. Considering the small size of BTESEthy sol, the penetration of the organosilica sol would occur during the coating procedure, resulting in an atomic mixing of C and Zr in the top layer of the membrane.

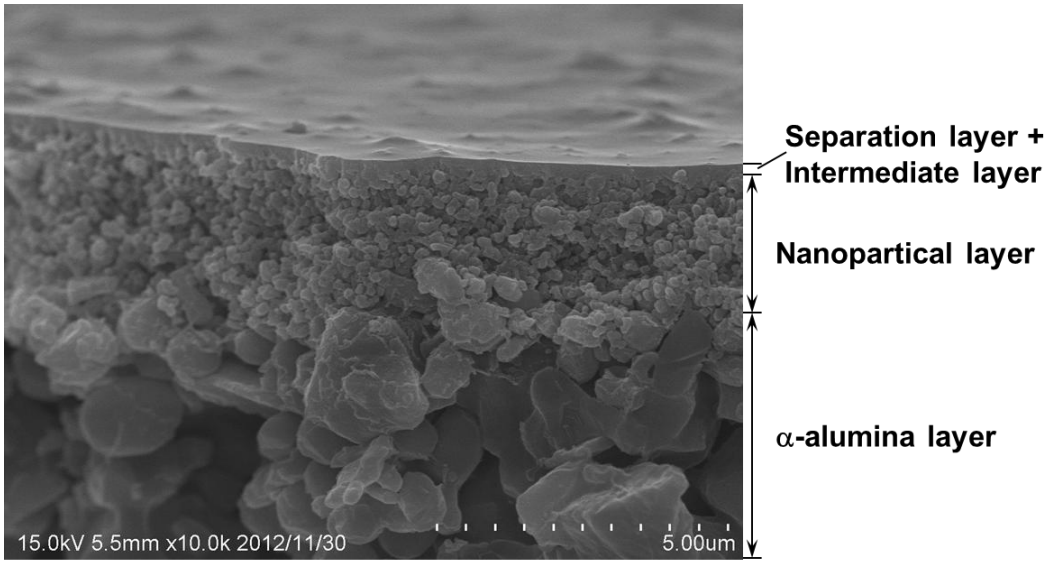

Figure 4-5. Cross-sectional SEM image of a BTESEthy membrane.

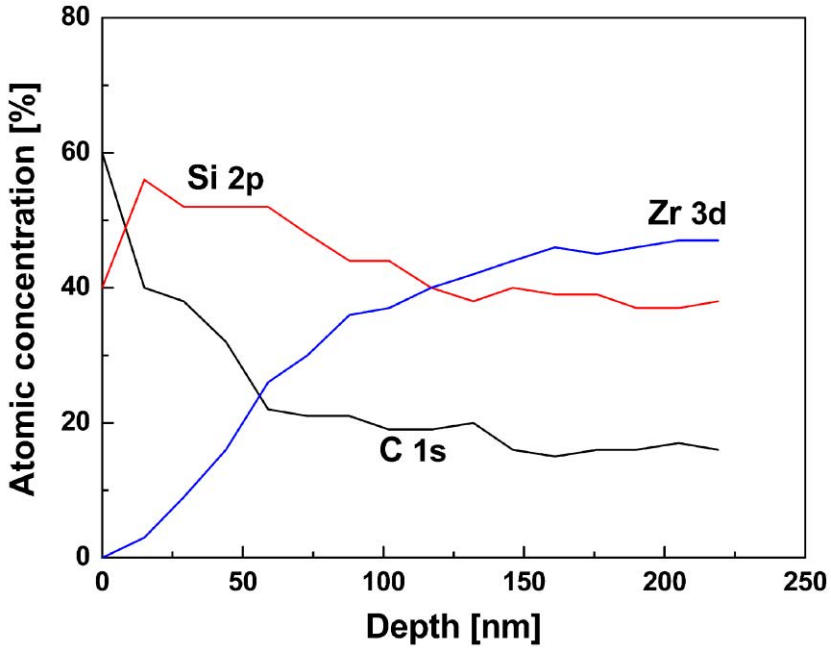

Figure 4-6. Depth profile of C 1s, Si 2p and Zr 3d in the BTESEthy membrane.

4.3.2 Temperature dependence of gas permeation

To investigate the separation efficiency of the BTESEthy membrane, the temperature dependence of gas permeance was measured using He, H_2, CO_2, N_2, C_3H_6, C_3H_8, and SF_6

in different molecular sizes, as presented in Figure 4-7. On the whole, the permeances of He, H_2 and N_2 decreased as temperature decreased, which is typical for activated permeation. In contrast, for adsorptive molecules such as CO_2, C_3H_6, C_3H_8, and SF_6, the permeances generally increased with decreasing temperature. This tendency may be caused by the adsorption effects, as the concentration gradient by adsorption increased with decreasing temperature. It is worth noting that the permeances of CO_2 and C_3H_6 appeared to peak at 100 °C, which can be explained by the balance between adsorption and diffusivity as follows. The number of adsorbed molecules increased as temperature decreased. Conversely, the enhanced adsorption caused a decrease in mobility at temperatures lower than the peak, hindering the diffusion of molecules through the membrane (liquid-like diffusion of pore filling molecules) [29].

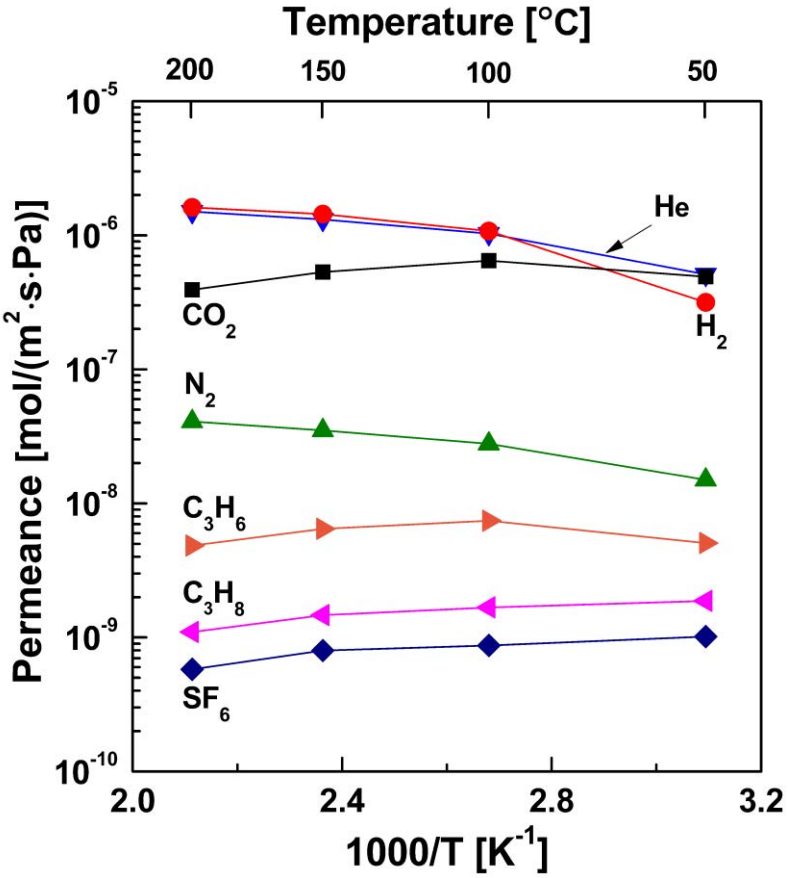

Figure 4-7. Temperature dependence of gas permeances for the BTESEthy membrane.

We further calculated the relevant permeance ratios of H_2/N_2, CO_2/N_2 and C_3H_6/C_3H_8 at various temperatures, as listed in Table 4-2. The BTESEthy membrane exhibited the highest H_2/N_2 permeance ratio of 39.5 at 200 °C, indicating the superior molecular sieving ability of the network structure. Surprisingly, a high permeance of CO_2 was observed (Figure 4-7), with the highest CO_2/N_2 selectivity of 32.7 at 50 °C, which was due to the strong adsorption of CO_2 on the network with π-bond electrons. Therefore, the BTESEthy membrane showed great potential for CO_2 separation. Additionally, the π-π interaction between the ethenylene bridges and the C_3H_6 molecules may contribute to a preferential C_3H_6 adsorption on the BTESEthy membrane, considering that the molecular sizes of C_3H_6 and C_3H_8 are quite close [30].

Table 4-2. Gas permeance ratios through the BTESEthy membrane at different temperatures.

Selectivity	50 °C	100 °C	200 °C
H_2/N_2	21.1	38.7	39.5
CO_2/N_2	32.7	23.3	9.6
C_3H_6/C_3H_8	2.7	4.4	4.4

4.3.3 Reverse osmosis performance and chlorine tolerance

The superior sieving ability and higher water affinity of BTESEthy membranes prompted us to study their desalination performances. The RO desalination performances were evaluated using a 2,000 ppm NaCl solution at a pressure that varied from 0.7 to 1.5 MPa (Figure 4-8). As the operating pressure increased, the water flux (J_v) and the salt rejection (R_{obs}) of the BTESEthy membrane increased continuously, whereas the water permeability (L_p) remained almost constant at approximately 2.2×10^{-13} $m^3/(m^2 \cdot s \cdot Pa)$. This can be well explained by the solution-diffusion (SD) model [31]. The transmembrane pressure difference ($\Delta P - \Delta \pi$) is the driving force for water transport across the membrane. Thus, the water flux increased linearly with increasing the operating pressure and water permeability, L_p, remained almost constant. However, the ion permeation, according to the SD model, was independent of the operating pressure. As the pressure increased, the

enhanced water permeation led to an increase in salt rejection from 97.9 to 99.2%.

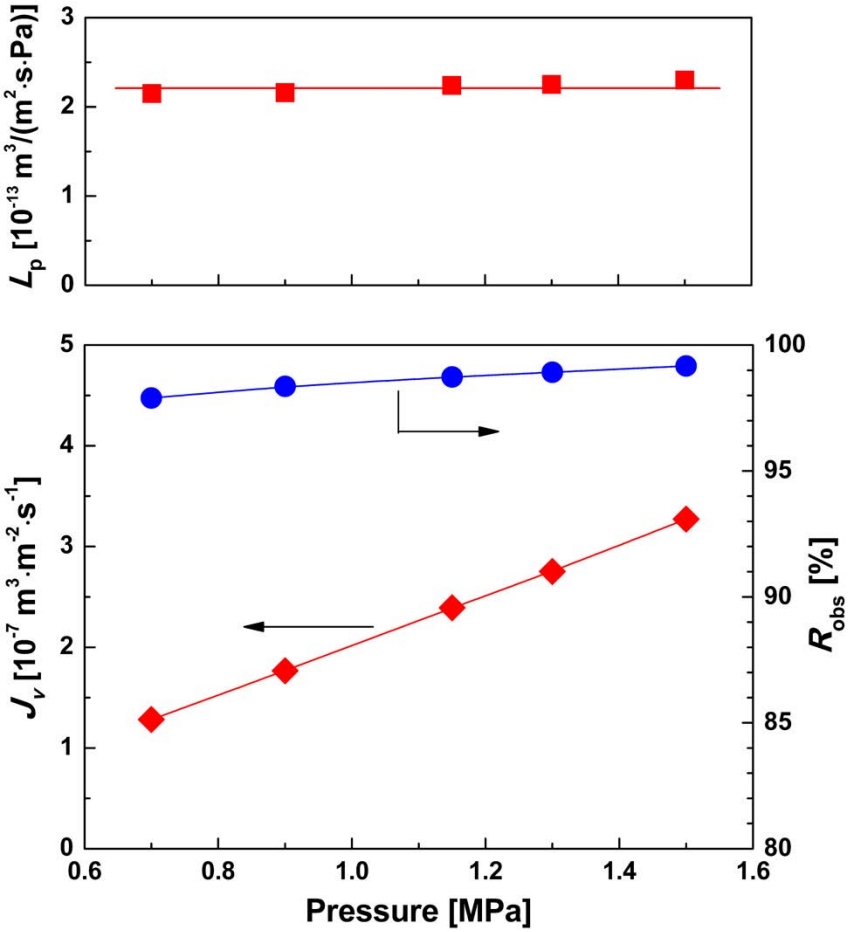

Figure 4-8. Effect of operating pressure on water flux, salt rejection, and water permeability.

The hydrothermal stability of the BTESEthy membrane was evaluated by performing a cycle in temperature. The change in temperature was conducted without agitating the feed solution in the RO cell. When the predetermined temperature was reached, the feed was agitated. After each step reached a steady state, the membrane performance was then tested. As shown in Figure 4-9, with an increase in feed temperature from 25 °C to 88 °C step by step, the water permeability of the BTESEthy membrane increased approximately 8-fold. Interestingly, the trade-off relationship between permeability and selectivity was not observed in this process. In contrary, the rejection showed almost no drop with temperature, which was 98.5% at 88 °C, from an initial value of 98.8% at 25 °C. This suggested that the pores of the membranes were still sufficiently small to enable

molecular sieving separation under such a high temperature. As the temperature returned to the starting temperature, the water permeability reduced gradually to around the initial level with keeping a high salt rejection, indicating a good hydrothermal stability of the BTESEthy membranes.

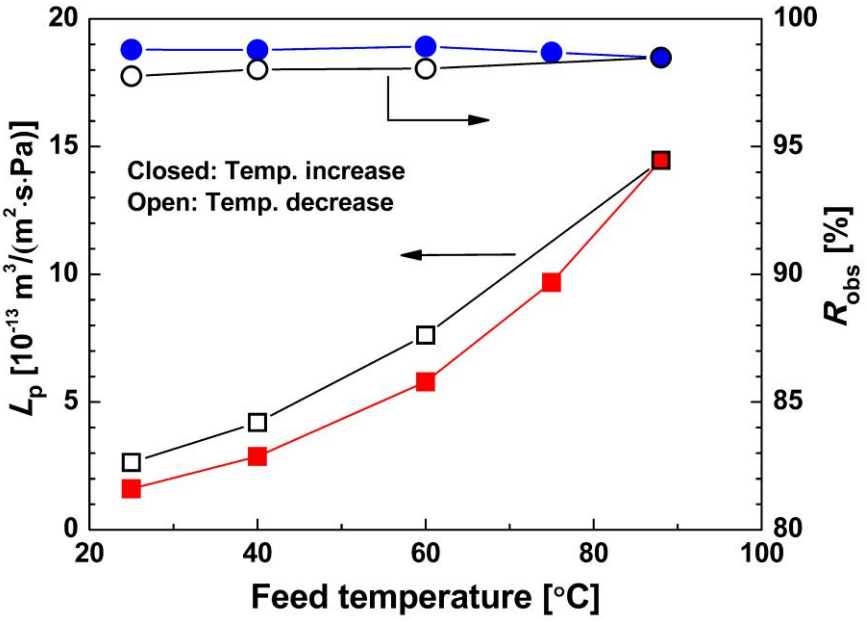

Figure 4-9. Water permeability and NaCl rejection for the BTESEthy membrane as a function of temperature cycles.

Chlorine resistance experiments were performed on the BTESEthy membrane by soaking tests. The BTESEthy membrane exhibited excellent chlorine tolerance owing to the inherently stable organosilica network, which lacks chemical functionalities that are susceptible to chlorine attack. As shown in Figure 4-10, after a total chlorine exposure of as much as 21,000 ppm·h, there was no obvious change in the NaCl rejection. In contrast, the rejection of the commercial polyamide RO membrane dropped dramatically after only ~7,000 ppm·h of chlorine exposure [32]. This high chlorine tolerance of BTESEthy membranes may offer great advantages over the commercial polyamide RO membranes.

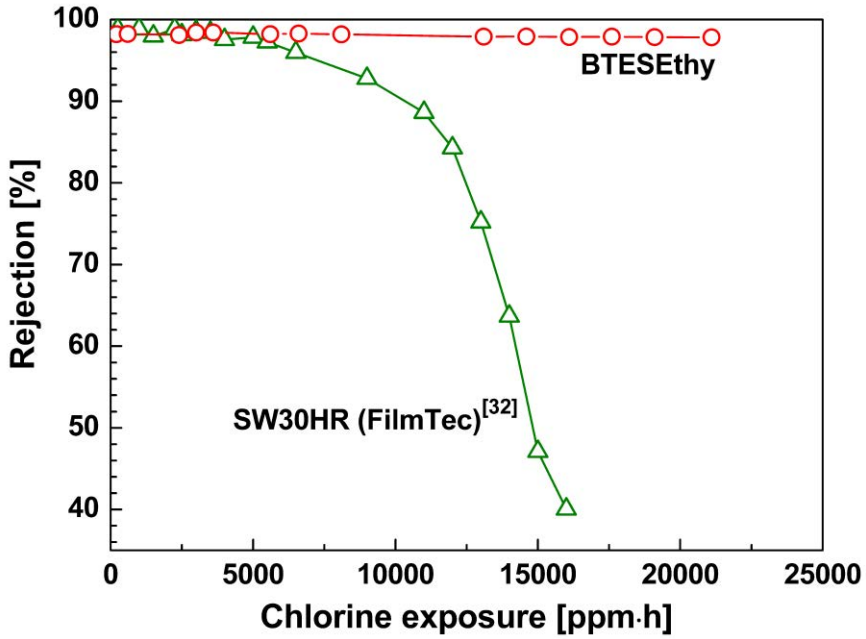

Figure 4-10. Chlorine resistance of the BTESEthy membrane (2000 ppm NaCl feed, 500 ppm chlorine as NaOCl, pH 7.0), compared to a SW30HR (FilmTec) polyamide membrane (2000 ppm NaCl feed, 500 ppm chlorine as NaOCl, pH 9.5).

4.3.4 Aqueous ozone modification

To further improve the water permeability, ozone-assisted modification was examined on the BTESEthy membranes. In these experiments, the membranes were periodically exposed to a 1 ppm level of ozone aqueous solution for a certain period of time. Figure 4-11 illustrates the water permeability and NaCl rejection as a function of ozone exposure. The water permeability increased continuously with exposure time, and the rejection decreased gradually. After a total exposure of 2 hours, the water permeability of the membrane increased more than 7-fold, and the salt rejection decreased by 11.7% due to the increased permeation of NaCl. The substantial improvement in water permeability can be explained by the change in chemical structures, as confirmed by FTIR analysis of the BTESEthy films (Figure 4-12). The following characteristic bands were mainly related to the BTESEthy framework: C–H stretching vibrations in the vinyl unit (~2980 cm^{-1}); C=C stretch (~1620 cm^{-1}); Si–O–Si stretch (1020-1200 cm^{-1}); Si–OH stretch (~920 cm^{-1}); and Si–C stretch (~790 cm^{-1}) [33,34]. Obviously, a decrease in the intensities of C=C stretching vibrations was observed with exposure time, indicative of the reaction of the

C=C bond with ozone. The mechanism for the ozonolysis of ethenylene-bridged organosilicas was discussed in detail by Polarz and his co-workers [21]. Ozone treatment resulted in cleavage of the C=C and Si–C bonds and eventually in the formation of new silanol groups. The formation of silanol groups in the organosilica network greatly enhanced the H_2O-affinity of the membrane, thus leading to high water permeability. Unlike the gas-phase ozone treatment, ethenylene bridges in the network did not completely react with the aqueous ozone in this study. Even after ozone exposure for 120 min, the characteristic C=C vibration bands could be observed in the FTIR spectra (Figure 4-12). A more likely explanation is that the ethenylene bridges exposed on the surface of channel walls seemed to react with the aqueous ozone, and the bridging groups embedded inside the channel walls remained, probably due to very low levels of ozone and limited exposure time.

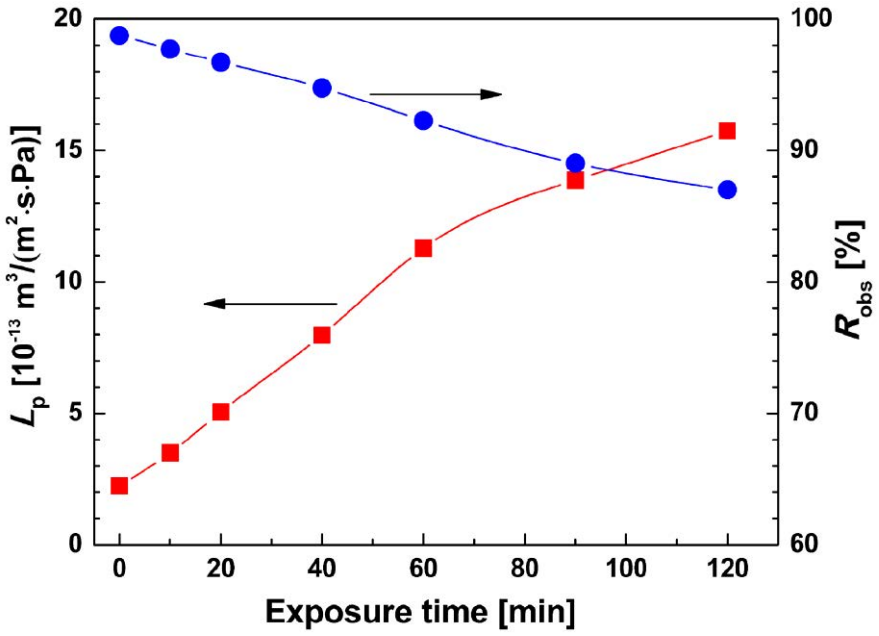

Figure 4-11. Effect of ozone treatment on water permeability and salt rejection of the membrane (25 °C, 1.15 MPa and 2000 ppm-NaCl).

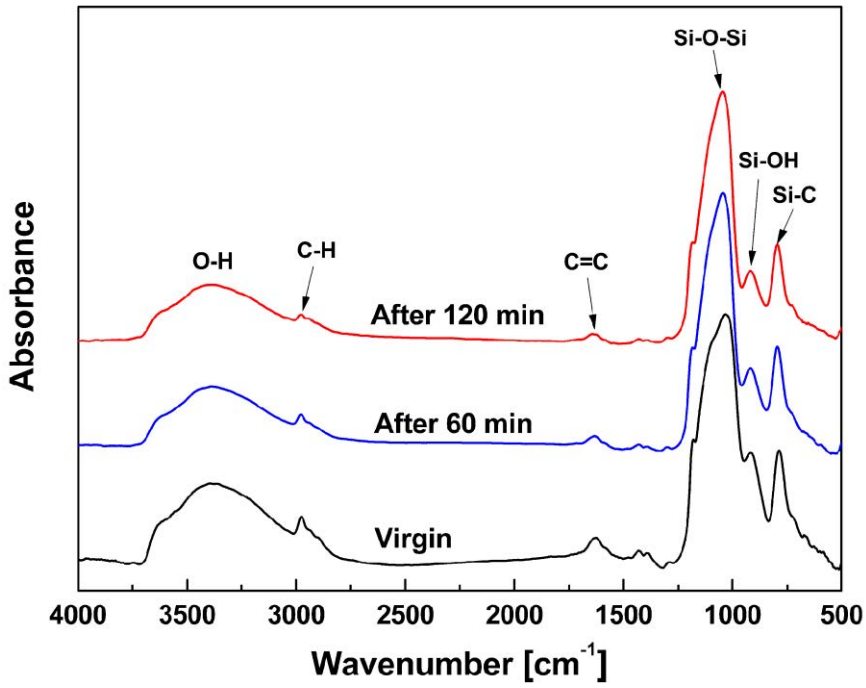

Figure 4-12. FTIR spectra of the BTESEthy film before and after ozone treatment.

With respect to molecular separation membranes, we concentrated more on the effective pore size change after ozone modification, which was reflected by molecular weight cut-off (MWCO). Figure 4-13 shows the change in the MWCO of the BTESEthy membrane, using a series of neutral solutes of different sizes: ethanol (Stokes diameter (Sd): 0.4 nm), isopropanol (Sd: 0.48 nm), glucose (Sd: 0.73 nm), and sucrose (Sd: 0.94 nm) [35]. The MWCO, defined at 90% rejection, of the virgin membrane was approximately 50 Da. Clearly, with an increase in the ozone treatment time, the MWCO increased to ca. 90 Da after 40 min, and further increased to ca. 120 Da after 120 min, indicating a gradual increase in effective membrane pore size. Despite a decrease in NaCl rejection due to the increased pore size, the BTESEthy membrane was still capable of molecular sieving for large molecules such as glucose and sucrose with rejection higher than 98%. Therefore, ozone modification may present new options for tailoring membrane pore sizes according to specific separation requirements.

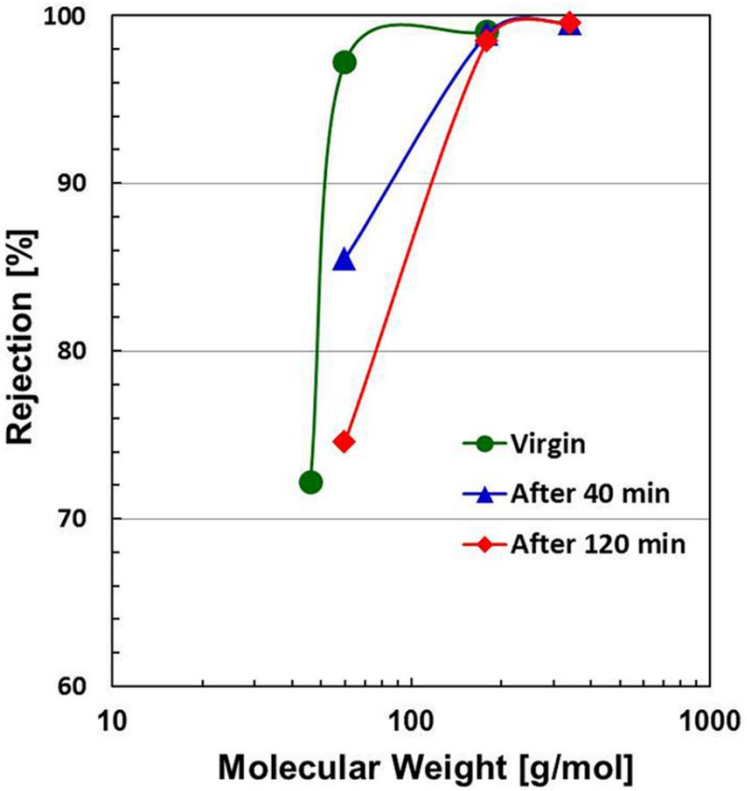

Figure 4-13. Change of MWCO curves after ozone treatment.

4.3.5 Trade-off of RO performances

Figure 4-14 shows the trade-off relationship between NaCl rejection and water permeability for zeolite and organosilica RO membranes. Generally speaking, BTESEthy-derived organosilica membranes showed better desalination performance than typical zeolite RO membranes such as ZSM-5 and silicalite. Even at a low pressure of 1.15 MPa, BTESEthy membranes almost completely (>98.5%) rejected NaCl. Compared to BTESE membranes, the water permeability of BTESEthy membranes was approximately doubled with no drop in rejection, simply by adjusting the bridging groups of the network. Furthermore, the water permeability of the BTESEthy membranes was significantly improved by a simple ozone modification. For example, despite a moderate rejection decrease from 98.8 to 92.3% after a 60 min exposure, the water permeability reached 1.1×10^{-12} $m^3/(m^2 \cdot s \cdot Pa)$, close to that of the commercial seawater RO membrane SW30HR [36].

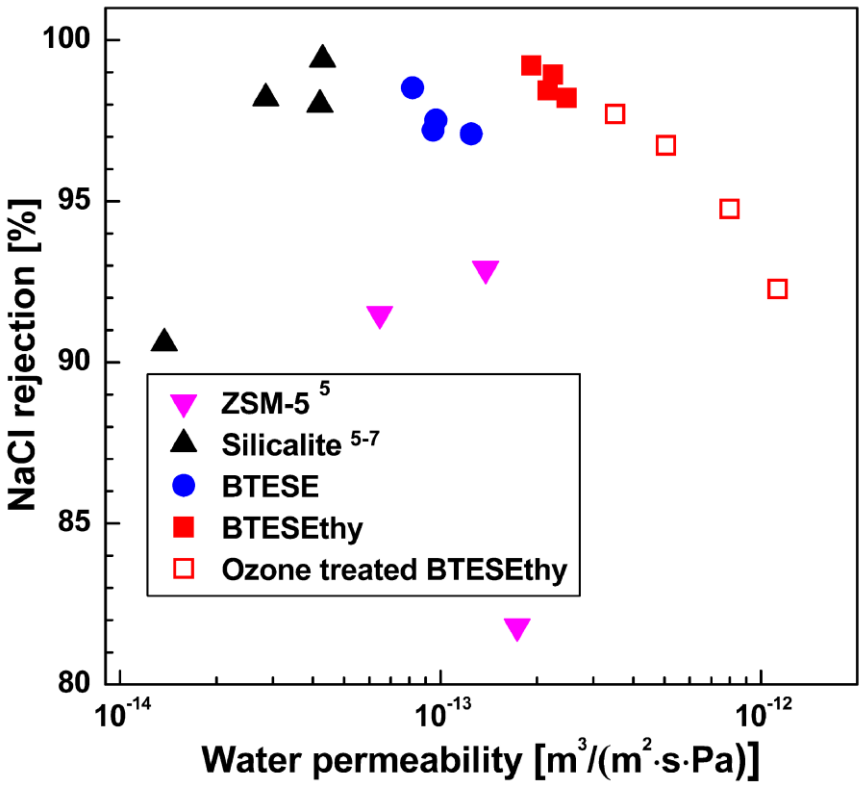

Figure 4-14. Trade-off of desalination performances for zeolite (25 °C, 2.76 MPa, and 0.1 M NaCl) and organosilica (25 °C, 1.15 MPa, and 2000 ppm NaCl) RO membranes.

To elucidate the electron density distribution and the structure of the BTESE and BTESEthy networks, quantum chemical calculations were carried out. For the calculations, model molecules with a trimeric 15-membered ring structure were employed (Figure 4-15), since these seem to be the smallest strain-free systems among the cyclic oligomers. The siloxy linkages on the silicon atoms in the real systems were replaced by methoxy groups in the models for simplification to minimize the computation time. The geometries were optimized by semi empirical calculations using the PM6 set of parameters and the electrostatic potentials (ESPs) were computed at the optimized geometries at the B3LYP/6-31G(d) level of theory. The optimized geometries have a rather round-shaped cyclic structure, but for the BTESEthy model, the ring is slightly ellipsoidal (Figure 4-15). The shortest inner ring through space C•••C distance was 4.6 Å for the BTESEthy model, while that for the BTESE model was 4.2Å, suggesting a more open pore structure of the BTESEthy system, probably due to the increased rigidity in the

ethenylene-bridged network. The electrostatic potentials (ESPs) of both models showed that the negative potentials were mainly localized inside the rings. However, the BTESEthy model exhibited a higher contrast for positive and negative potentials, compared with the BTESE model, which led to an enhanced H_2O-affinity for the BTESEthy channels by hydrogen-bonding and/or dipole-dipole interaction.

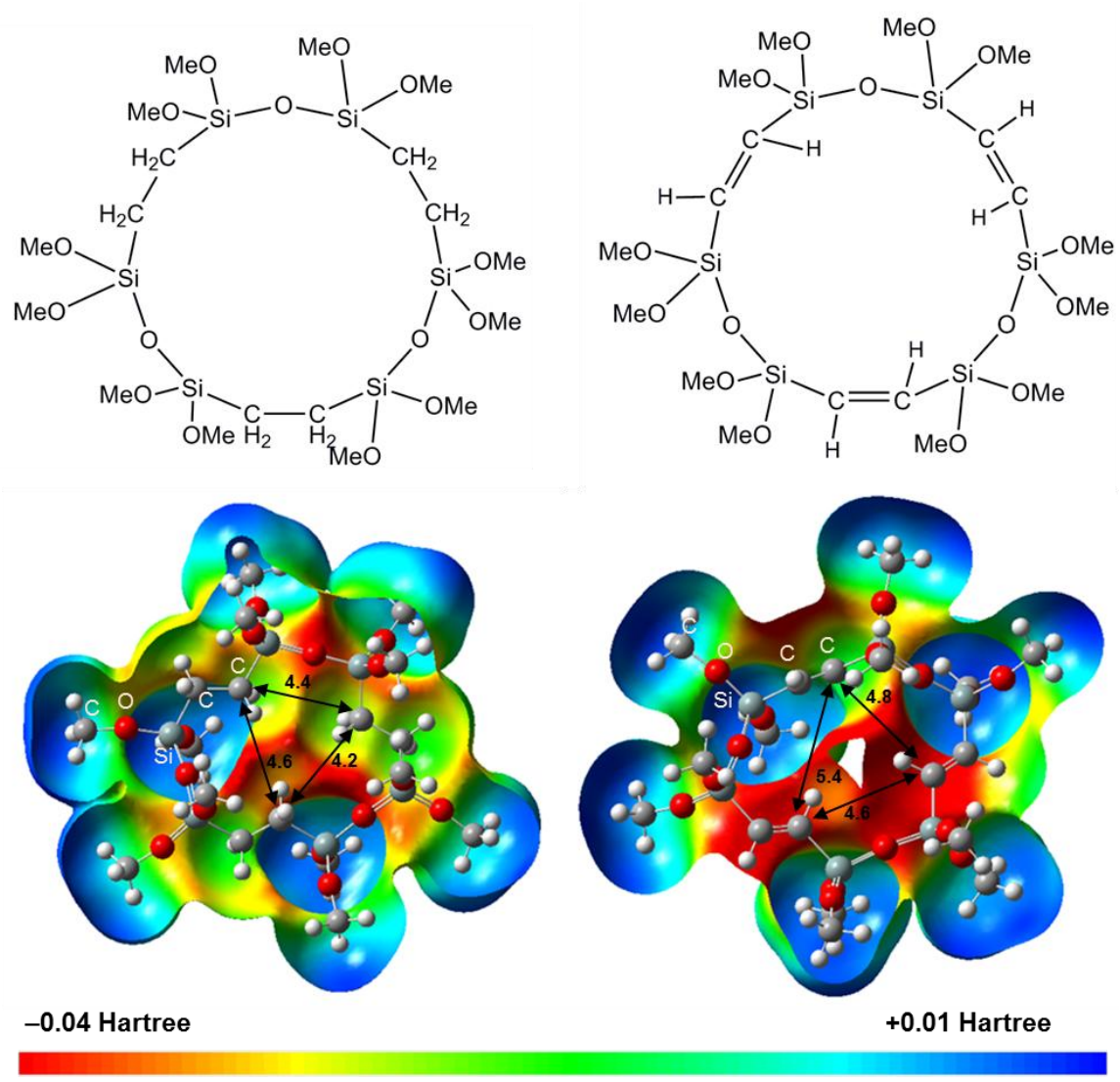

Figure 4-15. Optimized structures and ESPs for models of (left) BTESE and (right) BTESEthy networks derived from quantum chemical simulations at PM6//B3LYP/6-31G(d). Numbers indicate through space inner ring C•••C distances/Å. Colors range from -0.04 to +0.01 Hartree with orange and blue denoting extremely electron-rich and deficient regions, respectively.

4.4 Conclusions

We developed the first organosilica membrane derived from BTESEthy for water purification by reverse osmosis (RO). A thin and defect-free separation layer was obtained by optimizing the sol synthesis. Due to the introduction of ethenylene bridges in the network, the BTESEthy material exhibited a large BET surface area and superior water affinity. In gas permeation measurements, a high permeance of CO_2 with high CO_2/N_2 selectivity was observed for BTESEthy membranes at low temperatures, which shows great promise for CO_2 separation applications. RO measurements demonstrated that increasing the operating pressure resulted in a continuous increase in flux and salt rejection, while water permeability remained almost constant. BTESEthy membranes exhibited excellent chlorine resistance owing to the stable organically bridged network structure. Moreover, a significant improvement in water permeability was achieved by the aqueous ozone modification of the BTESEthy membrane, due to the great enhancement of water affinity by the reaction of the ethenylene bridges with ozone. Meanwhile, the effective pore size increased gradually with the ozone modification, which could present new options for tailoring membrane pore sizes. Compared with BTESE membranes, when using BTESEthy membranes, a simple adjustment of the bridging groups to more polarizable and rigid ethenylene linkages, doubled the water permeability with no drop in rejection.

References

[1] M. Elimelech, W.A. Phillip, The future of seawater desalination: Energy, technology, and the environment, *Science* 333 (2011) 712-717.

[2] K.P. Lee, T.C. Arnot, D. Mattia, A review of reverse osmosis membrane materials for desalination-development to date and future potential, *J. Membr. Sci.* 370 (2011) 1-22.

[3] D. Li, H.T. Wang, Recent developments in reverse osmosis desalination membranes, *J. Mater. Chem.* 20 (2010) 4551-4566.

[4] V.T. Do, C.Y. Tang, M. Reinhard, J.O. Leckie, Degradation of polyamide nanofiltration and reverse osmosis membranes by hypochlorite, *Environ. Sci. Technol.* 46 (2012) 852-859.

[5] L.X. Li, N. Liu, B. McPherson, R. Lee, Enhanced water permeation of reverse osmosis through MFI-Type zeolite membranes with high aluminum contents, *Ind. Eng. Chem. Res.* 46 (2007) 1584-1589.

[6] L.X. Li, J.H. Dong, T.M. Nenoff, Transport of water and alkali metal ions through MFI zeolite membranes during reverse osmosis, *Sep. Purif. Technol.* 53 (2007) 42-48.

[7] N. Liu, L.X. Li, B. McPherson, R. Lee, Removal of organics from produced water by reverse osmosis using MFI-type zeolite membranes, *J. Membr. Sci.* 325 (2008) 357-361.

[8] R.M. de Vos, H. Verweij, High-Selectivity, High-Flux Silica Membranes for Gas Separation, *Science* 279 (1998) 1710-1711.

[9] B.N. Nair, K. Keizer, H. Suematsu, Y. Suma, N. Kaneko, S. Ono, T. Okubo, S.I. Nakao, Synthesis of Gas and Vapor Molecular Sieving Silica Membranes and Analysis of Pore Size and Connectivity, *Langmuir* 16 (2000) 4558-4562.

[10] H.L. Castricum, A. Sah, R. Kreiter, D.H.A. Blank, J.F. Vente, J.E. ten Elshof, Hybrid ceramic nanosieves: stabilizing nanopores with organic links, *Chem. Commun.* 2008, 1103-1105.

[11] H.L. Castricum, A. Sah, R. Kreiter, D.H.A. Blank, J.F. Vente, J.E. ten Elshof, Hydrothermally stable molecular separation membranes from organically linked silica, *J. Mater. Chem.* 18 (2008) 2150-2158.

[12] R. Kreiter, M.D.A. Rietkerk, H.L. Castricum, H.M. van Veen, J.E. ten Elshof, J.F.

Vente, Stable hybrid silica nanosieve membranes for the dehydration of lower alcohols, *ChemSusChem* 2 (2009) 158-160.

[13] M. Kanezashi, K. Yada, T. Yoshioka, T. Tsuru, Design of Silica Networks for Development of Highly Permeable Hydrogen Separation Membranes with Hydrothermal Stability, *J. Am. Chem. Soc.* 131 (2009) 414-415.

[14] H.L. Castricum, G.G. Paradis, M.C. Mittelmeijer-Hazeleger, R. Kreiter, J.F. Vente, J.E. ten Elshof, Tailoring the Separation Behavior of Hybrid Organosilica Membranes by Adjusting the Structure of the Organic Bridging Group, *Adv. Func. Mater.* 21 (2011) 2319-2329.

[15] R. Xu, J.H. Wang, M. Kanezashi, T. Yoshioka, T. Tsuru, Development of Robust Organosilica Membranes for Reverse Osmosis, *Langmuir* 27 (2011) 13996-13999.

[16] G.G. Paradis, R. Kreiter, M.M.A. van Tuel, A. Nijmeijer, J.F. Vente, Amino-functionalized microporous hybrid silica membranes, *J. Mater. Chem.* 22 (2012) 7258-7264.

[17] M. Barczak, P. Borowski, A. Dąbrowski, Structure-adsorption properties of ethylene-bridged polysilsesquioxanes and polysiloxanes functionalized with different groups, *Colloids Surf., A* 347 (2009) 114-120.

[18] B.J. Melde, B.T. Holland, C.F. Blanford, A. Stein, Mesoporous Sieves with Unified Hybrid Inorganic/Organic Frameworks, *Chem. Mater.* 11 (1999) 3302-3308.

[19] K. Nakajima, I. Tomita, M. Hara, S. Hayashi, K. Domen, J.N. Kondo, A stable and highly active hybrid mesoporous solid acid catalyst, *Adv. Mater.* 17 (2005) 1839-1842.

[20] M. Sasidharan, S. Fujita, M. Ohashi, Y. Goto, K. Nakashima, S. Inagaki, Novel synthesis of bifunctional catalysts with different microenvironments, *Chem. Commun.* 47 (2011)10422-10424.

[21] S. Polarz, F. Jeremias, U. Haunz, Materials Surgery-Reactivity Differences of Organic Groups in Hybrids, *Adv. Funct. Mater.* 21 (2011) 2953-2959.

[22] R. Xu, J.H. Wang, M. Kanezashi, T. Yoshioka, T. Tsuru, Reverse osmosis performance of organosilica membranes and comparison with the pervaporation and gas permeation properties, *AIChE J.* 59 (2013) 1298-1307.

[23] H. Bader, J. Hoigne, Determination of ozone in water by the indigo method, *Water*

Res. 15 (1981) 449-456.

[24] D.J. Tobler, S. Shaw, L.G. Benning, Quantification of initial steps of nucleation and growth of silica nanoparticles: An in-situ SAXS and DLS study, *Geochim. Cosmochim. Acta* 73 (2009) 5377-5393.

[25] L.T. Zhuravlev, The surface chemistry of amorphous silica. Zhuravlev model, *Colloids Surf., A* 173 (2000) 1-38.

[26] M. Jaroniec, M. Kruk, J.P. Olivier, Standard Nitrogen Adsorption Data for Characterization of Nanoporous Silicas, *Langmuir* 15 (1999) 5410-5413.

[27] K.J. Shea, D.A. Loy, Bridged Polysilsesquioxanes. Molecular-Engineered Hybrid Organic-Inorganic Materials, *Chem. Mater.* 13 (2001) 3306-3319.

[28] M. Kanezashi, K. Yada, T. Yoshioka, T. Tsuru, Organic-inorganic hybrid silica membranes with controlled silica network size: preparation and gas permeation characteristics, *J. Membr. Sci.* 348 (2010) 310-318.

[29] Y. Takata, T. Tsuru, T. Yoshioka, M. Asaeda, Gas permeation properties of MFI zeolite membranes prepared by the secondary growth of colloidal silicalite and application to the methylation of toluene, *Micropor. Mesopor. Mater.* 54 (2002) 257-268.

[30] M. Kanezashi, M. Kawano, T. Yoshioka, T. Tsuru, Organic-inorganic hybrid silica membranes with controlled silica network size for propylene/propane separation, *Ind. Eng. Chem. Res.* 51 (2012) 944-953.

[31] D.R. Paul, Reformulation of the solution-diffusion theory of reverse osmosis, *J. Membr. Sci.* 241 (2004) 371-386.

[32] G.M. Geise, H.S. Lee, D.J. Miller, B.D. Freeman, J.E. McGrath, D.R. Paul, Water purification by membranes: The role of polymer science, *J. Polym. Sci., Part B: Polym. Phys.* 48 (2010) 1685-1718.

[33] D. Esquivel, E. De Canck, C. Jimenez-Sanchidrian, P. Van Der Voort, F.J. Romero-Salguero, Formation and functionalization of surface Diels-Alder adducts on ethenylene-bridged periodic mesoporous organosilica, *J. Mater. Chem.* 21 (2011) 10990-10998.

[34] S. Sankaraiah, J.M. Lee, J.H. Kim, S.W. Choi, Preparation and Characterization of Surface-Functionalized Polysilsesquioxane Hard Spheres in Aqueous Medium,

Macromolecules 41 (2008) 6195-6204.

[35] X.L. Wang, T. Tsuru, S. Nakao, S. Kimura, The electrostatic and steric-hindrance model for the transport of charged solutes through nanofiltration membranes, *J. Membr. Sci.* 135 (1997) 19-32.

[36] E.S. Hatakeyama, C.J. Gabriel, B.R. Wiesenauer, J.L. Lohr, M.J. Zhou, R.D. Noble, D.L. Gin, Water filtration performance of a lyotropic liquid crystal polymer membrane with uniform, sub-1-nm pores, *J. Membr. Sci.* 366 (2011) 62-72.

Chapter 5

Comparative study on structure-property of bridged organosilica membranes with ethane, ethylene and acetylene groups

5.1 Introduction

Hybrid organically bridged silica has attracted much interest due to their unique properties such as high surface area, tunable hydrophobicity/hydrophilicity, and high hydrothermal stability [1-3]. These hybrid silica-based materials, commonly referred to as periodic mesoporous organosilicas (PMOs), can be prepared via hydrolysis and condensation of bridged organosilanes $(R'O)_3Si\text{-}R\text{-}Si(OR')_3$ in the presence of a structure-directing agent [4,5]. The versatility of functional organic bridges in the resulting network can provide an opportunity to tune the bulk properties and make them promising for applications such as catalysis, adsorption, drug delivery and separation [6-9].

However, for molecular separation application, the pore size of PMOs, which typically range from ~2 to 10 nm, seems too large to exhibit molecular sieving ability. A significant breakthrough came with the development of microporous organosilica membranes with pore diameters of ~0.4 nm [10,11]. Castricum *et al.* first developed microporous organosilica membranes by co-condensation of bis(triethoxysilyl)ethane (BTESE) and methyltriethoxysilane (MTES). The resulting membrane showed a quite stable performance of 2 years for the pervaporative dehydration of butanol at 150 °C [10,11]. In their subsequent work, the BTESE membrane exhibited a high degree of acid stability in long-term measurements at a pH value of ~2 [12]. Qi *et al.* also reported high hydrothermal stability of Nb-doped BTESE membranes for CO_2 separation [13]. Our research group proposed a "spacer" technique to control silica networks, where the ethane groups were introduced to design a loose structure for development of a highly permeable

hydrogen separation membrane [14]. Recently, we examined the possibility of using BTESE-derived organosilica membranes for RO desalination under aggressive environments. The membrane exhibited excellent resistance to chlorine and exceptional hydrothermal stability, as well as superior salt rejection of >97% [15].

To date, most investigation focus on the BTESE-derived organosilica membranes since the Si-C-C-Si unit is almost the minimum for the hybrid silica network, which benefits the formation of small and rigid pores. From this point of view, development of organosilica membranes with unsaturated ethylene or acetylene bridges deserves more attention as they are easily accessible for chemical modification while maintaining the rigid pores for molecular sieving. The only difference is the single vs. double vs. triple bond of each organic bridge and therefore, it would be great research interest to investigate if this difference has some influence on the physical and chemical properties of materials. Ethenylene-bridged organosilica (BTESEthy) membrane has been developed for water desalination in our recent work, which shows great promise as a new type of promising RO membrane materials [16]. In this study, we developed acetylene-bridged (–C≡C–) organosilica membranes using bis(triethoxysilyl)acetylene (BTESA) as a novel precursor. Moreover, a comparative study was undertaken on organosilica materials with ethane, ethylene and acetylene bridges, providing insight into the relationship between the network structure and the bulk properties of these materials.

5.2 Experimental

5.2.1 Sol preparation

1,2-Bis(triethoxysilyl)acetylene (BTESA, 98%) sol was synthesized by hydrolysis and polymerization reaction of $(EtO)_3SiC{\equiv}CSi(OEt)_3$ with water and HCl, in ethanol. A required amount of BTESA was mixed with ethanol. Subsequently, premixed water and HCl were added dropwise to the precursor mixture under continuous stirring. The molar composition of the reactants was BTESA/H_2O/HCl = 1: 60: 0.1, and the weight percent of BTESA was kept at 5.0 wt%. The solution was stirred for 2 h at 25 °C before coating. 1,2-bis(triethoxysilyl)ethane (BTESE) and 1,2-Bis(triethoxysilyl)ethylene (BTESEthy)

sols were prepared under the same conditions as the BTESA sol.

5.2.2 Membrane preparation and characterization

Tubular α-alumina microfiltration membranes (porosity, 50%; average pore size, 1μm; outside diameter, 10 mm; and, length, 100 mm) were used as the supports. First, α-alumina particles (average particle size is 1.9 μm and 0.2 μm, respectively) were deposited onto the outer surface of the support using the SiO_2-ZrO_2 colloidal sol (2 wt.%) as a binder, and the substrate was fired at 550 °C for 30 min. This procedure was repeated 6 times to form the particle layer. Then, SiO_2-ZrO_2 (molar ratio of Si/Zr = 1/1, 0.5 wt.%) colloidal sols were coated on the particle layer by the hot-coating methods, where the substrate was first heated up to around 180 °C before coating, followed by quickly contacting the substrate with a wet cloth with the SiO_2-ZrO_2 sols. Subsequently, the substrate was fired at 550 °C for 15min in air. This hot-coating and calcination procedures were repeated approximately 6 times to form an intermediate layer. Finally, the BTESA sol was deposited onto the intermediate layer by wipe coating using a wet cloth with the BTESA sol (0.5 wt.%), followed by a flash calcination at 300 °C in air for 20 min.

The size distribution of the sols was measured by dynamic light scattering (DLS) at 25 °C using a Malvern Zetasizer Nano-ZS (ZEN3600). Thermogravimetric (TG) analysis (DTG-60, Shimadzu, Japan) was conducted on the organosilica powder for the evaluation of decomposition behavior of the remaining organic components in air and N_2, respectively, with a heating rate of 10 °C min^{-1}. Fourier Transform Infrared Spectrometer (FT/IR-4100) was applied to confirm the chemical structure of the BTESA films. Films for FTIR and static contact angle (CA) measurements were obtained by coating the organosilica sols onto clean silicon wafers, followed by calcination at 300 °C for 20 min.

5.2.3 Membrane performance

Single gas permeation measurements were performed at 200 °C using a high-purity of He, H_2, CO_2, N_2, C_3H_6, C_3H_8, and SF_6. Prior to measurement, the membrane was dried for 8-10 h in a He flow of 20 mL/min at 200 °C to remove the adsorbed water from the membrane pores. The permeate stream was kept at atmospheric pressure, and the pressure drop through the membrane was maintained at 1 bar. The permeation rate was measured

using a soap-film flow meter.

Water desalination experiments were carried out using a 2,000 ppm NaCl solution at 25°C, and molecular weight cut-off (MWCO) measurements were performed using 500 ppm neutral solutes: ethanol, isopropanol, glucose, and sucrose. RO experiments were conducted using a typical RO testing apparatus as previously described [17]. The feed solution, pressurized with a plunger pump, was vigorously agitated in the RO cell, and the retentate was recycled at an approximate flow of 30 mL min^{-1}. Water permeability, L_p, was calculated from the volume flux, J_v, divided by the effective transmembrane pressure, $\Delta P - \Delta\pi$.

$$J_v = L_p(\Delta P - \Delta\pi)$$

where L_p is the water permeability and, ΔP ($=P_1 - P_2$) and $\Delta\pi$ ($=\pi_1 - \pi_2$) are the differences in applied pressure and osmotic pressure, respectively. The observed rejection, R_{obs}, can be expressed as follows:

$$R_{obs} = (1 - C_p/C_f) \times 100\%$$

The concentrations of feed (C_f) and permeate (C_p) were measured with a conductivity meter for NaCl and a total organic carbon analyzer (Shimadzu, TOC-V_E) for neutral solutes.

5.3 Results and Discussion

Size distribution of the BTESE, BTESEthy and BTESA sols with an alkoxide concentration of 0.3 mol L^{-1} was determined by dynamic light scattering at 25 °C, as presented in Figure 5-1. Freshly synthesized (~ 2h for hydrolysis and polymerization reaction) BTESE sol showed a bimodal size distribution with mean radius of 4.7 nm, likely due to a small fraction of polymerization reaction of the monomer species [18]. In contrast, a narrow size distribution was observed for freshly prepared BTESEthy and BTESA sols, with mean radius of 1.9 and 2.1 nm, respectively. In general, the small sol size and narrow size distribution was desirable for preparing a thin, microporous separation layer. [19].

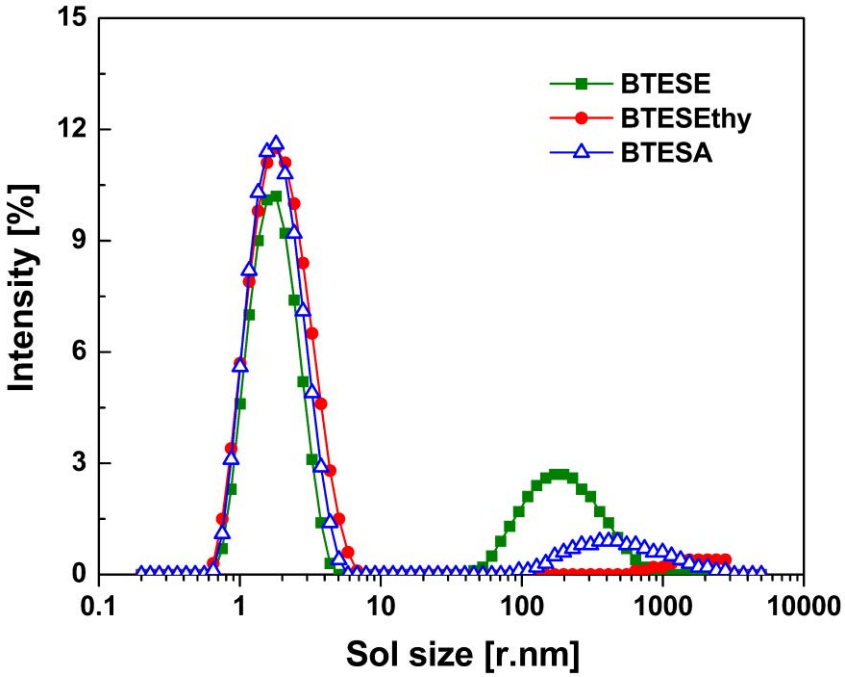

Figure 5-1. Size distribution of the BTESE, BTESEthy and BTESEthy sols determined by DLS.

Thermogravimetric (TG) analysis was conducted to evaluate the thermal stability of the organically bridged silica network. TG measurement was initiated after drying the sample at 100 °C for 2 hours under air or N_2 flow. As shown in Figure 5-2 (left), the weight loss of BTESA-derived gel powder in air and N_2 atmosphere at 800 °C was 17.4 and 13.6%, respectively. TG weight residue decreased at 200-400 °C probably due to evaporation of adsorbed water and dehydration of the silanol groups. Another decrease in weight was observed above approximately 400 °C, and was more pronounced in air than in N_2, which suggests the decomposition of acetylene groups in the network [20,21]. Figure 5-2 (right) shows the TG curves of BTESE, BTESEthy and BTESA gels in N_2 atmosphere. There was no big difference of the behavioral weight loss for the three materials. Therefore, organosilica membranes derived from BTESE, BTESEthy and BTESA were expected to be thermally stable at least up to 300 °C.

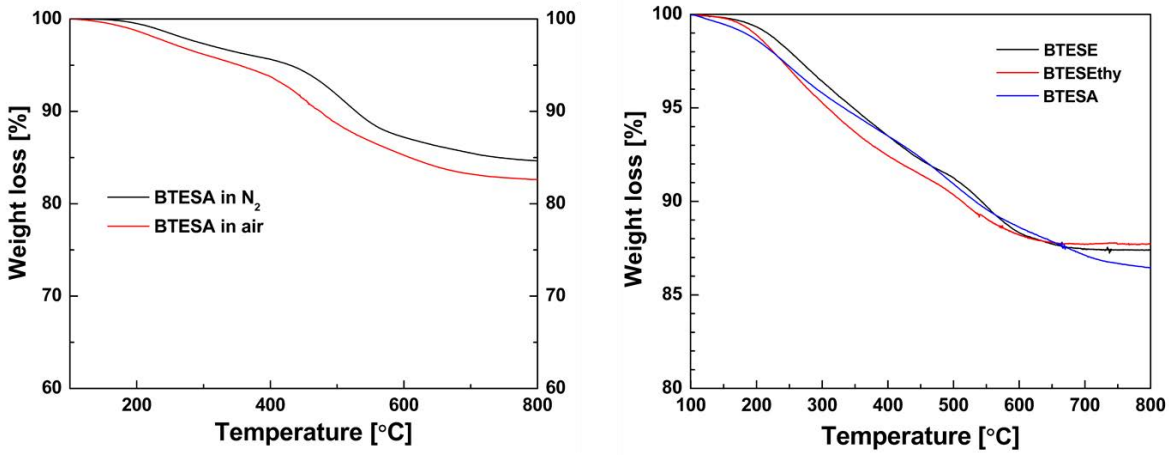

Figure 5-2. (left) TG analysis of BTESA gels in air and N_2 atmosphere with a heating rate of 10 °C/min, and (right) comparison of TG curves of BTESE, BTESEthy, and BTESA gels in N_2 atmosphere.

Figure 5-3 shows FTIR spectra of the BTESE, BTESEthy and BTESA films. The following absorptions were mainly related to the structure of the organosilica networks: C=C stretch (~1640 cm^{-1}); C≡C (~2100 cm^{-1}); O-H stretch (~3000-3600 cm^{-1}); C-H vibrations at ~1410 cm^{-1} (CH_2 bend), ~2890 cm^{-1} (CH_2 stretch), ~2980 cm^{-1} (=CH stretch); Si-O-Si stretch (1020-1200 cm^{-1}); Si-OH stretch (~920 cm^{-1}); and Si-C stretch (~790 cm^{-1}) [22-24]. The presence of these characteristic bands verified the formation of the related organosilica networks.

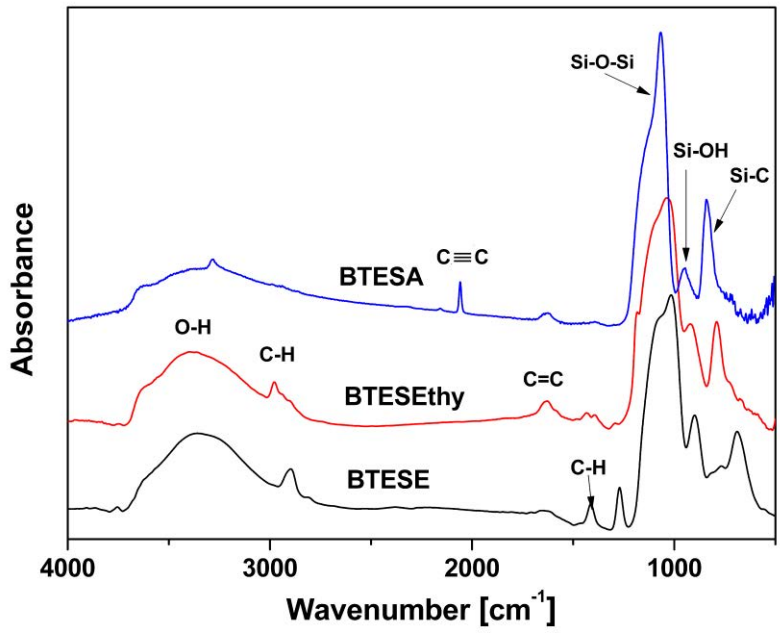

Figure 5-3. FTIR spectra of BTESE, BTESEthy and BTESA films.

Single gas permeance was measured using He, H_2, CO_2, N_2, C_3H_6, C_3H_8, and SF_6 for the three membranes with different bridging groups, as presented in Figure 5-4. The relevant permeance ratios of H_2/N_2, H_2/SF_6 were listed in Table 5-1. On the whole, the BTESA membrane exhibited higher permeance with lowest permeance ratios of H_2/N_2, H_2/SF_6, suggesting its relatively loose structure. The incorporation of acetylene bridges imparted higher rigidity within the networks, which would prevent the collapse of pores and the formation of dead-end pores during the calcination process, hence affording a more open and accessible pore structure [25]. In contrast, higher permeance ratios of H_2/N_2 and H_2/SF_6 were observed for BTESE and BTESEthy membranes, indicating their superior molecular sieving ability. Additionally, the π-π interaction between unsaturated bridging groups and the C_3H_6 molecules may contribute to a preferential C_3H_6 adsorption on the BTESEthy and BTESA membranes, respectively, considering that the molecular sizes of C_3H_6 and C_3H_8 are quite close [26].

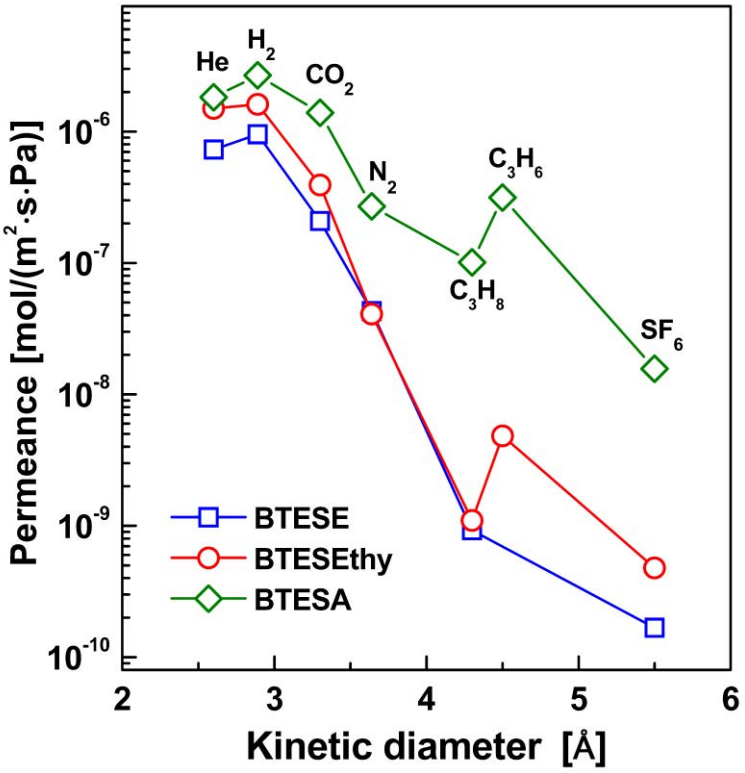

Figure 5-4. Comparioson of gas permeance properties for BTESE, BTESEthy and BTESA membranes at 200 °C.

Table 5-1. Gas permeance ratios.

Membrane	H_2/N_2	H_2/SF_6
BTESE	22.2	5700
BTESEthy	39.5	2590
BTESA	10.3	789

Figure 5-5 shows the time course of the RO performance for the BTESA membrane. During a continuous running of > 8 h, the water permeability was maintained at 8.5×10^{-13} $m^3/(m^2\cdot s\cdot Pa)$, which is about 8 times higher than that of the BTESE membrane. This high water permeability was attributed to the incorporation of polarizable and rigid acetylene bridges in the networks, which make the membrane network more hydrophilic and more open. However, the NaCl rejection of the BTESA membrane was relatively low, only at the level of ~95%, probably due to its larger pore size.

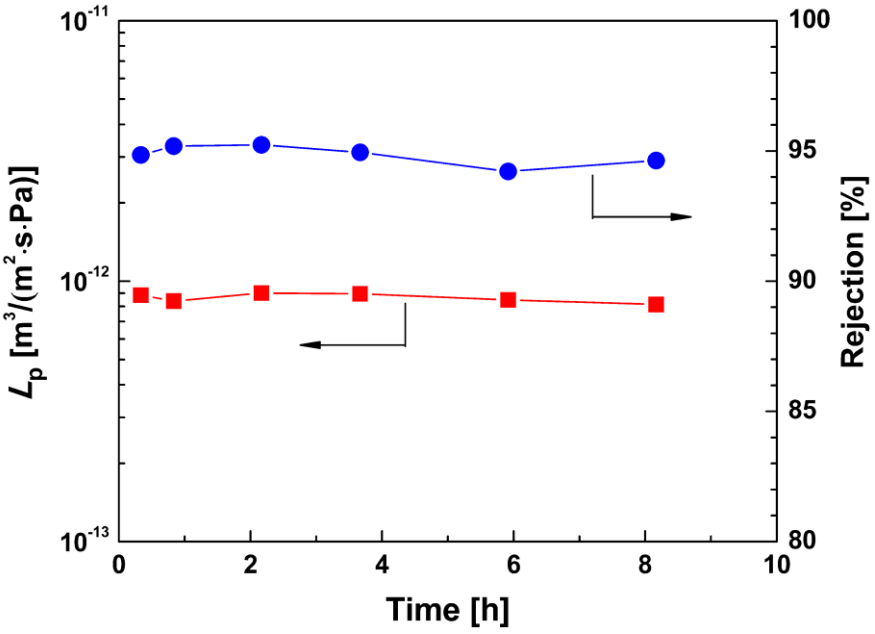

Figure 5-5. Time course of RO performances for the BTESA membrane.

The effective pore sizes of the BTESA membranes were evaluated by measuring the MWCO using a series of neutral solutes with different size: isopropanol (Stokes diameter (Sd): 0.48 nm), glucose (Sd: 0.73 nm) and sucrose (Sd: 0.94 nm) [27,28]. Figure 5-6

shows the MWCO curves of the BTESA membrane and a comparison with the BTESE membrane, the BTESEthy membrane and the commercial polyamide RO membrane, SW30HR [29]. The MWCO, defined at 90% rejection, of BTESA membrane was approximately 100 Da, distinctly larger than that of ~50 Da for BTESE and BTESEthy membranes. This result indicated that a larger effective pore size was obtained by introduction of acetylene bridges in the organosilica network, which is consistent with gas permeation results.

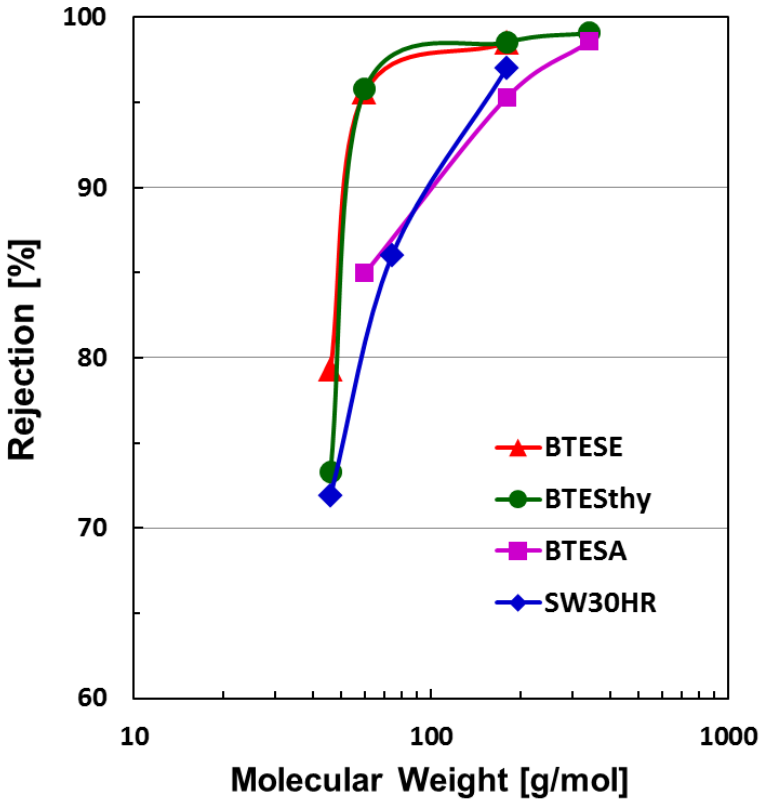

Figure 5-6. Comparison of molecular weight cut-offs for BTESE, BTESEthy, BTESA membranes and the commercial polyamide RO membrane, SW30HR (Dow FilmTec).

Figure 5-7 shows the trade-off relationship between NaCl rejection and water permeability for zeolite and organosilica RO membranes. Generally speaking, the organosilica membranes showed higher water permeability and roughly the same level of salt rejection, compared with the typical zeolite RO membranes such as ZSM-5 and silicalite [30-32]. Even at a low pressure of 1.15 MPa, BTESE and BTESEthy membranes

almost completely (>97%) rejected NaCl. Despite a relatively low NaCl rejection, the water permeability of the BTESA membranes reached up to 8.5 × 10^{-13} $m^3/(m^2 \cdot s \cdot Pa)$, mainly due to its more hydrophilic properties and larger pore size. Table 5-2 shows water contact angles of BTESE, BTESEthy and BTESA films. BTESEthy and BTESA films with unsaturated bridges showed low contact angles, suggesting their higher surface hydrophilicity. More importantly, a uniform distribution of bridging groups leads to the increased hydrophilicity not only on the membrane surface but also inside the membrane (within the pore channels of the network) [33,34]. This increased hydrophilicity from inside to surface may plays a leading role in the improved water permeability.

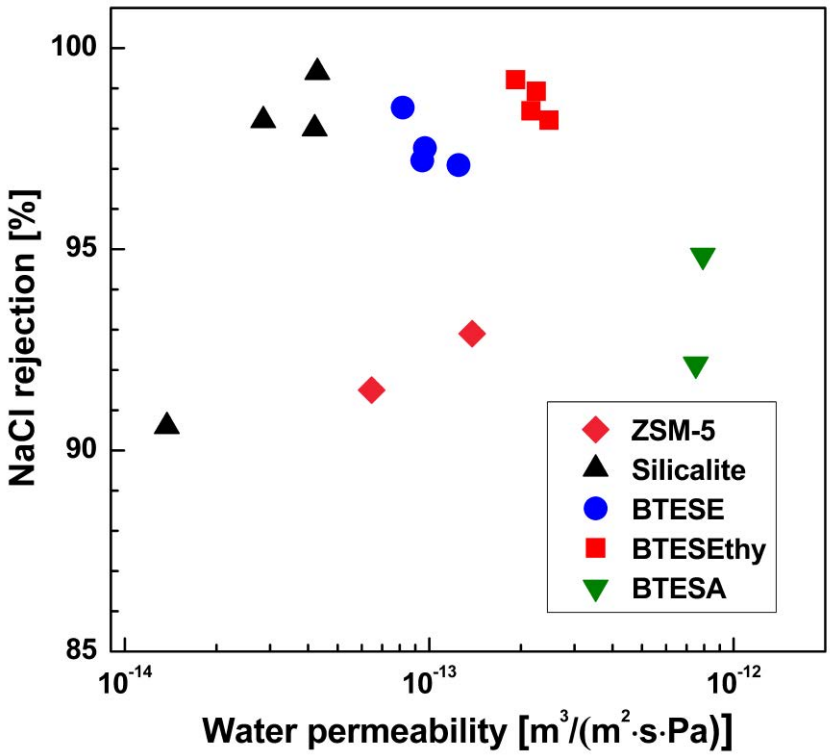

Figure 5-7. Trade-off of water permeability vs. salt rejection for zeolite (25 °C, 2.76 MPa, and 0.1 M NaCl) and organosilica (25 °C, 1.15 MPa, and 2000 ppm NaCl) RO membranes.

Table 5-2. Contact angles (CA) of BTESE, BTESEthy and BTESA films.

Sample	CA (°)
BTESE	66.8 ± 1.4
BTESEthy	50.4 ± 2.1
BTESA	48.4 ± 1.3

To elucidate the electron density distribution and the structure of the BTESE, BTESEthy and BTESA networks, quantum chemical calculations were carried out. As shown in Figure 5-8, model molecules with a trimeric 15-membered ring structure were employed for the calculations, because these seem to be the smallest strain-free systems among the cyclic oligomers. The siloxy linkages on the silicon atoms in the real systems were replaced by methoxy groups in the models for simplification to minimize the computation time. The geometries were optimized by semi-empirical calculations using the PM6 set of parameters and the electrostatic potentials (ESPs) were computed at the optimized geometries at the B3LYP/6-31G(d) level of theory. The optimized geometries shows that the inner ring through space C•••C distance increased gradually from BTESE to BTESA, suggesting more and more open pore structure of the models, probably due to the increased rigidity in the network. The electrostatic potentials (ESPs) of the three models showed that the negative potentials were mainly localized inside the rings. However, the BTESA and BTESEthy models exhibited higher contrast for positive and negative potentials, compared with the BTESE model, which led to an enhanced H_2O-affinity for the channels by hydrogen-bonding and/or dipole-dipole interaction.

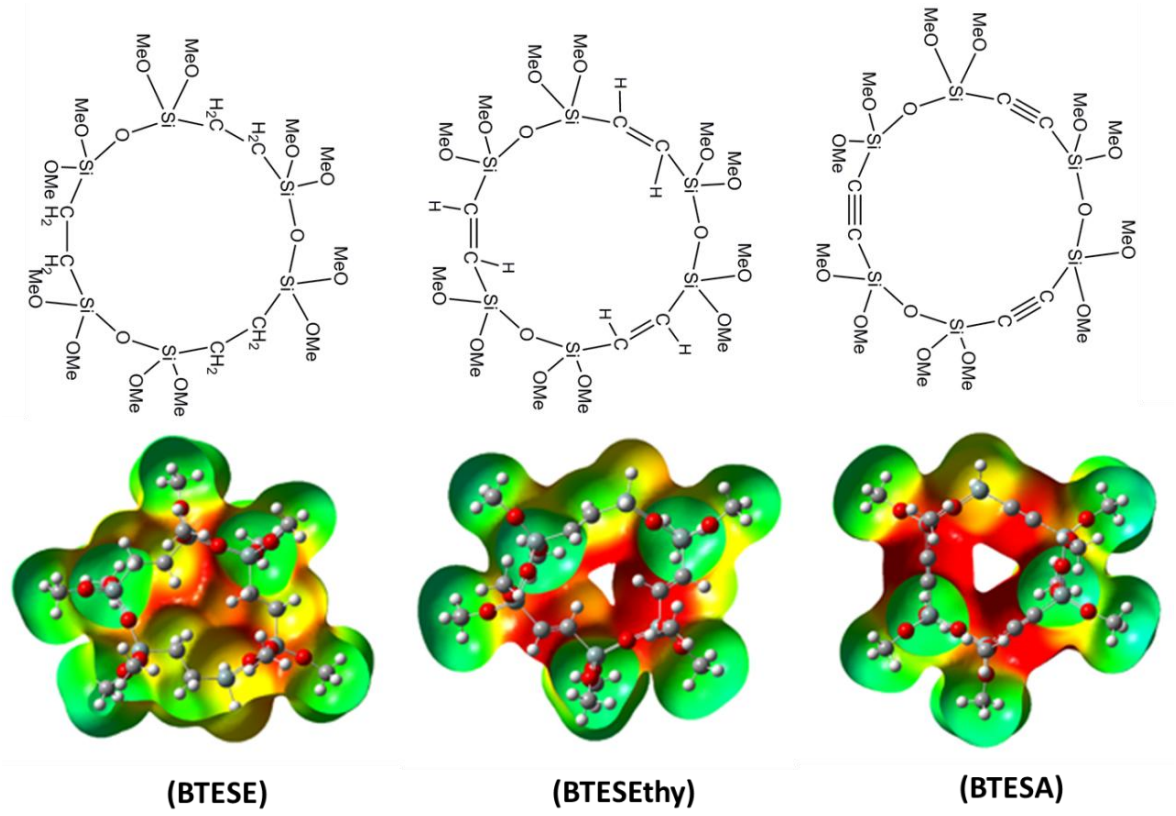

Figure 5-8. Optimized structures and ESPs for models of (left) BTESE, (middle) BTESEthy, and (right) BTESA networks derived from quantum chemical simulations at PM6//B3LYP/6-31G(d).

5.4 Conclusions

We developed acetylene-bridged (–C≡C–) organosilica membranes and comparatively studied the properties of the organosilica materials with ethane, ethylene and acetylene bridges. A narrow size distribution with small sol size was obtained for BTESA sols by optimizing the sol synthesis. Like BTESE and BTESEthy membranes, the BTESA membrane was also expected to be thermally stable up to 300 °C in air. The BTESA membrane exhibited high permeance with low permeance ratios of H_2/N_2, H_2/SF_6, due to its more loose structure caused by the introduction of more rigid acetylene bridges within the networks. MWCO measurements indicated that BTESA membranes possessed a larger effective pore size than BTESE and BTESEthy membranes, resulting in a relatively low rejection of NaCl in reverse osmosis. The water permeability of the BTESA membranes reached up to approximately 8.5×10^{-13} $m^3/(m^2 \cdot s \cdot Pa)$, which was close to that of the

commercial seawater RO membrane SW30HR [29]. Compared with BTESE and BTESEthy membranes, the great improvement in water permeability for the BTESA membranes mainly resulted from the increased hydrophilicity within the acetylene-bridged organosilica network, as well as the resulted larger pore size.

Reference

[1] A. Thomas, Functional Materials: From Hard to Soft Porous Frameworks, *Angew. Chem., Int. Ed.* 49 (2010) 8328-8344.

[2] F. Hoffmann, M. Cornelius, J. Morell, M. Froeba, Silica-based mesoporous organic-inorganic hybrid materials, *Angew. Chem., Int. Ed.* 45 (2006) 3216-3251.

[3] K.J. Shea, D.A. Loy, Bridged Polysilsesquioxanes. Molecular-Engineered Hybrid Organic-Inorganic Materials, *Chem. Mater.* 13 (2001) 3306-3319.

[4] K.J. Shea, D.A. Loy, A mechanistic investigation of gelation. The sol-gel polymerization of precursors to bridged polysilsesquioxanes, *Acc. Chem. Res.* 34 (2001) 707-716.

[5] T. Asefa, M.J. MacLachlan, N. Coombs, G.A. Ozin, Periodic mesoporous organosilicas with organic groups inside the channel walls, *Nature* 402 (1999) 867-871.

[6] Q.H. Yang, J. Liu, L. Zhang, C. Li, Functionalized periodic mesoporous organosilicas for catalysis, *J. Mater. Chem.* 19 (2009) 1945-1955.

[7] M. Kubo, K. Ishiyama, A. Shimojima, T. Okubo, Effect of organic groups on hydrogen adsorption properties of periodic mesoporous organosilicas, *Micropor. Mesopor. Mater.* 147 (2012) 194-199.

[8] C.X. Lin, S.Z. Qiao, C.Z. Yu, S. Ismadji, G.Q. Lu, Periodic Mesoporous Silica and Organosilica with Controlled Morphologies as Carriers for Drug Release, *Micropor. Mesopor. Mater.* 117 (2009) 213-219.

[9] V. Rebbin, R. Schmidt, M. Fröba, Spherical Particles of Phenylene-Bridged Periodic Mesoporous Organosilica for High-Performance Liquid Chromatography, *Angew. Chem., Int. Ed.* 45 (2006) 5210-5214.

[10] H.L. Castricum, A. Sah, R. Kreiter, D.H.A. Blank, J.F. Vente, J.E. ten Elshof, Hybrid ceramic nanosieves: stabilizing nanopores with organic links, *Chem. Commun.* 2008, 1103-1105.

[11] H.L. Castricum, A. Sah, R. Kreiter, D.H.A. Blank, J.F. Vente, J.E. ten Elshof, Hydrothermally stable molecular separation membranes from organically linked silica, *J. Mater. Chem.* 18 (2008) 2150-2158.

[12] H.M. van Veen, M.D.A. Rietkerk, D.P. Shanahan, M.M.A. van Tuel, R. Kreiter, H.L. Castricum, J.E. ten Elshof, J.F. Vente, Pushing membrane stability boundaries with HybSi® pervaporation membranes, *J. Membr. Sci.* 380 (2011) 124-131.

[13] H. Qi, J. Han, N.P. Xu, H.J.M. Bouwmeester, Hybrid organic-inorganic microporous membranes with high hydrothermal stability for the separation of carbon dioxide, *ChemSusChem* 3 (2010) 1375-1378.

[14] M. Kanezashi, K. Yada, T. Yoshioka, T. Tsuru, Design of Silica Networks for Development of Highly Permeable Hydrogen Separation Membranes with Hydrothermal Stability, *J. Am. Chem. Soc.* 131 (2009) 414-415.

[15] R. Xu, J.H. Wang, M. Kanezashi, T. Yoshioka, T. Tsuru, Development of Robust Organosilica Membranes for Reverse Osmosis, *Langmuir* 27 (2011) 13996-13999.

[16] R. Xu, M. Kanezashi, T. Yoshioka, T. Okuda, J. Ohshitac, T. Tsuru, Tailoring the affinity of organosilica membranes by introducing polarizable ethenylene bridges and aqueous ozone modification, *ACS Appl. Mater. Interfaces* (2013) doi: 10.1021/am401056a, in press.

[17] R. Xu, J.H. Wang, M. Kanezashi, T. Yoshioka, T. Tsuru, Reverse osmosis performance of organosilica membranes and comparison with the pervaporation and gas permeation properties, *AIChE J.* 59 (2013) 1298-1307.

[18] D.J. Tobler, S. Shaw, L.G. Benning, Quantification of initial steps of nucleation and growth of silica nanoparticles: An in-situ SAXS and DLS study, *Geochim. Cosmochim. Acta* 73 (2009) 5377-5393.

[19] H.L. Castricum, G.G. Paradis, M.C. Mittelmeijer-Hazeleger, R. Kreiter, J.F. Vente, J.E. ten Elshof, Tailoring the Separation Behavior of Hybrid Organosilica Membranes by Adjusting the Structure of the Organic Bridging Group, *Adv. Func. Mater.* 21 (2011) 2319-2329.

[20] T. Tsuru, T. Nakasuji, M. Oka, M. Kanezashi, T. Yoshioka, Preparation of hydrophobic nanoporous methylated SiO_2 membranes and application to nanofiltration of hexane solutions, *J. Membr. Sci.* 384 (2011) 149-156.

[21] H.R. Lee, T. Shibata, M. Kanezashi, T. Mizumo, J. Ohshita, T. Tsuru, Pore size controlled silica membranes with disiloxane alkoxides for gas separation, *J. Membr. Sci.*

383 (2011) 152-158.

[22] P.H.T. Ngamou, J.P. Overbeek, R. Kreiter, H.M. van Veen, J.F. Vente, I.M. Wienk, P.F. Cuperus, M. Creatore, Plasma-deposited hybrid silica membranes with a controlled retention of organic bridges, *J. Mater. Chem. A* 1 (2013) 5567-5576.

[23] D. Esquivel, E. De Canck, C. Jimenez-Sanchidrian, P. Van Der Voort, F.J. Romero-Salguero, Formation and functionalization of surface Diels-Alder adducts on ethenylene-bridged periodic mesoporous organosilica, *J. Mater. Chem.* 21 (2011) 10990-10998.

[24] J.M. Schmeltzer, L.A. Porter, M.P. Stewart, J.M. Buriak, Hydride Abstraction Initiated Hydrosilylation of Terminal Alkenes and Alkynes on Porous Silicon, *Langmuir* 18 (2002) 2971-2974.

[25] D.A. Loy, J.P. Carpenter, S.A. Yamanaka, M.D. McClain, J. Greaves, S. Hobson, K.J. Shea, Polymerization of Bis(triethoxysilyl)ethenes. Impact of Substitution Geometry on the Formation of Ethenyleneand Vinylidene-Bridged Polysilsesquioxanes, *Chem. Mater.* 10 (1998) 4129-4140.

[26] M. Kanezashi, M. Kawano, T. Yoshioka, T. Tsuru, Organic-Inorganic Hybrid Silica Membranes with Controlled Silica Network Size for Propylene/Propane Separation, *Ind. Eng. Chem. Res.* 51 (2012) 944-953.

[27] X.L. Wang, T. Tsuru, S. Nakao, S. Kimura, The electrostatic and steric-hindrance model for the transport of charged solutes through nanofiltration membranes, *J. Membr. Sci.* 135 (1997) 19-32.

[28] Y. Kiso, K. Muroshige, T. Oguchi, M. Hirose, T. Ohara, T. Shintani, Pore radius estimation based on organic solute molecular shape and effects of pressure on pore radius for a reverse osmosis membrane, *J. Membr. Sci.* 369 (2011) 290-298.

[29] E.S. Hatakeyama, C.J. Gabriel, B.R. Wiesenauer, J.L. Lohr, M.J. Zhou, R.D. Noble, D.L. Gin, Water filtration performance of a lyotropic liquid crystal polymer membrane with uniform, sub-1-nm pores, *J. Membr. Sci.* 366 (2011) 62-72.

[30] L.X. Li, J.H. Dong, T.M. Nenoff, Transport of water and alkali metal ions through MFI zeolite membranes during reverse osmosis, *Sep. Purif. Technol.* 53 (2007) 42-48.

[31] L.X. Li, N. Liu, B. McPherson, R. Lee, Enhanced water permeation of reverse

osmosis through MFI-Type zeolite membranes with high aluminum contents, *Ind. Eng. Chem. Res.* 46 (2007) 1584-1589.

[32] N. Liu, L.X. Li, B. McPherson, R. Lee, Removal of organics from produced water by reverse osmosis using MFI-type zeolite membranes, *J. Membr. Sci.* 325 (2008) 357-361.

[33] Y.D. Xia, W.X. Wang, R. Mokaya, Bifunctional Hybrid Mesoporous Organoaluminosilicates with Molecularly Ordered Ethylene Groups, *J. Am. Chem. Soc.* 127 (2005) 790-798.

[34] C. Vercaemst, M. Ide, P.V. Wiper, J.T.A. Jones, Y.Z. Khimyak, F. Verpoort, P. Van Der Voort, Ethenylene-Bridged Periodic Mesoporous Organosilicas: From E to Z, *Chem. Mater.* 21 (2009) 5792-5800.

Chapter 6

Conclusions

6.1 Summary of this study

The research presented in this dissertation focus on the development and design of microporous organosilica membranes for water purification applications. Bridged organosilica materials derived from BTESE, BTESEthy and BTESA, were developed as promising molecular separation membranes for water desalination by reverse osmosis (RO). The transport mechanism in RO was discussed for the innovative organosilica membrane. In addition, the comparison of structure-property of these organosilica membranes with different bridging groups was described. The main conclusions in this thesis were summarized as follows:

1. A robust microporous organosilica membrane has been developed by a sol-gel technique for water desalination. The organosilica membranes derived from bis(triethoxysilyl)ethane (BTESE) show a molecular weight cut-off below 100 Da and exhibit superior molecular sieving ability in the RO process. BTESE membranes showed exceptional hydrothermal stability in temperature cycles up to 90 °C, due to the introduction of an inherently stable, organically bridged silica network structure, significantly broadening the application fields of the organosilica membranes. Moreover, these organosilica RO membranes already show excellent chlorine stability under a wide range of chlorine concentrations; e.g., after a total chlorine exposure of up to 35,000 ppm·h, there was no obvious change in separation performance.

2. BTESE-derived organosilica membranes calcined at 300 °C exhibited higher salt rejection and lower water flux compared with the membrane prepared at 100 °C in RO desalination. Increasing the operating pressure led to an increase in water flux and salt rejection, while the flux and rejection decreased as salt concentration increased. The water

flux decreased linearly as the salt concentration increased from 500 to 10000 ppm, and the salt rejection decreased slightly with salt concentration. The nearly constant salt permeability in this concentration range suggested the molecular sieving mechanism for the organosilica RO membranes. Observed activation energies for permeation were larger for membranes with a smaller pore size, and were considerably larger than the activation energies for water viscosity. The applicability of the generalized SD model was examined in RO and PV desalination processes, and the quantitative differences in water permeance were accurately predicted by the application of generalized transport equations.

3. Ethenylene-bridged microporous organosilica membrane has been developed via the sol-gel technique. The BTESEthy material exhibited a large BET surface area and superior water affinity than that of ethane-bridged organosilicas. High permeance of CO_2 with high CO_2/N_2 selectivity was explained in relation to the strong CO_2 adsorption on the network with π-bond electrons. The introduction of polarizable ethenylene bridges in the network structure led to improved water permeability and high NaCl rejection (>98.5%) in reverse osmosis (RO). Moreover, a significant improvement in water permeability was achieved by the aqueous ozone modification of the BTESEthy membrane, due to the great enhancement of water affinity by the reaction of the ethenylene bridges with ozone. After 60 min of ozone exposure, the water permeability reached 1.1×10^{-12} $m^3/(m^2 \cdot s \cdot Pa)$, which is close to that of a commercial seawater RO membrane. Meanwhile, molecular weight cut-off measurements indicated a gradual increase in the effective pore size with ozone modification, which could present new options for tailoring membrane pore sizes.

4. Acetylene-bridged organosilica membranes were prepared and the properties of BTESA were compared with the previous organosilica materials with ethane and ethylene bridges. BTESA sols showed a relatively narrow size distribution with small sol size. Similar to BTESE and BTESEthy membranes, the BTESA membrane was thermally stable up to 300 °C in air. Compared with BTESE and BTESEthy membranes, BTESA membranes exhibited higher permeance and lower selectivity in gas permeation, due to its more loose structure. MWCO measurements suggested that BTESA membranes had the largest

effective pore size among the three membranes, resulting in a relatively low rejection of NaCl. However, BTESA membranes exhibited highest water permeability of up to approximately 8.5×10^{-13} $m^3/(m^2 \cdot s \cdot Pa)$ in RO, owing to the introduction of the more polarizable and rigid acetylene bridges in the silica network.

6.2 Outlook

We have demonstrated that bridged organosilica is a highly promising class of materials for RO desalination due to their excellent chlorine stability and superior hydrothermal stability. Compare to the commercialized polyamide-based RO membranes, the water permeability of these organosilica membranes still seems low, mainly due to the hydrophobic nature of the organic bridges. Therefore, in-depth studies should focus on adjusting the structure of the organic bridging groups by direct incorporation of more hydrophilic bridging groups or post-modification of the organosilica networks, to further improve the water permeability and salt rejection while maintaining its robustness.

List of Publications

Journal Articles:

(1) Rong Xu, Jinhui Wang, Masakoto Kanezashi, Tomohisa Yoshioka and Toshinori Tsuru, Development of robust organosilica membranes for reverse osmosis, *Langmuir*, **27** (2011) 13996-13999.

(2) Rong Xu, Jinhui Wang, Masakoto Kanezashi, Tomohisa Yoshioka and Toshinori Tsuru, Reverse osmosis performance of organosilica membranes and comparison with the pervaporation and gas permeation properties, *AIChE J.*, **59** (2013) 1298-1307.

(3) Rong Xu, Masakoto Kanezashi, Tomohisa Yoshioka, Tetsuji Okuda, Joji Ohshitac and Toshinori Tsuru, Tailoring the affinity of organosilica membranes by introducing polarizable ethenylene bridges and aqueous ozone modification, *ACS Appl. Mater. Interfaces*, **5** (2013) 6147-6154.

Conference:

(1) Rong Xu, Jinhui Wang, Masakoto Kanezashi, Tomohisa Yoshioka and Toshinori Tsuru, Hybrid organosilica membranes with high chlorine resistance for desalination, *The 6th Sino-Japan Symposium on Chemical Engineering*, June 21-24, 2011, Wuhan, China.

(2) Rong Xu, Masakoto Kanezashi, Tomohisa Yoshioka and Toshinori Tsuru, Organic-inorganic hybrid silica membranes with high hydrothermal stability and high chlorine tolerance in reverse osmosis, *The 43rd Autumn Meeting, The Society of Chemical Engineers of Japan*, September 14-16, 2011, Nagoya, Japan.

(3) Rong Xu, Masakoto Kanezashi, Tomohisa Yoshioka and Toshinori Tsuru, Tailoring the

structure of hybrid organosilica membranes for water desalination, *The 7th Conference of Aseanian Membrane Society (AMS7)*, July 4-6, 2012, Busan, Korea.

(4) Rong Xu, Masakoto Kanezashi, Hiroki Nagasawa, Tomohisa Yoshioka and Toshinori Tsuru, Adjusting the bridging groups of organosilica membranes toward high water permeability, *The 8th Conference of Aseanian Membrane Society (AMS8)*, July 16-19, 2013, Xi′an, China.

Acknowledgements

I would like to express my deepest gratitude to my advisor, Prof. Toshinori Tsuru, for his guidance, inspiration and encouragement in every stage of my Ph.D study. His profound learning and perseverance in the pursuit of scientific challenges have provided me with lifetime benefits.

I am very grateful to Prof. Tomohisa Yoshioka, Prof. Masakoto Kanezashi, and Prof. Hiroki Nagasawa for their kind assistant in my experiments and insightful discussion on my research work. I would also like to thank grateful to Prof. Joji Ohshita and Prof. Watara Nishijima in my dissertation committee for reading my thesis in their busy schedule.

I am thankful to my tutor, Mr. Toshinobu Shibata, for his warm-hearted assistance in my research work and daily life, when I came to Japan. I would like to thank all other group members in the Separation Engineering Lab, for their sustained help and all the good moments we spent together.

Lastly, I would like to thank my wife, Xilan Feng, for her endless encouragements and support through the entire three-year journey. I also wish to thank my son and daughter, whose births bring more happiness to my life.

July 2013

Rong Xu